KARADENIZ TECHNICAL UNIVERSITY
THE GRADUATE SCHOOL OF NATURAL AND APPLIED SCIENCES

GEOLOGICAL ENGINEERING DEPARTMENT

THE GEOLOGICAL, MINERALOGICAL AND GEOCHEMICAL PROPERTIES OF THE MAGNETITE-RICH CYPRUS TYPE Cu-Fe-Au VMS SYSTEM IN ORTAKLAR, GAZIANTEP.

MASTERS THESIS

Huseini ZAKARIA

JUNE 2017
TRABZON

KARADENİZ TECHNICAL UNIVERSITY

THE GRADUATE SCHOOL OF NATURAL AND APPLIED SCIENCES

GEOLOGICAL ENGINEERING DEPARTMENT

THE GEOLOGICAL, MINERALOGICAL AND GEOCHEMICAL PROPERTIES OF THE MAGNETITE-RICH CYPRUS TYPE Cu-Fe-Au VMS SYSTEM IN ORTAKLAR, GAZIANTEP.

Huseini ZAKARIA

This thesis is accepted to give the degree of

"MASTER OF SCIENCE"

By

The Graduate School of Natural and Applied Sciences at
Karadeniz Technical University

The Date of Submission : **15 / 05 /2017**

The Date of Examination : **01 / 06 /2017**

Supervisor : **Prof. Dr. Necati TÜYSÜZ**

Trabzon 2017

KARADENİZ TECHNICAL UNIVERSITY

THE GRADUATE SCHOOL OF NATURAL AND APPLIED SCIENCES

DEPARTMENT OF GEOLOGICAL ENGINEERING

HUSEINI ZAKARIA

THE GEOLOGICAL, MINERALOGICAL AND GEOCHEMICAL PROPERTIES OF THE MAGNETITE-RICH CYPRUS TYPE Cu-Fe-Au VMS SYSTEM IN ORTAKLAR, GAZIANTEP

Has been accepted as a thesis of

MASTER OF SCIENCE

after the Examination by the Jury Assigned by the Administrative Board of the Graduate School of Natural and Applied Sciences with the Decision Number 1702 dated 16 / 05 / 2017

Approved By

Chairman : Prof. Dr. Halim MUTLU .....

Member : Prof. Dr. Necati TÜYSÜZ .....

Member : Doç. Dr. Gülten YAYLALI ABANUZ .....

Prof. Dr. Sadettin KORKMAZ

Director of Graduate School

PREFACE

This study was undertaken initially under the supervision of Prof. Dr. Miğraç Akçay and completed under the supervision of Prof. Dr. Necati Tüysüz as a Master's degree thesis at the Geological Department of Karadeniz Technical University. This is in part fulfilment of the requirements for the award of Master of Science degree in Geological Engineering.

I would like to acknowledge the Turkish Government for supporting and providing me the platform to further my education in this wonderful country under the Türkiye Bursları Graduate scholarship.

My utmost gratitude go to Prof. Dr. Miğraç Akçay and Prof. Dr. Necati Tüysüz who devoted their time, resources and knowledge in making sure this thesis turned out right after supporting this study with their experience and directions. I wish to express my appreciation to research assistant Oğuzhan Gümrük for his immense support before and after I arrived in Karadeniz Technical University for his unlimited help, support and guidance throughout my studies in Karadeniz Technical University and to Associate Professor Gülten Yaylalı Abanuz for her thorough review of this thesis.

My sincere gratitude goes to the senior geologist and mine Director of Miryildiz Mining Company during the time of field research in the name of Mr. Recep Yaşar who shared not only his knowledge and experience but also his time and devotion to guide me throughout and after my field research. In addition, to Esra Yakar who worked tirelessly during the sample preparation, laboratory works and discussions.

I cannot forget to mention the academic guidance and motivation I received from the lecturers and research assistants of the Geological Department of Karadeniz Technical University in the names of Professor Mehmet Arslan, Professor Yener Eyuboğlu, Associate Prof. Emel Abdioğlu and Merve Yildiz just to mention a few.

My final gratitude goes to my family especially my father for his immense support throughout my educational life Alhaj Zakaria Huseini and my wife Salamatu Abbas for her love, patience and full support and to my friends with whom I missed our outings and play times due to putting together this work.

Huseini ZAKARIA

Trabzon, 2017

TEZ ETIK BEYANNAMESİ

Yüksek Lisans Tezi olarak sunduğum ‘Geological, Mineralogical and Geochemical Characteristics Of the Magnetite-rich Cyprus type Cu-Fe-Au VMS system in Ortaklar, Gazientep.’başlıklı bu çalışmayı baştan danışmanım Prof. Dr. Miğraç Akçay ve daha sonra danışmanım Prof. Dr. Necati Tuysuz‘un sorumluluğunda tamamladığımı, verileri/örnekleri kendim topladığımı, deneyleri/analizleri ilgili laboratuarlarda yaptığımı/yaptırdığımı, başka kaynaklardan aldığım bilgileri metinde ve kaynakçada eksiksiz olarak gösterdiğimi, çalışma sürecinde bilimsel araştırma ve etik kurallara uygun olarak davrandığımı ve aksinin ortaya çıkması durumunda her türlü yasal sonucu kabul ettiğimi beyan ederim. 01/06/2017.

Huseini ZAKARIA

TABLE OF CONTENTS

Master Thesis

SUMMARY

THE GEOLOGICAL, MINERALOGICAL AND GEOCHEMICAL PROPERTIES OF THE MAGNETITE-RICH CYPRUS TYPE Cu-Fe-Au VMS SYSTEM IN ORTAKLAR, GAZIANTEP.

Huseini ZAKARIA

Karadeniz Technical University
The Graduate School of Natural and Applied Sciences
Geology Graduate Program
Supervisor: Prof. Dr. Necati TÜYSÜZ
2017, 93 Pages, (5) Appendix

Located in the Şahinbey district of Gaziantep in the southeastern part of Turkey within the Koçali complex, the Ortaklar Fe-Cu-Au Deposit is a magnetite-rich VMS deposit lying within volcano-sedimentary units including N-MORB type basalts of Upper Triassic - Lower Cretaceous ophiolite characterized by nappes and thrusts. With an estimated reserve of 2.5 million tonnes of ore comprising 45% Fe, 3% Cu, and 0.5 ppm Au, the deposit is composed of tectonically separated discrete ore lenses of various lengths. This deposit consists of pyrite, magnetite, chalcopyrite and sphalerite as ore minerals in decreasing abundance with chlorites, carbonates and quartz as gangue phases. Hydrothermal alteration has affected a wide portion of the study area and is characterized by an inner propylitic zone at the central section characterised by Mg-rich chlorites (chlinochlore) and the calculated chlorite geothermometry produced temperatures in the range of 225 to 255^{0}C. It is underlain by minor silicification grading into argillic alteration zone. Late-stage carbonate alteration crosscuts all the volcano-sedimentary strata. δ^{34}S values obtained from pyrites and chalcopyrites range from +2.5‰ to 4.6‰ indicating a magmatic source for the sulphur with a calculated temperature range of 202 to 364^{0}C. The δ^{18}O values for the quartz and magnetite spans from 8.9 to 28.9‰ and from -5.0 to 8.3‰, respectively with a calculated temperature range of 250–427^{0}C. Calculated δ^{18}O values for the fluids in equilibrium with these minerals have a broad range between 3.39 and 23.32‰. δ^2H isotopic composition of the waters extracted from the fluid inclusions in quartz associated with the mineralization vary from -52 to -73‰. Such δ^{18}O and δ^2H compositions are highly likely related to a magmatic fluid source modified by interaction with underlying rocks. The geothermometric data together with mineral paragenetic studies and field observations indicate that ore deposition occurred in two stages. A high temperature magnetite-rich first stage and a sulphide-rich second stage followed by a waning stage.

Key Words: Ortaklar, Cu-Fe-Au, VMS, O-H-S isotopes, hydrothermal alteration, Ore textures

Yüksek Lisans

ÖZET

ORTAKLAR (GAZİANTEP) MANYATİT-ZENGİN KIBRIS TİPİ Cu-Fe-Au VMS YATAĞ'INI JEOLOJİK, MİNERALOJİK VE JEOKİMYASAL ÖZELLİKLERİ

Huseini ZAKARIA

Karadeniz Teknik Üniversitesi
Fen Bilimleri Enstitüsü
Jeoloji Mühendisliği Anabilim Dalı
Danışman: Prof. Dr. Necati TÜYSÜZ
2017, 93 Sayfa, 5 Sayfa Ek

Ortaklar Cu-Fe-Au Yatağı, Gaziantep'in Şahinbey ilçesinde, Türkiye'nin güneydoğusunda bulunan Koçali kompleksi içinde Bölgesi N-MORB tipi bazaltlar da dahil olmak üzere volkanik-sedimenter birimler knappes ve bindirmeler ile karakterize edilen Üst Triyas-Alt Kretase ofiyolit içerisinde yer alan manyetit-zengin bir VMS yataktır. % 45 Fe, % 3 Cu ve 0.5ppm Au içeren 2,5 milyon ton cevherin tahmini rezervi ile, çeşitli uzunluklarda tektonik olarak ayrılmış ayrı cevher merceklerinden oluşur. Bu yatağı, klorit, karbonat ve kuvarsın gang fazları olarak azalan cevher mineralleri olarak pirit, manyetit, kalkopirit ve sfaleritten oluşmaktadır. Hidrotermal alterasyon, çalışma alanının geniş bir bölümünü etkilemiş ve orta bölümde, Mg zengini kloritler (chlinochlore) ile karakterize edilen iç propilitit zon ile karakterize edilmiştir ve hesaplanan klorit jeotermometri 225-250 °C aralığında sıcaklık veriyor. Bu alterasyon derecelendirmesinin altında küçük silisleşme olup, arjilik alterasyon zonuna sınıflandırıyor. Geç evre karbonat alterasyonu bütün volkano-sedimenter tabakaları çaprazlamaktadır. Piritler ve kalkopiritlerden elde edilen $\delta^{34}S$ değerleri, + 2.5 ‰ - 4.6 ‰ arasında değişir ve hesaplanan ortalama sıcaklık aralığı 205 ila 367^0C olan sülfür için magmatik bir kaynak gösterir. Kuvars ve manyetit için $\delta^{18}O$ değerleri, 8.9 ila 28.9 ‰ ve -5.0 ila 8.3 ‰ arasındadır, hesaplanan sıcaklık 250-427^0C arasındadır. Bu minerallerle dengede olan akışkanlar için hesaplanmış $\delta^{18}O$ değerleri, 3.39 ile 23.32 ‰ arasında geniş bir aralığa sahiptir. Bu $\delta^{18}O$ ve $\delta^{2}H$ bileşimleri, altta yatan kayaçlarla etkileşim yoluyla değiştirilen magmatik bir sıvı kaynağıyla büyük olasılıkla ilişkilidir. Jeotermometrik veriler, mineral parajenez çalışmaları ve saha gözlemleri ile birlikte iki aşamalı cevher çökelti olduğunu göstermektedir. Yüksek sıcaklığa sahip manyetit bakımından zengin bir ilk aşamada ve ardından sülfit bakımından zengin ikinci aşamada ve sonra bir azalan aşamada oluşmuştur.

Anahtar Kelimeler: Ortaklar,Cu-Fe-Au, VMS, O-H-S izotopları, Hidrotermal alterasyon, Cevher dokuları.

TABLE OF FIGURES

Page No.

TABLE OF TABLES

Page No.

TABLE OF SYMBOLS

Am	: Amphibole
Bn	: Bornite
Ccp	: Chalcopyrite
CF-IRMS	: Continuous-Flow Isotope-Ratio Mass Spectrometer
Chl	: Chlorite
Cl	: Clay
Cpx	: Clinopyroxene
Csa	: "hot dry-summer" climates
Cu	: Copper
E-MORB	: Enriched Mid Ocean Ridge Basalts
Ep	: Epidote
Fe	: Iron
fO_2	: Oxygen fugacity
g	: gram
G	: Gangue
H	: Hydrogen
HFS	: High Field strength
ICP-MS	: Iductively Coupled Plasma Mass Spectrometry
ICP-OES	: Inductively Coupled Plasma Optical Emission Spectrometry
IRMS	: Isotope-ratio mass spectrometry
kV	: Kilovolt
Mag	: Magnetite
Mar	: Marcasite
nA	: Nanoampere
O	: Oxygen
OIB	: Ocean Island Basalts
Opq	: Opaque
Opx	: Orthopyroxene
Pl	: Plagioclase
Px	: Pyroxene

Py : Pyrite

Qtz : Quarts

S : Sulphur

Sp : Sphalerite

Srp : Serpentine

TAB : Tauride Anatolian Belt

TC/EA : Thermo-Finnigan thermo-combustion elemental analyzer

VMS : Volcanogenic Massive Sulphide

VSMOW : Vienna Standard Mean Ocean Water

XRD : X-ray Diffraction

$\delta^{18}O$: Oxygen Isotope Composition

$\delta^{2}H$: Hydrogen isotope composition

$\delta^{34}S$: Sulphur Isotope Composition

ΔC : Change in Concentration

1. GENERAL INFORMATION

1.1. Study Purpose

This study was carried out to understand the geologic, tectonic and mineralization history of the Ortaklar Volcanogenic Massive Sulphides (VMS) deposit located in the Şahinbey district of Gaziantep in Turkey. In order to achieve this objective, mapping of and delineating the alteration pattern in the vicinity of the mineralised area, studying the petrographic and petrochemical features of volcanic rocks occurring in the area, and stable isotopes (O, H and S isotopes) geochemistry of quartz, magnetite, pyrite and chalcopyrites from the ore constitute major portion of this study. Although fluid inclusion studies were supposed to form a major chapter of the study, no measurable fluid inclusions were found to help achieve this objective. Microprobe analyses on rock forming minerals and the ore minerals were carried out to provide a complete micrometer-scale quantitative chemical analysis of the constituents of the minerals. Based on all these studies, attempts were made to decipher the geology and geological structures in the study area, the geometry of the ore, the types of ore and the alteration and alteration patterns associated with the mineralization. Not only that but also attempts were made to determine the mineral paragenesis and the relationship between the sulphides and magnetites.

1.2. Geographical Location

The study area is located in the south of Ortaklar village in the south-eastern part of Turkey, approximately 32 km west of Gaziantep. The licenced area is bounded by coordinates of 37° 0'46.30"E 37° 2'34.54"N, 37° 1'40.28"E 37° 2'38.18"N, 37° 1'38.59"E 37° 2'58.50"N and 37° 0'53.58"E 37° 3'4.04"N in the Gaziantep-Şahinbey district. It forms part of the division N38-d4 of the 1:25000 scale topographical map of Turkey. The route to Ortaklar Deposit is a first and second-class tarred road network from Gaziantep city centre towards west. The mine site has a distance of about 500m from the Ortaklar village southwards, which can be accessed by untarred road networks, created mainly for mining purposes.

It takes about 40 minutes to drive from Gaziantep to the Ortaklar village. The main road near the Gaziantep University connects to Burç yolu after about 6km passing by the zoological garden next to the University heading towards Yeşilpınar. The distance from Yeşilpinar to Belenkoy village on the Belenköy village road is about 24km and from Belenköy village to the Ortaklar village road is approximately 7.5km. Ortaklar is about 5km west of Belenköy, 5.12km southwest of Sarikaya and 4.16km northwest of Akbayır (Fig 1.1).

Figure 1.1. Google earth view of the study area (Insert -Turkey map)

1.3. Geomorphology, Climate and Vegetation

The area is made up of hilly and mountainous ranges bounding the northern and southern sector ranging from about 600m to 850m above sea level. The height of the mountains increase northwards. Gaziantep province has a hot-summer Mediterranean climate (Csa in the Koeppen climate classification) with influences of a continental climate during winter with hot, dry summers and cool, wet and occasionally snowy winters. The average temperature in Gaziantep is 15.5°C while the average annual rainfall is 529 mm. Steppe plants cover most bare grounds with long stretches of limestone plateau covered by olives and pistachio trees at 500 m to 600 m altitude.

1.4. Previous Studies

Detailed geological studies have been undertaken in the Adiyaman region on the same Tauride Anatolian belt in which the deposit falls by Varol et al, (2011) who divided the Koçali complex as the Tarasa Unit, the Konak Unit, the Cilo Limestones and the Kale Ophiolite. They determined the age of the volcanic sequences as Late Triassic (middle Carnian to Rhaetian) based on the radiolarian data from the associated pelagic rock units. They also concluded that the geochemical data obtained indicates the presence of two different types of Late Triassic volcanic rock groups characterized by E-MORB and OIB mantle sources, and that the samples from the Kocali Complex occurring in Adiyaman region has characteristics of N-MORB type mantle source and was affected by crustal contamination. Yıldırım et al, (2016) studied the geological, mineralogical, hydrothermal alteration and ore formational history of the study area and concluded that the Ortaklar Deposit formed in two stages: a sulphide-rich magnetite-poor first stage and a magnetite-rich sulphide-poor second stage. The Ortaklar Deposit has an estimated 2.5 million tonnes of ore reserve comprising 45% Fe, 3% Cu and 0.5ppm Au (Yildirim et al, 2016). These studies provided a general formation model for the mineralization in this study.

1.5. General Geology of South Eastern Anatolia

South East Anatolian suture belt (Fig 1.2) is a region bounded by the Anatolide-Tauride terrain to the north and the Arabian plate to the south. The Anatolide-Tauride terrane forming the bulk of the southern Turkey and showing a Palaeozoic stratigraphy similar to the Arabian Platform is interpreted as being the remnants of Tethyan seaways (Varol et al, 2011) and its oceanic crust known as ophiolites and ophiolite melanges. Notable evolution of the southern Neotethyan seaway began by rifting in the Triassic period and terminated by continent-continent collision during the Miocene (Şengör and Yılmaz, 1981, Robertson, 2007) creating the Tauride-Anatolia belt (TAB) marking the southern edge of the Eurasian plate and the northern edge of the Arabian plates.

The main events separating the TAB from the Arabian plate took place in Cretaceous resulting in the northward subduction of Neotethys below the TAB forming the Bitlis - Zagros active margin (Aagard et al, 2005; Robertson et al, 2004; Rolland et al 2011; Kuşcu and Friedman, R., 2013a). During this subduction event, most of the oceanic lithosphere belonging to the Southerly Ocean, Neotethys between Arabian plate and TAB was consumed

firstly by an intra-oceanic subduction that also resulted in supra-subduction zone (SSZ) ophiolites. These SSZ ophiolites were then emplaced over the southern margin of the TAB forming the Malatya- Keban metamorphics (Robertson et al., 2005; Kuşcu et al., 2013a). This was followed by the closure of the Neotethys oceanic basin that resulted in an active margin along the Bitlis – Zagros subduction zone between 83 - 79 Ma (Kuşcu and Friedman, 2013). The subduction resulted in voluminous calc-alkaline intrusive magmatism emplaced into Malatya - Keban and Bitlis – Pötürge metamorphics. This short-lived subduction was terminated due to collision between Arabian plate and TAB, which is marked by the emplacement of the ophiolitic nappes over the Bitlis - Pötürge metamorphic massifs. The high temperature metamorphism of the Bitlis – Pötürge was dated as 74 - 71 Ma (Gencouğlu and Turhan, 1984; Rolland et al., 2011), which was interpreted as the timing of continental lithospheric subduction (underthrusting) underneath TAB before the final suturing of Arabian and Eurasian plates (Rolland et al., 2011). Following the underthrusting of the metamorphics underneath TAB, the whole region experienced a post-collisional extension due to decrease in the convergence rate between Arabian and Eurasian plates (Savostin et al., 1986); Kuşcu et al., 2013a) and delamination or rollback of the subducted slab between 77 to 54 Ma (Kuşcu et al., 2013a; Rolland et al., 2011) that exhumed the metamorphic basement, uncovered previously obducted ophiolites, and filled the basins with Maastrichtian to Paleocene subaerial and submarine sedimentary rocks.

The Activation of the northward movement of the Arabian plate with respect to the Eurasian plate resulted in emplacement of very large bodies of ophiolites with underlying tectonic slices of ophiolites mixed with different lithologies (melanges?) during the mid-Cretaceous over the Anatolide-Tauride terrane (Okay, 2008). With the initiation of continental collision in the Palaeocene due to the closure of the southern Neotethys Ocean, the Anatolide-Tauride terrane was internally sliced and formed a south to southeast verging thrust pile. The contraction continued until the Early to Mid-Miocene in western Turkey and is still continuing in the eastern Anatolia. The lower parts of the thrust pile found in the north (Tavşanlı Zone, Afyon Zone and the Menderes Massif) were regionally metamorphosed, while the upper parts (Taurides) found in the south form unmetamorphosed large cover nappes or superficial nappes composed mainly of a stack of thrust sheets of Palaeozoic and Mesozoic sedimentary rocks. The resulting orogenic zone (Bitlis-Zagros orogen) was formed during this continental collision and the remnants of the Tethyan Ocean

are marked by southeastern Anatolian Suture Belt (Goncuoglu et al., 1997) or the Assyrian Zagros suture in southeastern Anatolia (Okay and Tüysüz, 1999).

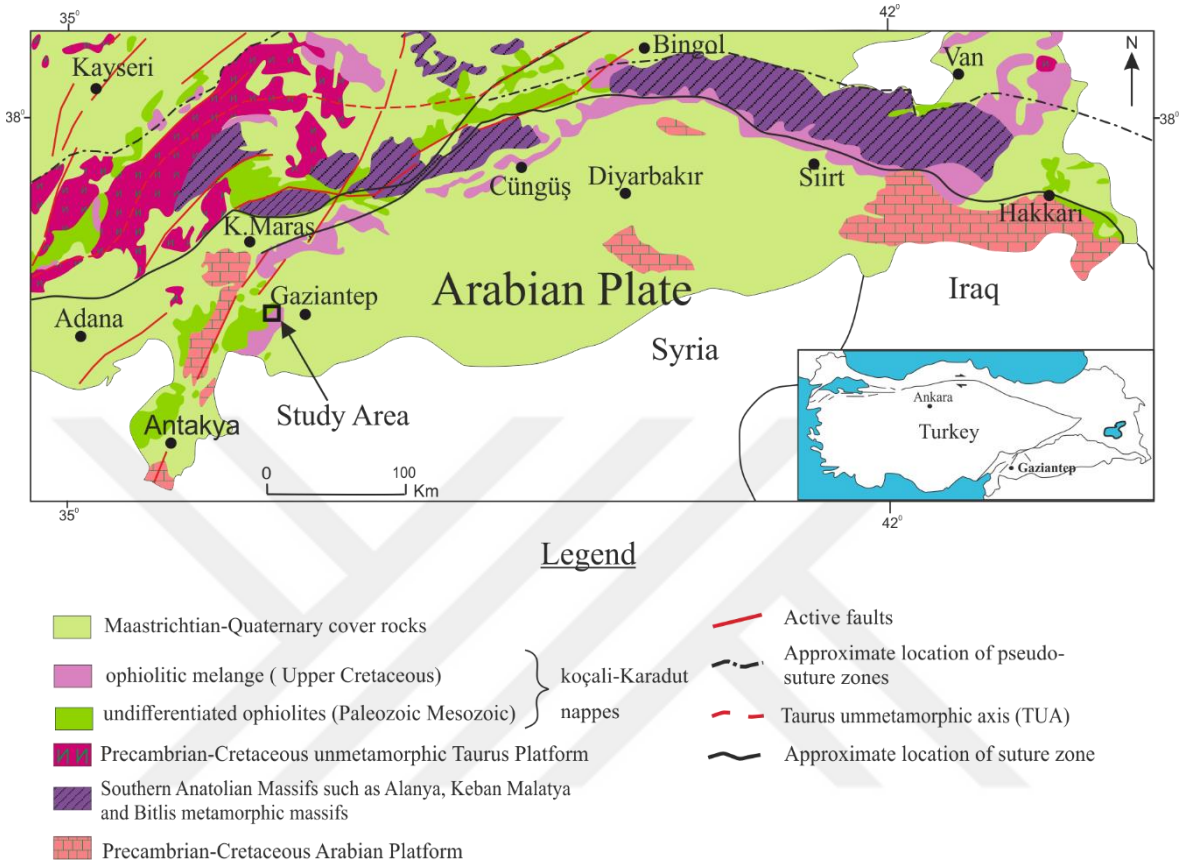

Figure 1.2. General Geological Map of part of the Tauride and Arabian platform with study area indicated. (Modified from Yılmaz and Yılmaz (2013))

The Southeastern Anatolian suture belt has been differentiated into three tectonic zones, (namely the Arabian Platform, an imbricated zone and a Nappe zone) by Yılmaz and Yiğitbaş (1990), Yilmaz (1993) and Elmas and Yilmaz (2003). However, Şenel (2002) identified two main distinct structural units, the Anatolian autochthon (corresponding to the Arabian platform) and nappes. The nappes thrusting-over the SE Anatolian Autochthon can be grouped into three main packages, named as the Bitlis-Malatya Nappe, the Koçali-Karadut nappes and the Cüngüş-Hakkari Nappe.

The Bitlis-Malatya Nappe is composed of high-grade metamorphic schists and gneisses surrounded by an envelope of low-grade slate, phyllite, marble, and metacherts. Constituting the lowermost unit of the nappes, the Koçali- Karadut system is made up of ophiolite and ophiolite melanges with flysches, pelagic rock suites and clastic sediments that

can be divided into different allochthonous units such as the Koçali Complex, Karadut Complex, Cilo limestones and Hatay ophiolites (Varol et al., 2011). In the Cüngüs-Hakkari Nappes, the Cüngüş is the lower structural unit composed of thin-medium-thick bedded, green, gray, greenish gray, yellowish gray sandstones, siltstones and marl (Pirençek, 1990; Yilmaz and Duran, 1997) with local conglomerates and thin limestone intercalations. The Hakkari formation is the upper structural unit made up of thin-medium-thick, gray, green, greenish gray, reddish sandstones, shale and limestones (Yilmaz and Duran, 1997).

2. METHODOLOGY

All procedures and methods used for this study can be divided into four broad categories which are; fieldwork, laboratory works, analytical methods and procedures and Office works.

2.1. Field Research

The fieldwork began in June 2015 and continued throughout the summer of the same year with intermittent breaks. In January 2016, collection of samples from new drill holes was done as a follow up work for better visualization and understanding of the ore behaviour.

2.1.1. Collection of Field Maps

A generalized geological map produced by Miryildiz Mining Company to map out the lithological units and to produce lithostratigraphical view using drillhole data was obtained prior to the fieldwork. This map was used as a basis for mapping and all units shown on the map were visited in an attempt to check their lithological boundaries. The detailed mine map also produced by Miryildiz Mining Company in May 2015 was used as a guidance for the preparation of 1:2000-scaled geological map of the mining area. Both maps were finalised also by comparing them with maps obtained from the General Directorate of Mineral Research and Exploration (MTA) of Turkey.

2.1.2. Sample Collection

For the purpose of petrographic studies of the wall rocks occurring in the mining area, sixty (60) thin sections (35 for volcanics and 25 for sedimentary) were prepared in the thin section preparation laboratory of the Geology Department at the Karadeniz Technical University. Twenty two (22) samples were collected from three different cores of diamond core drill holes drilled by Miryildiz Mining Company, with additional hand samples from the underground galleries to study the petrography and petrochemistry of lithological units.

2.2. Laboratory Works

2.2.1. Sample Preparations for Sections

In total, 124 samples were prepared for petrographic, mineral paragenetic and fluid inclusions studies. Thin sections preparation were carried out in the thin section preparation laboratory of the Geology Department at Karadeniz Technical University. The selected rock samples for thin sections were first cut into 10mm thick slices with a rock saw. Next, the surfaces of the rock slices were polished with abrasives and mounted on thin wet glass surfaces. One side of the glass slides was also polished to enhance mounting process. The surface of the rock slice was cleaned and made perfectly flat and free of grooves and pits. A thin layer of Canada balsam was spread over the surface of the rock slice and the glass slide evaporated to a preferred hardness. Rock slice and glass slide were removed quickly and the balsam coated surfaces were put in contact. The slice and slide were pressed together to remove bubbles and allow the mount to cool. Excess part of the samples were cut away, and the surface polished to a thickness of about 0.03mm.

Polished sections preparations were carried out at the polished section preparation laboratory of the Geology Department in Karadeniz Technical University. For this process, the samples were first cut and trimmed into appropriate sizes to identify and study the textural relationships between different minerals followed by grinding and polishing to obtain a well-polished surface. Grinding was done by using sequential sized diamond plates ranging from 120 mesh to 600 mesh to level and remove all oxidized and weathered materials from the surfaces in 2 to 3 minutes time intervals for each diamond plate mounted on to automated grinding and polishing machine. Polishing was then made using the same machine with different polishing diamond plates of 1200 mesh to 8000 mesh combined with polishing powder abrasives of 0.05μm to 0.03μm sizes. Polished sections were studied in the research laboratory and fluid inclusion laboratory of the Geology Department of Karadeniz Technical University while microprobe analyses were undertaken at the department of Lithospheric Research in the University of Vienna.

Preparation of fluid inclusions sections were made in the same thin section and polished section preparation laboratory. 14 samples were prepared by cutting the samples containing few quartz veins into smaller sizes, grinded to give two opposite flat surfaces and then highly polished at one surface. The surface was made perfectly flat, free of grooves and pits and polished to achieve a very smooth, scratch-free surface. A thin layer of Canada

balsam was spread over the glass slide to cover the area of the polished surface of the rock slice. Rock slice and glass slide were removed quickly and the balsam coated surfaces were put in contact. The slice and slide were pressed together to remove bubbles and allowed the mount to cool and hardened for about 24 hours. After that, excess parts were sawed off and the surface ground to a thickness of about 30μ to 50μ. The same polishing stages were also applied to this new surface.

2.2.2. Sample Preparation for Stable Isotope Analysis

For H, O and S isotopic analyses, 10g each of quartz, magnetite, pyrites and chalcopyrite grains were selected from mineralized zones of drillcore samples and hand samples collected from the underground galleries of the mine area, crushed into smaller pieces and sieved to get desirable sizes at the Karadeniz Technical University Geological Engineering department's sample preparation laboratory. Quartz grains were collected for H and O isotopic analyses, magnetite grains for O isotopic analysis, and pyrites and chalcopyrite grains were collected for S isotopic analysis. Cleaning of magnetite dust particles from the quartz, pyrite and chalcopyrite samples were done at the Mining department of Karadeniz Technical University through a handheld ultrasonic cleaner with alcohol. Samples were washed by pouring them into the alcohol and agitating the combination using the ultrasonic cleaner for about 3 minutes. The samples were washed with clean tap water and left to dry to give clean mineral grains. The purity of mineral separates were checked by XRD measurements carried out at the Physics Department. Mineral separates that contained impurities of other minerals were re-selected to remove any impurities.

2.2.3. Sample Preparation for Chemical Analysis

Twenty-two fresh and altered volcanic and sedimentary rocks were selected and prepared for the chemical analysis. Sixteen of these samples were taken from three different drill holes, three hand sample from underground and three samples from the mine pits. After removing any zones of surficial weathering, these rocks were cut into pieces, crushed and pulverized in a low-chrome steel bowl in the sample preparation laboratory of the Geological Department at Karadeniz Technical University, and sent to ACME lab in Canada for chemical analysis.

2.3. Analytical Methods and Procedures

2.3.1. Chemical Analysis

After rock sampling and sample preparations, altered and least altered samples were sent for chemical analysis, which provided the needed data for geochemical classifications and mass calculations for the hydrothermal alterations. Whole rock samples were analysed for major elements, trace elements and rare earth elements (REE) analysis. All the elements were determined by Inductively Coupled Plasma Emission Spectrometry (ICP-ES) where prepared sample were mixed with $LiBO_2/Li_2B4O_7$ flux. Crucibles were fused in a furnace. The cooled beads were dissolved in ACS grade nitric acid and analyzed by ICP and/or ICP-MS. Loss on ignition (LOI) was determined by igniting a sample split then measuring the weight loss. An additional 14 elements analyses from an aqua regia digestion were carried out to provide Au and volatile elements' data, which do not report as part of the Lithium metaborate/tetraborate fusion method. In this method, prepared samples were digested with a modified Aqua Regia solution of equal parts of concentrated HCl, HNO_3 and DI H_2O for one hour in a heating block or hot water bath. Samples were brought up to volume with dilute HCl. Sample splits of 0.5g were analysed with optional 15g or 30g digestion available.

2.3.2. Microprobe Analysis

Electron microprobe analysis (EPMA) was conducted at the Department of Lithospheric Research of the University of Vienna (Vienna, Austria). Analyses were made with an electron microscope equipped with Cameca SX Five brand 5 wavelength dispersive spectrometers. Instrumental conditions were adjusted to 40° finishing angle using 20 kV bombarding energy, 10nA bombarding current with an approximately 1μ diameter beam. All samples used in EPMA analysis were carbon coated with Cressigton brand carbon coating device. Natural and synthetic minerals and elements were used as calibration standards in the measurements of all minerals.

2.3.3. Stable Isotope Analysis

The S isotope samples were analysed at the Department of Earth and Planetary Sciences and Centre for Stable Isotopes in New Mexica, USA. Sulphur isotope measurements ($d^{34}S$) were conducted by Continuous Flow Isotope Ratio Mass Spectrometry

using a Costech Elemental Analyser coupled to a Thermo-Fisher Scientific Delta V Plus Advantage mass spectrometer via a Conflo IV interface. The $BaSO_4$ (0.2 - 0.3 mg) was combusted in a quartz tube packed with ultra-high purity copper wires and quartz chips (Fry et al., 2002) at 1020ºC in the presence of pure O_2 gas. The resulting SO_2 gas was then passed through a GC column and measured in the mass spectrometer. International standards (IAEA S-1, NBS123 and NBS127) and two laboratory standards (CP1 and CP2), covering a range of $\delta^{34}S$ values from –22.6‰ to 20.3‰, were run at the beginning, at intervals between samples and at the end of analytical sessions. Analytical precision calculated from the standards was ± 0.2 ‰ (1s standard deviation). Analyses were normalized to the standards listed above.

The $\delta^{18}O$ ratio and $\delta^{2}H$ were analysed at Queens University in Australia. For the Oxygen (silicates): Oxygen was extracted from 5 mg samples at 550-600°C according to the conventional BrF_5 procedure of Clayton and Mayeda (1963) and analyzed via dual inlet on a Thermo-Finnigan DeltaPlus XP Isotope-Ratio Mass Spectrometer (IRMS). $\delta^{18}O$ values are reported using the delta (δ) notation in units of permil (‰) relative to Vienna Standard Mean Ocean Water (VSMOW) international standard, with a precision of 0.1‰.

For the Hydrogen: Samples were weighed into silver capsules, degassed for 1 hour at 100°C then crushed and loaded into a zero-blank auto sampler. The hydrogen isotopic composition was measured using a Thermo-Finnigan thermo-combustion elemental analyzer (TC/EA) coupled to a Thermo-Finnigan DeltaPlus XP Continuous-Flow Isotope-Ratio Mass Spectrometer (CF-IRMS). $\delta^{2}H$ values are reported using delta (δ) notation in permil (‰), relative to Vienna Standard Mean Ocean Water (VSMOW), with a precision of 3‰.

3. GEOLOGICAL SETTING

Miryildiz Mining Company has a licenced area of 3,695,900 m^2 covering south of Ortaklar village with a pictorial view shown in figure 3.1. Wilson and Krummenercher, (1957), Rigo de Reghi and Cortesini, (1964), Sungurlu (1972, 1974), Güvench, (1963), Tuna, (1973) , Perinçek, (1979), Yoldemir (1987, 1988), Terlemez et al., (1992), Ulu et al., (1991), Yılmaz (1990, 1993), Yılmaz and Yıldırım, (1991), Yılmaz, (1993), Yiğitbaş and Yılmaz (1996), Robertson et al., (2006, 2007), Yidirim , et al., (2010) and Varol et al.(2011) undertook extensive regional geological and structural studies of the Adiyaman region which provided an inferential knowledge and also played a very important role in the geological modelling and understanding of the mineralization of the study area. Yildirim et al, (2016) provided detailed geological and geochemical studies (covering the ore and the wall rocks) and provided detailed ore paragenesis after mineralogical and isotopical studies.

Figure 3.1. Overview of the study area with the mine site

The Koçali Complex in the Kocali-Karadut Nappes is characterized by the presence of tectonically imbricated (overlapping) slices of pelagic rock suits (pelagic limestones, cherts etc), platform carbonates, clastics, serpentinites and basic volcanics (Sungurlu, 1973; Ricou and Marcoux, 1980; Bernoulli et al., 1990). The different rock units within this complex are described as a remnant of Southern Tethyan seaway (Kazmin et al., 1986; Bernoulli et al., 1990) or Southern Neotethys. Sungurlu (1973) subdivided the complex into three lithological associations: ultrabasics, volcanics, and sedimentary units. In the Adıyaman region, this complex was subdivided into the Tarasa, Konak, and Kale Formations by Perincek (1978; 1979a; 1979b).

The Tarasa Formation, corresponding to the volcanic unit of Sungurlu (1973), is composed of basalts, spilitic basalts, and diabase with a total thickness of 400-1000 m. The Konak Formation, up to 1800m thick, comprises limestones, radiolarites, volcanic rocks and silicified shales, and corresponds to the sedimentary units of Sungurlu (1973). Moreover, the Kale Formation, the uppermost tectonic unit of the Koçali Complex, corresponds to the ultrabasics of Sungurlu (1973) and includes serpentinites, diorites, diabases, and gabbros. According to Sungurlu (1973), the complex is aged as Upper Jurrasic-Lower Cretaceous. The Koçali Unit is trusted over by the Karadut Unit. Varol et al., (2011) redefined the Tarasa Formation as Tarasa unit, the Konak formation as the Konak unit and the Kale Formation as the Kale ophiolites.

3.1. Lithological Units

According to Yildirim et al. (2016), the study area is made up of serpentinized harzburgites, layered cumulates, isotropic gabbros, sheeted dykes, spilitic basalts, pillow basalts, mudstones, radiolarites and metalliferous sediments. The rocks can be described as tectonic slices and their lithostratigraphy cannot easily be followed due to high weathering and alteration, irregular alternation of the rock units and complex structural history. The northern part of the area consists of an ophiolite nappe made up of serpentinites overthrusting the Koçali melange zone composed of basic igneous rocks and sedimentary units (Fig. 3.2 and 3.3). The central portion of the area contains mostly basaltic volcanic rocks and a complex weathered unit made up of volcanic blocks with a sedimentary matrix.

Drill core and underground samples taken during this study provided the best samples for microscopic examinations and chemical analysis of the ultramafic and volcanic rocks as their equivalents collected on the surface were more weathered.

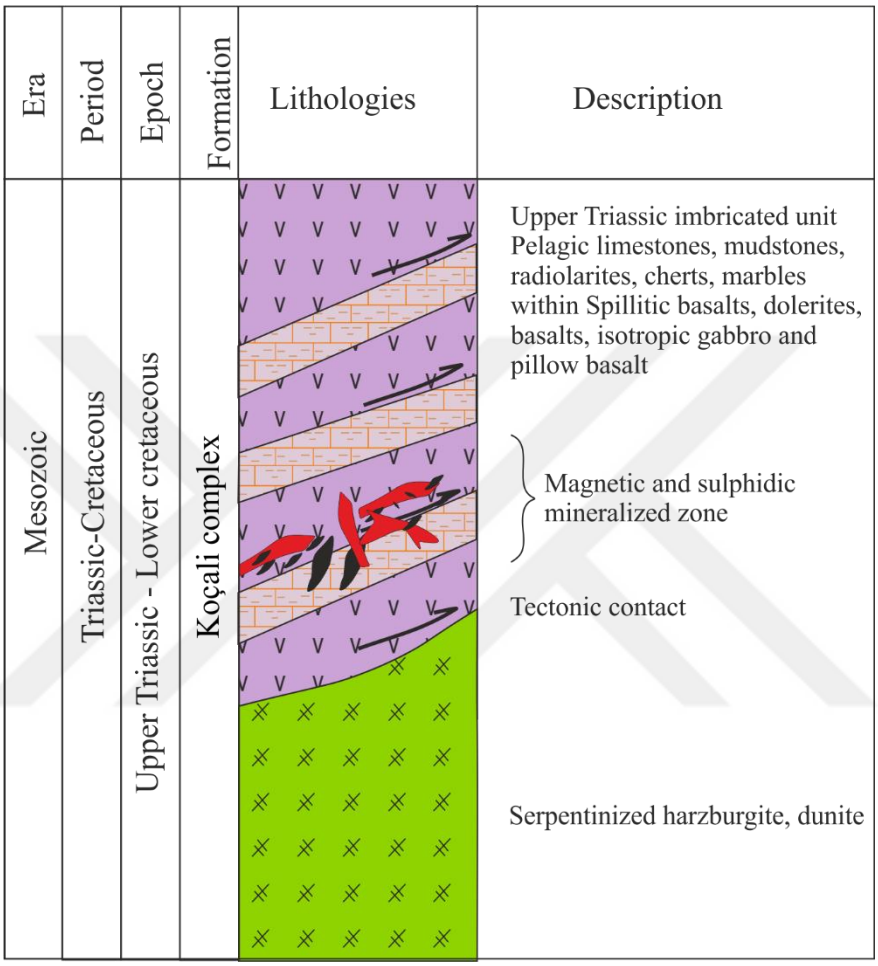

Figure 3.2. Stratigraphy of the study area.

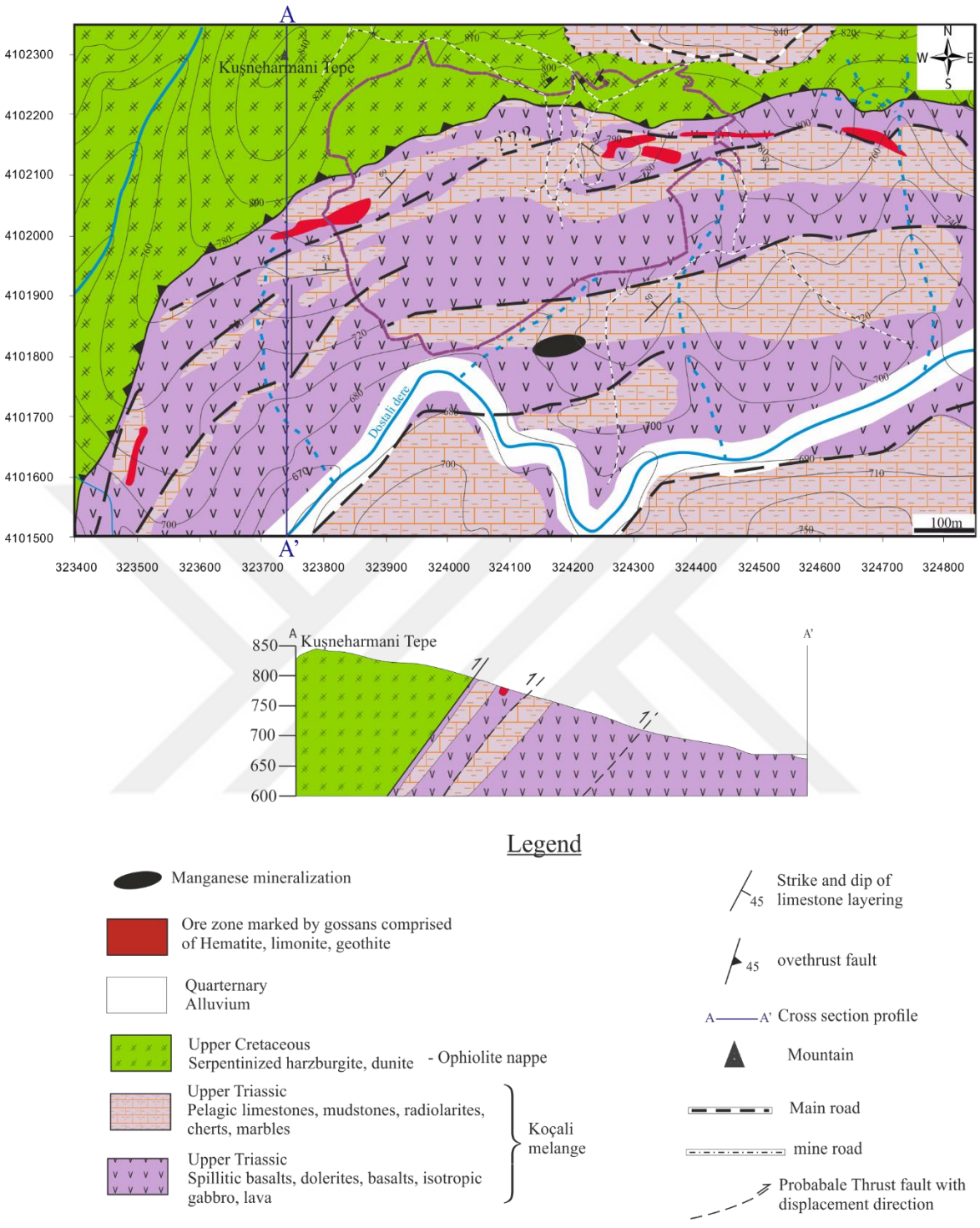

Figure 3.3. Geology of the Ortaklar Deposit with location of active mine site and geological cross section from north to south. Modified from (Bahçeci et al., 1984)

Serpentinized harburgite and dunites occupying approximately one-third of the study area lying over the other units with an overthrust contact are green coloured, massive and weathered with abundant joints probably caused by the overthrusting. Their exposed surfaces are dark green coloured having resinous lustre. The serpentinized harburgite exposed in the western pit are fine grained with soapy feel while the ones in the central portion of the mine area are coarse grained and tends to become finer towards the east. Under the microscope, they have porphyritic texture with highly altered (serpentinized) pyroxene porphyroblasts embedded in a highly altered serpentinized fine matrix.

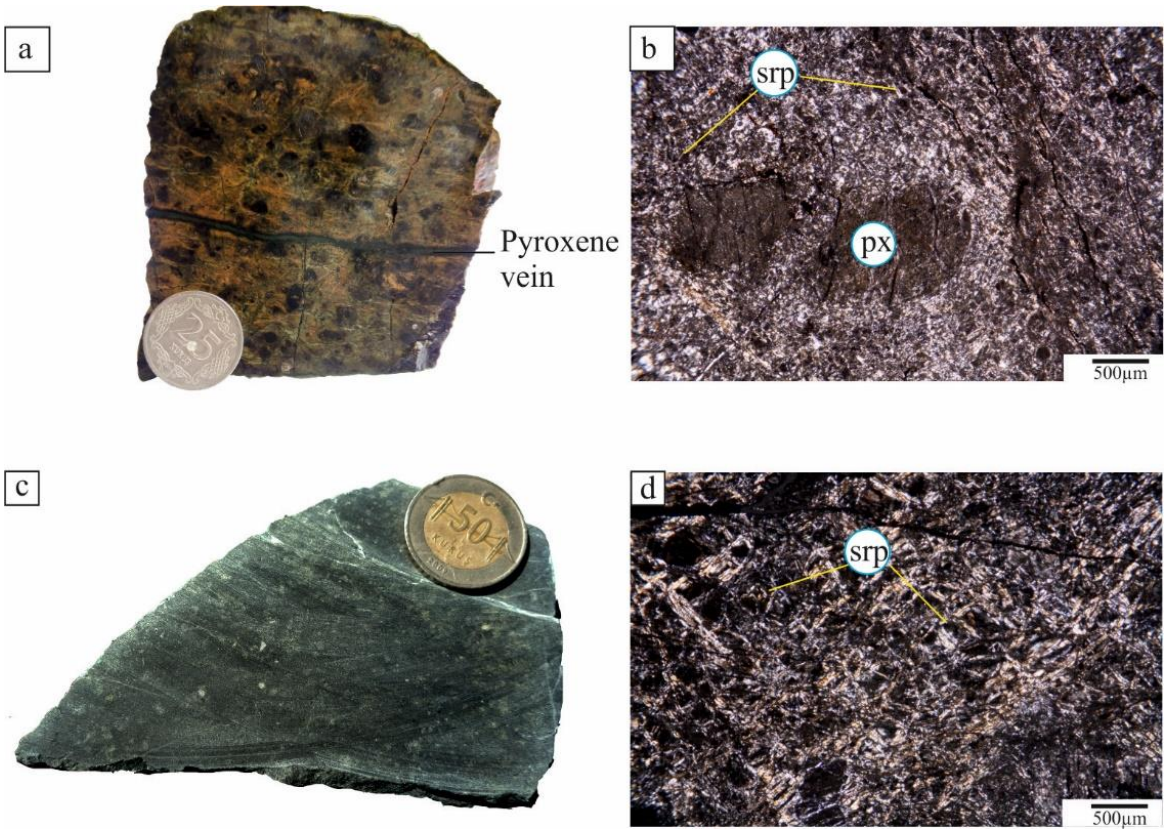

Figure 3.4. Hand specimen and microscopic view of the lithologies in ophiolite nappe in the Ortaklar Deposit. a) hand specimen of serpentinized harzburgite with a pyroxene vein, b) microscopic view of serpentinized harzburgite, c) hand specimen of serpentinite, and d) microscopic view of serpentinite. (Px: Pyroxene Srp: Serpentine)

The igneous components of the Ortaklar's Koçali complex made up of isotropic gabbro, dolerites, pillow lavas, basalts and spillitic basalts occur in the central and southern portion of the study area. Some are mixed with the sedimentary units in the eastern and western pit (Fig. 3.10). Pillow lavas are in the form of rounded blocks found underlying the

serpentinite units in the western pit according to the chief geologist because at the time of fieldwork, it was not safe to visit that area. They are massive, round blocks of volcanic materials with very fine-grained textures. Hand and drill core samples of the isotropic gabbros are massive, green coloured and fine textured but, under the microscope, they are made up of euhedrally formed grains of plagioclase, pyroxenes and opaque minerals exhibiting ophitic texture characterised by euhedral plagioclase surrounded by pyroxenes as shown in figure 3.5. The plagioclases exhibit both carlsbad and albite twins though the albite twins are faded due to hydrothermal alteration.

Hand samples of the dolerites have fined grained texture but under the microscope, they show ophitic texture containing plagioclase, pyroxene and opaque minerals with chlorites as an alteration product of the plagioclase found both as a matrix material and as subhedral porphyroblasts.

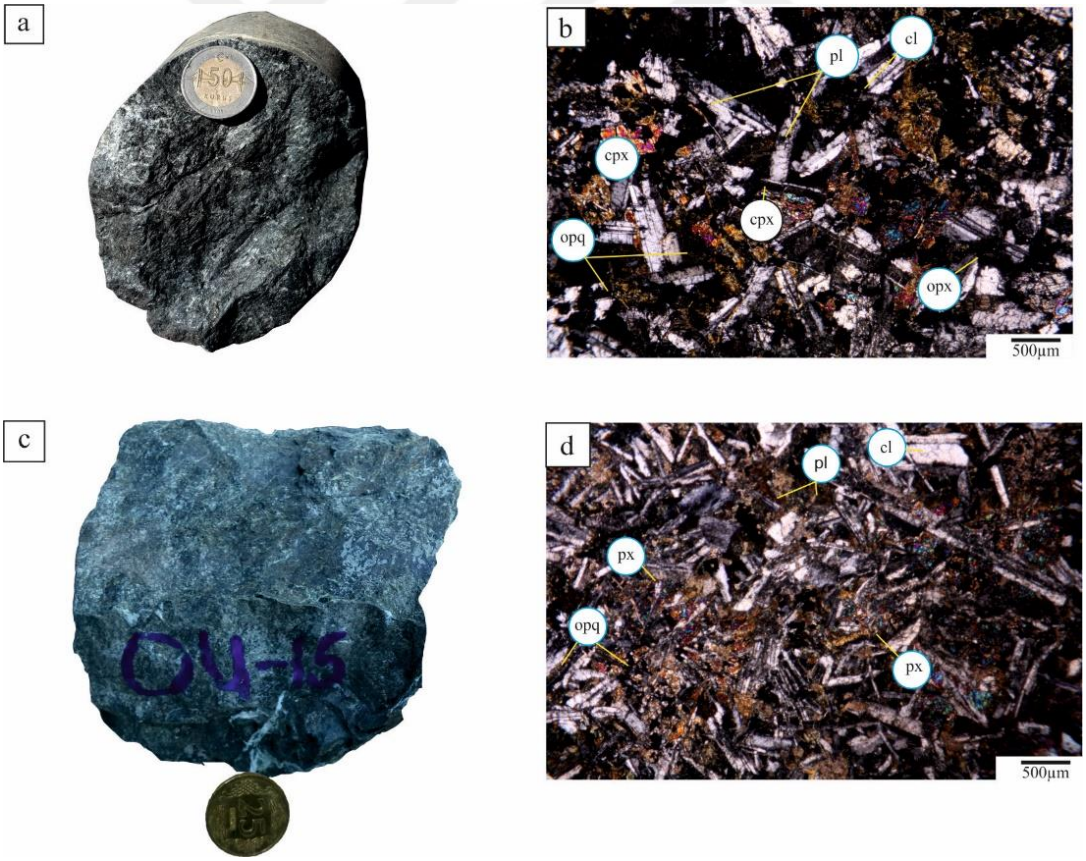

Figure 3.5. Hand specimen and microscopic view of basic igneous rocks of Koçali complex from the Ortaklar Deposit. a) hand specimen of the isotropic gabbro, b) microscopic view of the isotropic gabbro, c) hand specimen of the dolerite and d) microscopic view of the dolerite. (cl: Clay, cpx: Clinopyroxene, opx: Orthopyroxene, pl: plagioclase, opq: opaque)

The spillitic basalts occur in contact with the ore at certain locations. They are green looking fine-grained rocks with crosscutting calcite veins. Under the microscope, these rocks contain mostly plagioclase, few orthopyroxenes and clay minerals showing sub-ophitic texture (Fig 3.6b). The plagioclase are subhedral with albite twinning (labradorite) and some exhibiting oscillatory zoning. The spillitic basalts are hydrothermally altered with the olivine and pyroxenes converted into chlorites, smectites and iron oxides. Best samples of the basalts were found in the drill cores. They were exposed in the eastern, central and western parts of the study area. They are highly weathered in the pits and in the easternmost part of the study area, and occur as mixed up with the sedimentary units at certain areas. Under the microscope, these are fine-grained rocks with plagioclase laths, pyroxenes and clay minerals (Fig 3.6d).

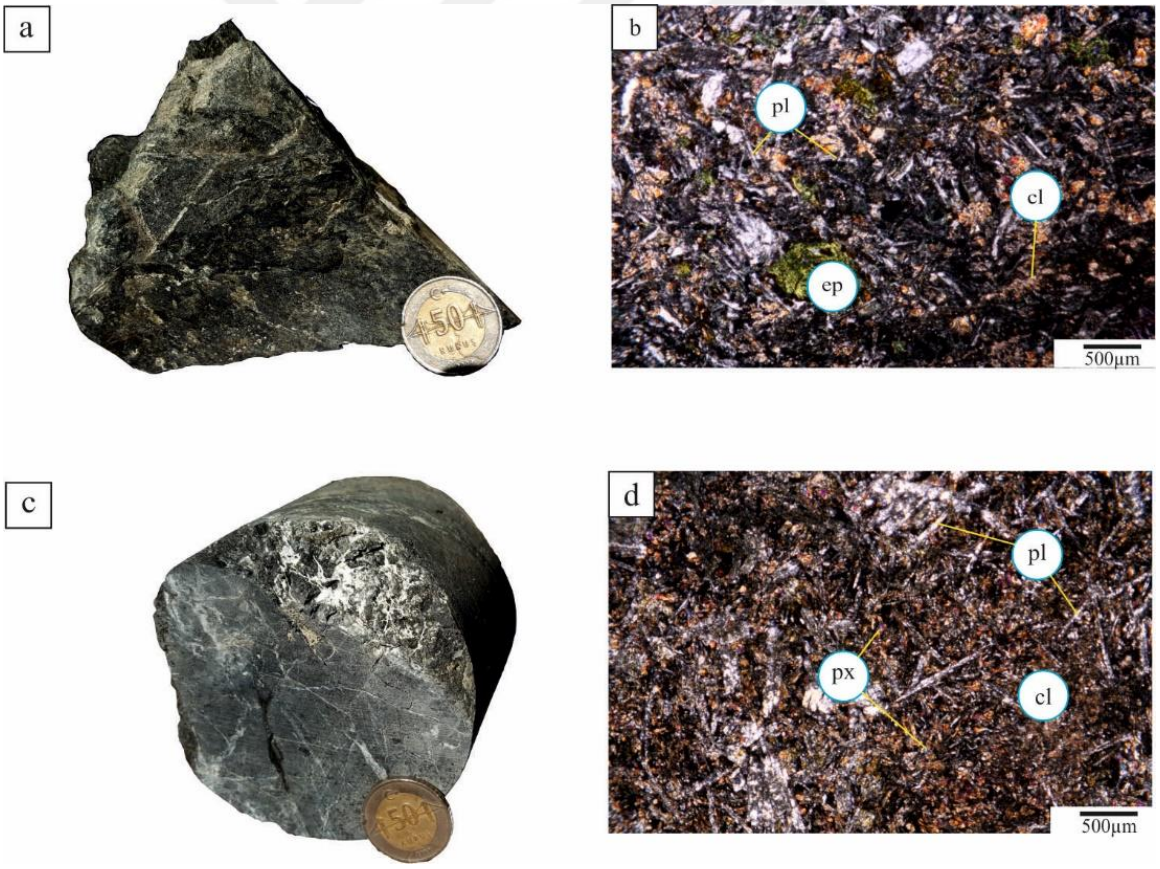

Figure 3.6. Hand Specimen and Microscopic view of basic igneous rocks of Koçali complex found within the Ortaklar Deposit. a) Hand specimen of the spillitic basalt b) microscopic view of the spillitic basalt, c) hand specimen of the basalt d) microscopic view of the basalt. (cl: Clay, ep: epidote, pl: Plagioclase, px: pyroxene)

Sedimentary units occurring in the study area are made up mostly of pelagic limestone, marbles, mudstones, radiolarites and cherts. The pelagic limestones, marbles and mudstones are found within the imbricated zone outcropping in contact with the volcanics. The pelagic limestone is composed of mass of calcareous tests of pelagic foraminifera while the mudstones are composed of mass of clays under the microscope as shown in figure 3.7. The massive ore is sometimes in direct association with the cherts and in other locations with mudstones-radiolarites. The sedimentary units occurring in the study area strike in the east-west direction overlying and sometimes intercalating with the volcanic rocks at the southern portion of the study area. Metalliferous sediments outcrop in the central and the eastern part of the study area. The limestones are usually stratified with thickness of the beds ranging from 2 cm to 20 cm. At some locations, the limestones are crystallized and/or silicified. The mudstones outcropping in the eastern, central and western portions of the area are fine-grained, massive textured at the surface with crosscutting calcite veins, and are soft and highly friable underground where they occur in contact with the ore. Usually in contact with the massive ore in drillcore samples, the cherts are usually very hard and reddish in colour and include micro-layering and micro-faults infilled with calcite and quartz veins.

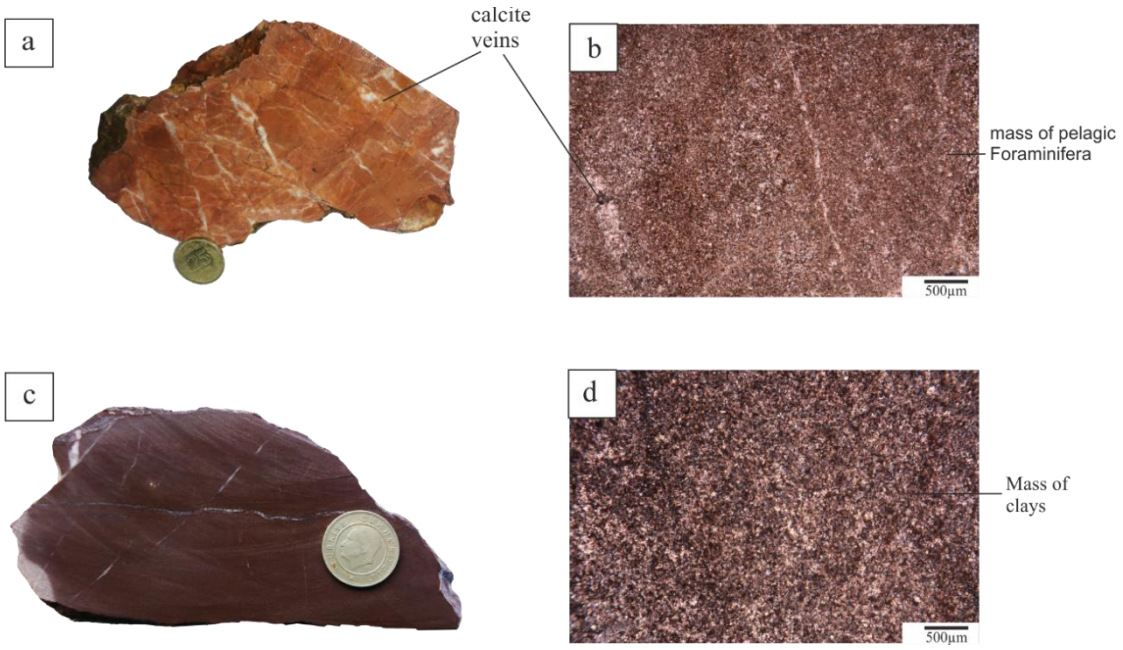

Figure 3.7. Hand specimen and microscopic view sedimentary rocks of Koçali complex found at Ortaklar Deposit. a) Hand specimen of pelagic limestone b) microscopic view of pelagic limestone c) hand specimen of mudstone d) microscopic view of the mudstone.

3.2. Lithogeochemistry

The whole rock and trace element chemical data obtained from the laboratory are given in the appendices. All the analysed rocks have basaltic composition with most of them plotting in the basalt field and some in the picrobasalt and tephritic basanite fields in the SiO_2 vs alkali diagram of Le Maître et al, (1989) as shown in figure 3.8a. It also indicates that the samples have a variable composition around subalkaline and alkaline dividing line of Le Maître et al, (1989). These scatters are due to intense effects of hydrothermal alteration and are artefacts of mobility of Si, Na and K. In figure 3.8a, two samples plotted out of the boundary due to reduction in Nb or increase in Y contents as a result of hydrothermal alteration converting the plagioclase, olivine and pyroxenes into clay minerals and other accessory phases. Yet, this shift in the chemistry of the basalts does not cause any change in their geochemical affinities as shown in fig 3.8b. La vs Yb diagram of Barrett and MacLean (1999) manifests that all of basaltic rocks from the immediate vicinity of the Ortaklar Deposit ore deposit have similar geochemical affinities and are all tholeiitic (Fig. 3.8b).

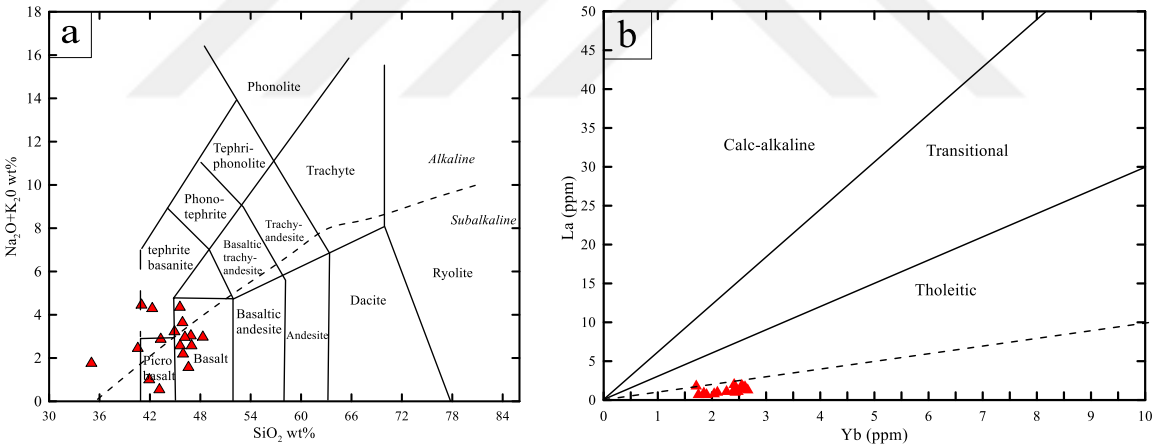

Figure 3.8. Magmatic discrimination diagrams of b.asic rocks from the Ortaklar Deposit. a) TAS diagram (Le Maitre et al, 1989), b) La vs Yb (Barrett and MacLean, 1999)

Trace element composition of basic igneous rocks is rather consistent and produce overall parallel patterns. N-MORB normalised plots using the normalising values of Sun and Mc Donough , (1989) show variable LIL element profiles deviating from the flat profile of N-MORB. This variability, especially in K and Rb data, shows that these rocks are affected by hydrothermal alteration, which may have changed the chemistry of feldspars. The HFS elements, though generally thought to be immobile, show slight variation from the straight line of the N-MORB with the entire element except P and Ti showing slightly

decreased levels. The most characteristic feature of this diagram is the strongly negative Nb anomaly; this "negative Nb anomaly" is unlikely to result from differential alteration because Nb is widely believed to be immobile under prevailing seafloor conditions (Pearce, 1982, 1983). Also volcanic rocks related to contemporaneous subduction (example volcanic arc basalts) typically exhibit a well-defined negative Nb anomaly, as seen in modern lavas erupted above subduction zones (Pearce, 1982). However, the Nb anomaly exhibited by the Ortaklar volcanic rocks might be attributed to Nb retained in rutile as a result of a small degree of melting of peridotite.

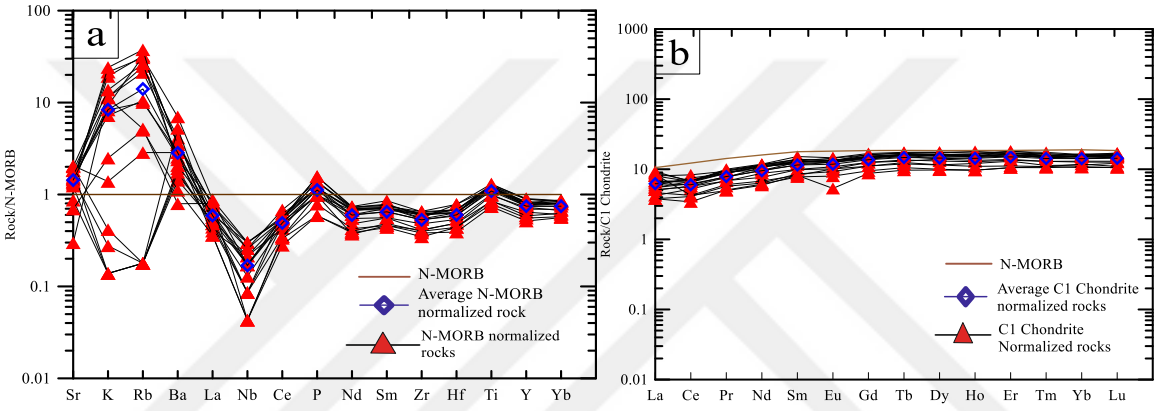

Figure 3.9. Spider diagrams of basic igneous rocks from the Ortaklar Deposit. a) N-MORB normalized multi-element diagram drawn based on N-MORB composition from Sun and McDonough (1989). b) C1 chondrite normalized REE diagram (drawn using normalising data of Sun and McDonough, 1995).

Like the HFS elements in the N-MORB-normalised multi-element diagram of Sun and McDonough (1989), C1 chondrite-normalised REE patterns are also similar to N-MORB values. The REE patterns of all analysed basalts are almost identical and have nearly flat trends with light REE being slightly more reduced than middle and heavy REE compared to N-MORB values. The flat pattern is also reflected in the Eu values, as most samples do not show any Eu anomaly. There is only one sample (S56.17) displaying slightly negative Eu anomaly (Fig. 3.9b), indicating plagioclase depletion in the sample (Rollinson, 1993)

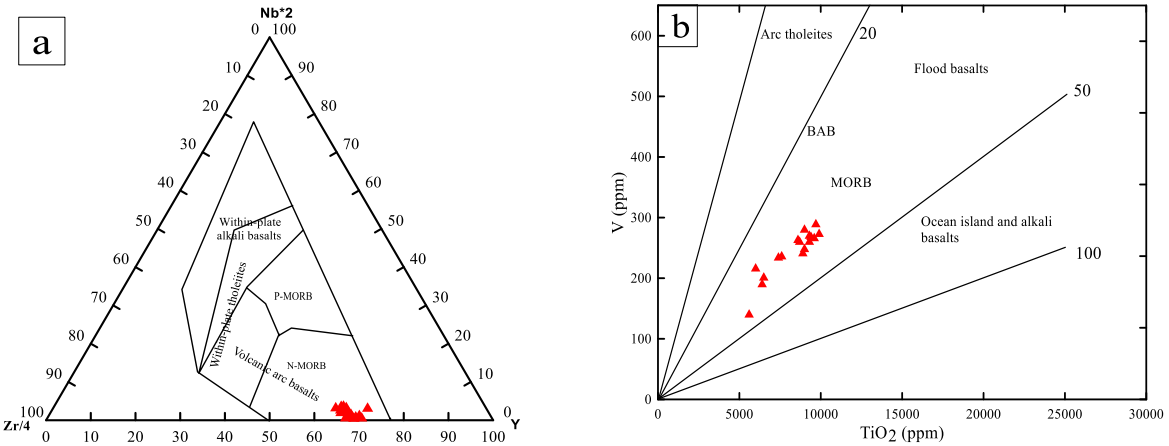

Figure 3.10. Tectonomagmatic discrimination diagrams of basic igneous rocks from th Ortaklar Deposit, a. Zr/4, Nb*2, Y ternary diagram (Meschede, 1986) b. Ti vs V diagram (Shervais, 1982)

The tectono-magmatic discrimination diagrams (Fig 3.10) of the basic igneous rocks from the Ortaklar Deposit show a Mid Ocean Ridge Basalt (MORB) affinity with figure 3.10a plotting directly in the N-MORB region. Another diagram to be used to understand the source region of the magma producing the basalts is the TiO_2 vs V plot of Shervais, (1982) (Fig 3.10b), which clearly supports the MORB affinity of the basalts. The basis of this diagram is the variation in the crystal/liquid partition coefficient for vanadium which ranges with increasing oxygen fugacity from >1 to <<1. Since Ti is always incompatible, the depletion of V relative to Ti is a function fO_2 of the magma and its source, the degree of partial melting and subsequent fractional crystallization (Shervais, 1982).

Using the immobile element Nb, Meschede (1986) suggested that different types of ocean floor basalts could be separated. With that, two different MORB, which are normal MORB or N-MORB, and the enriched MORB also known as E-MORB were recognized. The basic igneous rocks from the Otaklar deposit plotted in the N-MORB region on the Zr/4, Nb*2 and Y ternary diagram of Meschede (1986). Although these rocks have negative N-MORB normalized Nb anomaly, the HFS elements behavioural pattern strongly correlate with that of N-MORB.

3.3. Structural Geology

3.3.1. Bedding

Bedding planes and limestone stratifications are well exposed in the open pits in the Ortaklar Deposit. Generally, the ultramafics and volcanics lie over the sedimentary units towards south. The lithological boundary planes have strike values ranging from 200^0 to 270^0 and dips of 40^0-80^0 to the north and north-western mostly parallel to the overthrust planes of the ultramafics. The sedimentary units are stratified with each strata (bed) ranging in width from about 2 cm to 20 cm. The layers strike 270^0 in the E-W direction in the Eastern portion and the sedimentary rocks in the western portion have strikes of 200^0 to 260^0 with dips ranging from 50^0 to 60^0 in the north-western direction.

3.3.2. Tectonic Structures

Thrust faulting of the ophiolite nappes over the volcanic and sedimentary units occur across the study area with the fault dipping in the northern direction. Complex rock units are well exposed in both the eastern and western pits (Fig 3.11). The rock units found within the eastern and south-eastern parts of the area are highly altered and highly friable. In the drill logs, it can be easily ascertained that the rock units in the eastern part of the study area are highly tectonized and fragmented with complex signatures.

Folding can be inferred from measurements taken from the limestone units exposed in and around the Ortaklar Deposit. The limestone units in the western part of the study area have an average strike of 060^0 with an average dip of 69^0; those exposed in the central area have an average strike of 285^0 and dip of 50^0. The exposed stratified limestones found in the eastern area have an average strike of 090^0 with an average dip of 45^0.

The serpentinites in the study area are haphazardly jointed as shown in figure 3.12. There are three major sets of joints occurring in the serpentinites found in the northern area with recurring shearing indicating a highly deformational history associated within this unit. The first set of joints have an average strike of 200^o and a dip of 46^o; the second sets of joint have an average strike of 320^0 with a dip of 74^o; and the last set of joints have an average strike 025^o with a dip of 56^o. Haphazard jointing also occur within the sedimentary units with the volcanic units undergoing rather shearing episodes. Most shear zones occur within the serpentinized and volcanic units.

Figure 3.11. The field-view of the Koçali complex made up of volcanics and sedimentary rocks found in the eastern part of the study area.

Figure 3.12. A field-view of the jointed serpentinites in the study area

3.3.3. Mineral Veins

In addition, mineral veins are easily seen within the serpentinized rocks mostly made up of altered pyroxenes and carbonates. Within the volcano-sedimentary units magnesites veins with length of 1cm to 15cm crosscut this formation (Fig 3.13).

Figure 3.13. A field view of the magnesite vein in the study area.

4. ORE GEOLOGY

The licenced mine area occupies an area of 369.59 hectares situated at the south of the Ortaklar village, 32 km to the west of Gaziantep. The mine site lies within the Upper Triassic- Upper cretaceous Koçali complex bounded by serpentinites in the north and the imbricated volcano-sedimentary units composed of basaltic rocks, pelagic limestones, mudstones as tectonic slices in the south (Fig 3.3). Major mine activity occurs within the volcano-sedimentary units. The ore zones in the Ortaklar Deposit have undergone deformation and dislocation simultaneously with the host strata during obduction episodes. Positive topographic features (mounds) are the characteristics of most ophiolite hosted VMS deposits reflecting strong fault control on hydrothermal upflow. Distinctive mounds' absence in certain parts of the mineralized zone may be due to post volcanic fault truncation or as a function of their original deposition environment (Galley and Koski, 1999). Miryildiz mining company provides operational underground mines divided into eastern and western galleries created after the open pits ore were extracted. The mining activity mostly occurs along and across the NE-SW striking and the northerly dipping fault zone.

4.1. Localization and Visualization of the Ore Zone

The ore lenses in the Ortklar deposit are highly dismembered and are characterized by massive pyrite and marcasite, massive chalcopyrite, massive magnetite, brecciated magnetite + chalcopyrite + pyrite, stockwork and disseminated pyrite + chalcopyrite + sphalerite +magnetite as major ore phases with chlorite + carbonates + quartz as major gangue phases. Carbonate veins commonly occur within the volcano-sedimentary units. Striking mostly concordant to a long NE-SW trending thrust fault and the wall rocks with a dip of 60^{o}, the ore zone occurs within the tectonic slices of mudstones, radiolarites, spilitic basalts and pillow lavas as lenses or tabular bodies having a thickness of 10 to 100 meters and a total strike length of about 1 kilometre.

The ore zone covers an area of about 1 km along the NE-SW thrust fault occurring in the middle of the study area (Fig. 3.3), with the ore lenses clustering along a paleohorizontal direction (Fig 4.1). They are characterised and marked by zones of oxidation of different sizes composed of limonite, hematite and goethite. Azurites and malachite are also found occurring around the gossan zones. As shown in the two dimensional (X-Y and X-Z

coordinates) views of the mine site produced using GEOVIA Surpac (Fig. 4.1a and Fig. 4.1b), the drill holes are perpendicular to the ore zone with varying dip and azimuth. Despite the fact that the ore zones at the Ortaklar Deposit are mostly massive, they are usually discontinuous both vertically and horizontally. The topography of the mineralized zones is marked by mounds covered by gossans and vegetation. The lateral length of the individual lenses ranges from 30 m to as far as 400 m.

The x, z view (Fig. 4.1a and b) shows the cross sectional view of the mineralized area as at June 2015 with some of the drillholes cutting through the ore lenses. The deepest drillhole extends about 400 m cutting through alternating ore lenses separated by volcano-sedimentary strata. The ore lenses follow a linear trend dipping in a north and northeasten direction.

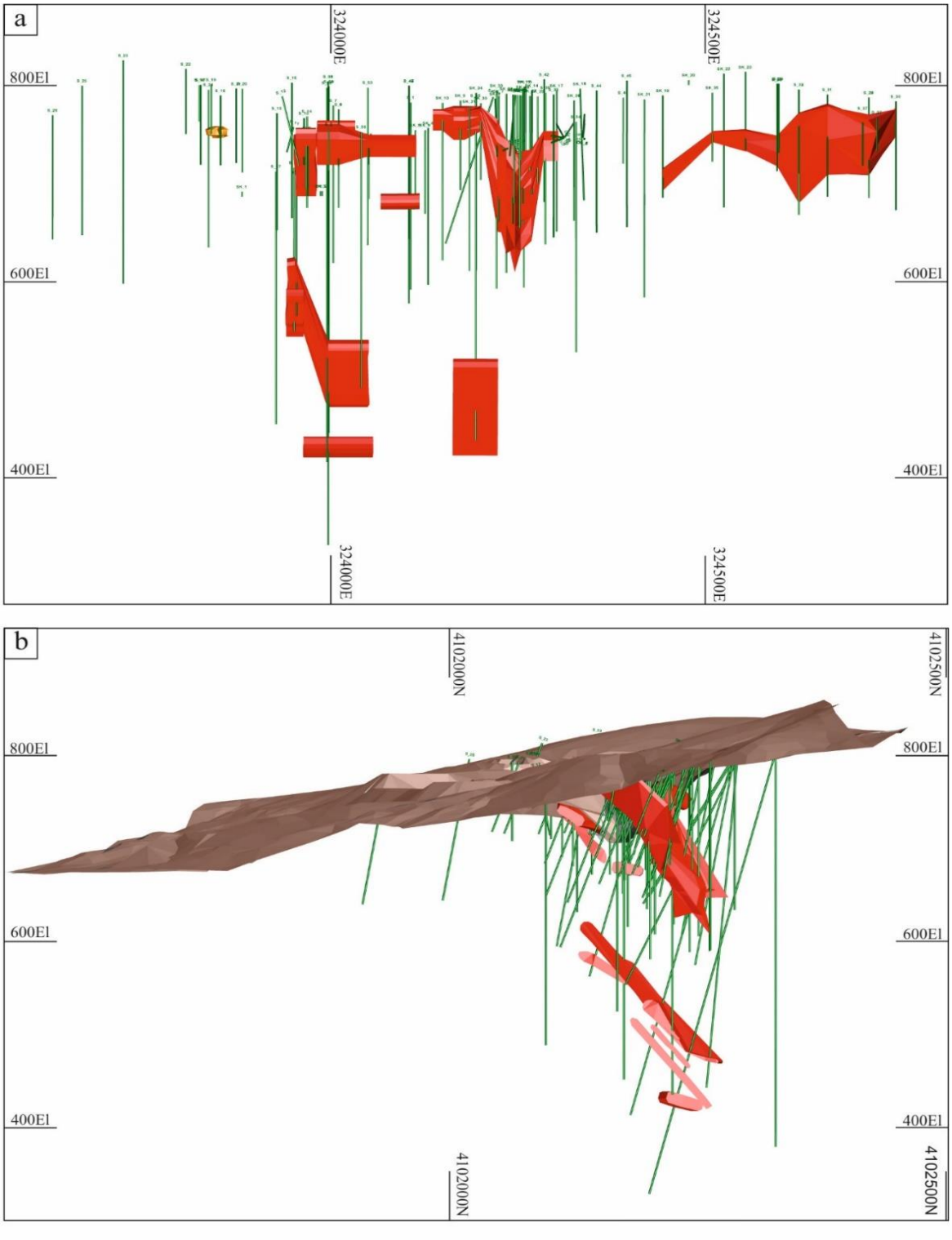

Figure 4.1. GEOVIA Surpac sections of the Ortaklar Deposit showing cross sectional views of the deposit together with drill holes (a) and the location of the ore lenses with respect to the surface (b).

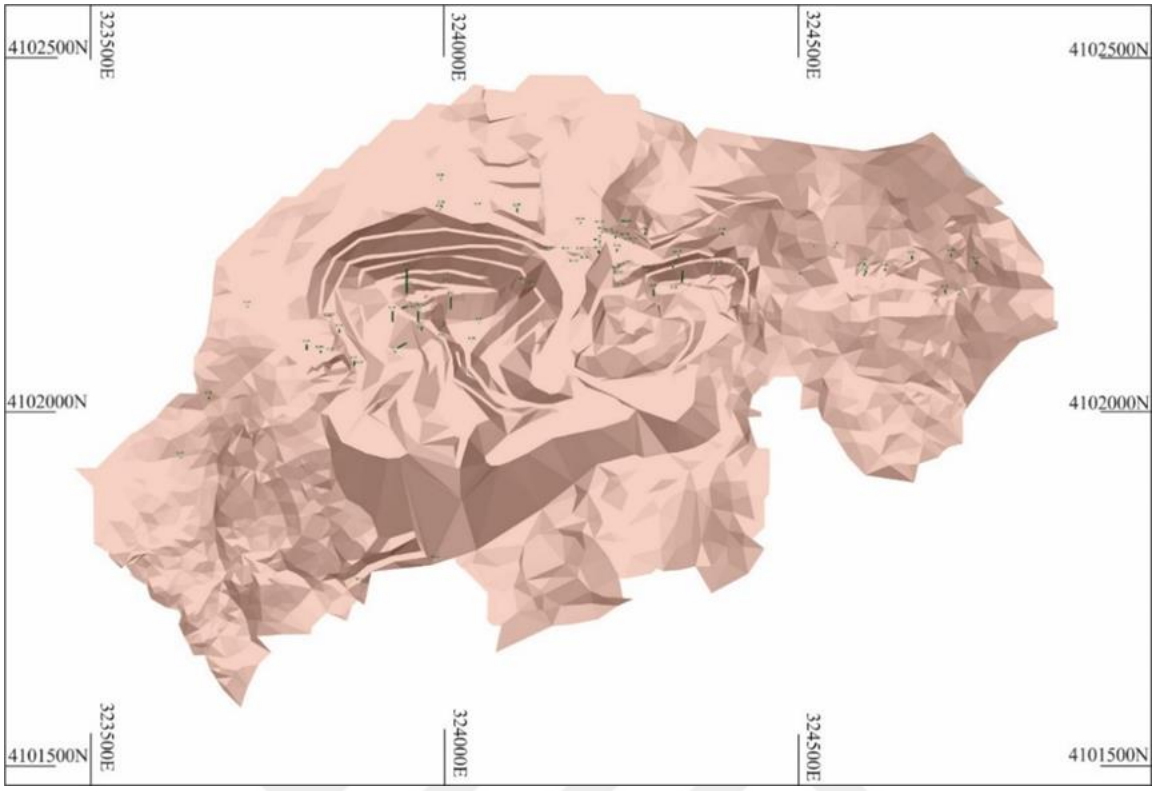

Figure 4.2. Generalised view of the Ortaklar Deposit, the location and direction of drillholes produced using GEOVIA surpac software.

The ore are in the form of lenses and shows textural variations both laterally and vertically. The megascopic examination of the ore in the field, both in the pit and underground, and the investigation of drill logs produced through detailed petrographic examinations of the rock samples collected along drill holes indicate that the ore zones are characterized by changes in their textural and mineralogical features (Fig 4.3). Diamond drill hole S52 was determined to be the best representative drill hole showing the vertical changes of the ore at the Ortaklar Deposit. The vertical ore zones within this hole are characterised by tectonic breakages and changes in lithologies along its entire continuity. Ore layers in the upper part of the hole are bounded by limestone, the middle zone ores by both limestone and volcanic units, and lower zone ores by only volcanic units. This, however, does not indicate a lithological control on the occurrence of the mineralisation since, volcano-sedimentary units and basic igneous rocks are totally mixed up as a result of thrusting. In fact, the thickest ore lens is found in the middle zone of the mineralised area (Fig. 4.3), where the ore lens is overlain by the sedimentary unit made up of cherts and pelagic limestone. The ore lens is also underlain by basalt, which is the main host rock as expected in VMS deposits formed in ophiolites.

The Ortaklar mineralized area are highly tectonised, dismembered and inconsistent in the textural properties of the ore lens. Detailed drill log of hole S52 which was the deepest mineralized drillhole at the time of conducting this study is summarised in figure 4.3 and the detailed description is as follows;

The upper mineralized zones contain slightly oriented brecciated sulphides hosted by sulphide matrix bounded by cherts and limestone. The breccias have lenslike/elipsoidal shapes with similar sizes (Fig 4.3) followed by a thick zone of sedimentary unit. At the middle mineralized zone, large brecciated magnetite with brecciated spheroidal sulphides are hosted by sulphide matrix. This is followed by large brecciated sulphides with ellipsoidal, spheroidal and semi spheroidal shapes which are hosted by sulphides and magnetite matrix. Brecciated massive sulphides further underlie this zone. Large brecciated magnetite reoccurs at a depth of 278.40m to 278.50m in addition to brecciated sulphides hosted by sulphide matrix. The lower mineralized zones are highly dismembered and characterised by melange of ultramafic materials, basalts, limestone and thin ore lens. Calcite signatures begin to be seen in addition to brecciated sulphides and magnetite at deeper levels. The calcite becomes prominent at a depth of 286.7 m to 310.70 m and the ore finally changes to massive magnetites with sulphide stockwork veins (Fig 4.3).

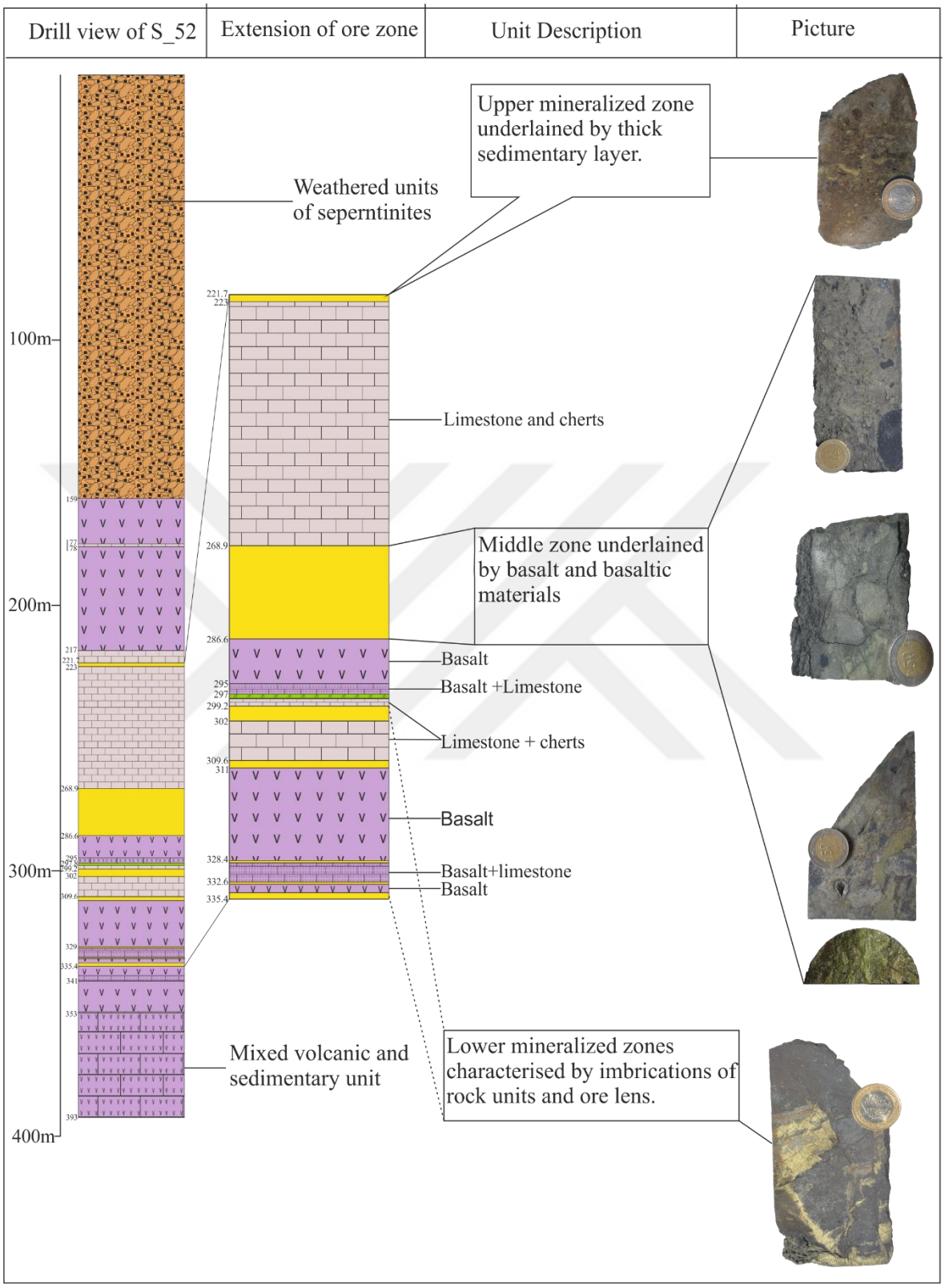

Figure 4.3. Vertical textural changes associated with the ore obtained from drill-hole number S52.

4.2. Types of Ore

The Ortaklar Deposit is made up of different type of ores with different textural characteristics. The observed ore types are:

I. Massive Ore
   -Massive sulphides
   -Massive magnetite
   -Massive sulphide-oxides
II. Stockwork-disseminated ore
III. Stockwork- veinleted ore
IV. Brecciated Ore

4.2.1. Massive Ore

Commonly found beneath the gossan zone and composed of both sulphides and oxides, massive types of ore which are 40 to 50 metres thick (Yildirim, et al., 2016), occur mainly in the upper and lower parts of the mineralized zone, and are divided into three subtypes, namely massive sulphide ore, massive oxide ore, and massive sulphide-oxide ore. Pyrite is the most dominant sulphide mineral followed by chalcopyrite in the massive sulphide ore. They are homogeneous having mineral grains in disorientated form. Most of the pyrites are sand sized with a size range of 2 mm to 5 mm and rounded while the chalcopyrite are hardly euhedral with rarely distinguishable individual mineral grains (Fig 4.4). Carbonate in the form of veinlets and disseminations is the common gangue minerals associated with the massive sulphides.

Magnetite is the primary oxide mineral in the massive oxide ore and it is found in both deep and near supergene zones at the mine site. Characteristically similar to the pyrites in sizes of bulk mineral grains, the massive magnetite ore is highly hygroscopic and mostly accompanied by other forms of oxides such as hematite and maghemite due to supergene oxidation of the primary oxides.

4.2.2. Stockwork Ore

This type of ore occurs at a depth of 126 m at the eastern part of the mine area. Although stockworks generally correspond to the lower zones of an ore body, the stockworks found at Ortaklar occur at the middle to upper zone of the mine area. This might have been due to tectonic activities occurring after mineralization resulting in dismembering, uplift and/or overturning of the ore lens. Representing the feeder channels of the mineralised body within the host rocks, this ore type is also subdivided into disseminated and veinleted ore types based on the distribution and modes of occurrence of ore minerals. Both subtypes occur at the same zones and have no preference with respect to their area of occurrence. The disseminated ore subtype is characterised mainly by pyrite and chalcopyrite disseminated within altered host rocks composed of silicified basalts and undifferentiated basaltic materials (Fig 4.4c). Magnetite is also present in abundance, though as minute grains mostly infilling the spaces between sulphides. Chlorite, quartz and pyroxenes are the gangue minerals associated with the disseminated ore type. Veinleted ore subtype, in contrast to the disseminated ore, consists mainly of crosscutting sulphides (Fig 4.4f) with minor quartz and carbonates occurring within the altered host rocks.

4.2.3. Brecciated Ore

This type of ore is widespread throughout the ore body. The intensity of brecciation increases with decreasing depth. Ranging from angular fragments to spheroidal fragments with a size range of 2 cm to 10 cm, this ore type is made up of both oxides (mainly magnetite) and sulphides (mainly pyrite and marcasite with lesser chalcopyrite). Large spheroidal fragments of sulphides and magnetite are cemented mainly by sand sized sulphides together with minute sizes of oxides (Fig 4.4g and Fig 4.4h), attributing a highly friable character to the ore. Brecciated ore contains fragments of both massive ore and disseminated and veinleted ores, showing that the event of brecciation took place after the deposition of ore.

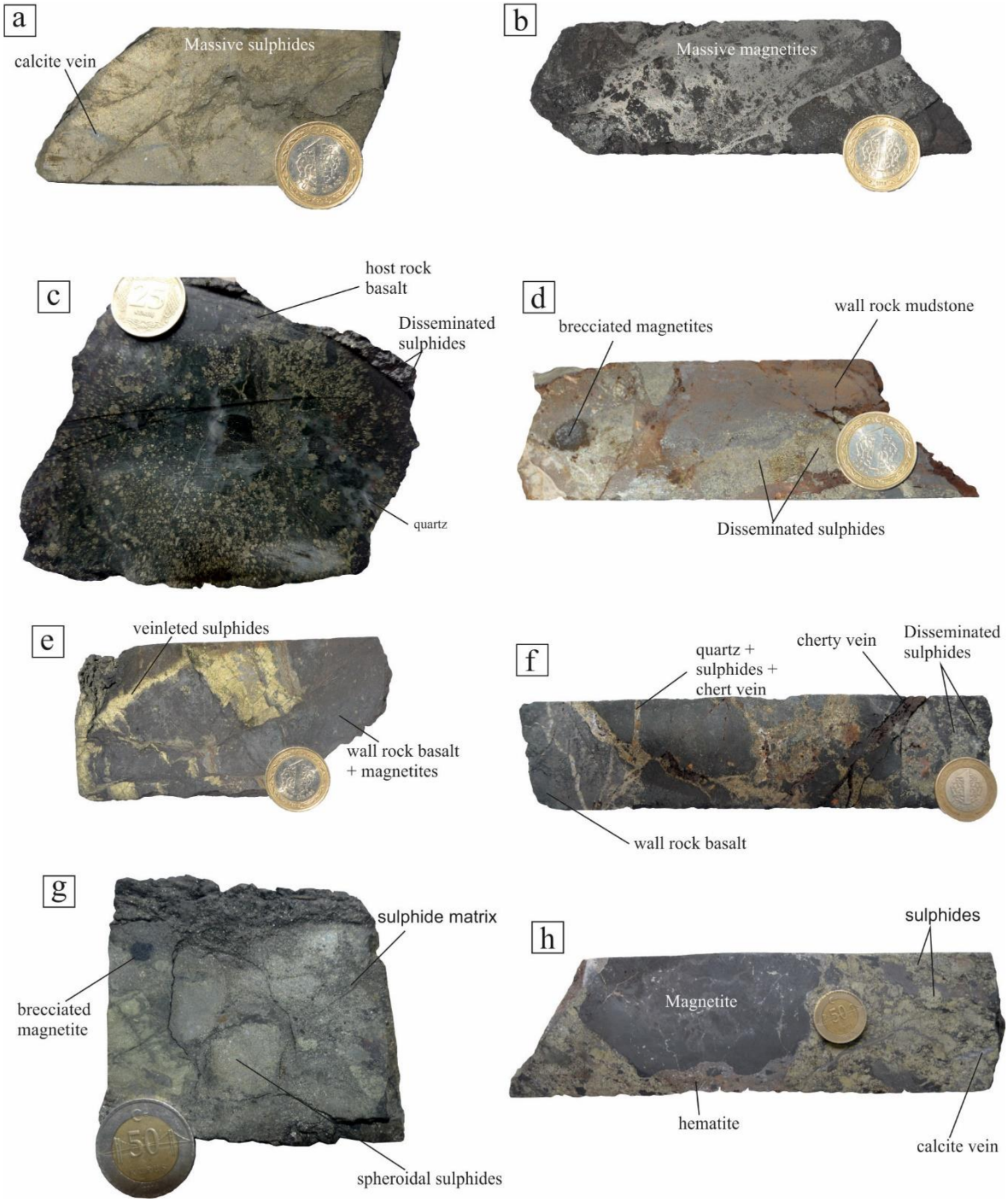

Figure 4.4. Megascopic views of the ore types found in the Ortaklar Deposit. A) Massive type of ore represented by the abundance of massive pyrite and marcasite (?). B) Massive oxide ore composed almost entirely of magnetites. C) Stockwork-dissminated type of ore represented by disseminations of pyrite within a silicified and chloritized basalt. E, F) Stockwork-veinleted ore with the sulphides crosscutting the wall rock basalts. D) Sample composed of both disseminated sulphides and brecciated magnetites within a transition zone. G,H) Brecciated ore of sulphides and magnetites within the ore lens.

4.3. Ore Petrography

4.3.1. Ore Mineralogy and Textures

The Ortaklar Deposit has a mineral paragenesis made up of pyrite, marcasite, magnetite and chalcopyrite as the main primary ore minerals (Yildirim, et al., 2016). Sphalerite occurs in rare quantities. The primary pyrite is rarely euhedral (cube shaped), and mostly subhedral and anhedral in morphology (Fig 4.5). The euhedral cube shaped pyrites are mostly found in the stockwork disseminated ore zones surrounded by gangue minerals such as quartz and chlorites, suggesting that they formed at relatively higher temperatures in a slower deposition process (Çiftçi et al, 2015). In the massive type of ore, pyrites are mostly subhedral and anhedral in shape with chalcopyrite in spaces between them (Fig 4.7).

Marcasite, is formed mainly as pseudomorph of pyrite by replacing the pyrites within its boundaries and along its cracks (Fig. 4.6). Found mainly in spatial association with pyrites and occasionally as replacements within it, chalcopyrite hardly exhibits any preferential shape under the microscope as shown in figure 4.10.

The stockwork zone is composed of mostly pyrites, chalcopyrites and magnetites in a disseminated pattern within a matrix of silicate minerals such as chlorites, quartz and pyroxenes (Fig 4.5). Disseminated textures reveals that sulphide minerals were derivatives of immiscible sulphide liquids (Ramdohr, 1981). The common secondary texture resulting from deformational episode in Ortaklar Deposit is the brecciated pyrite texture. Pyrites with very high brittle properties and low malleability in comparison to the other occurring ore minerals exhibit cataclastic textures in the ore samples (Fig 4.7). Crosscutting relation occur within the sulphide minerals where pyrites and sphalerite cut across chalcopyrite mineral grains as shown in figure 4.8.

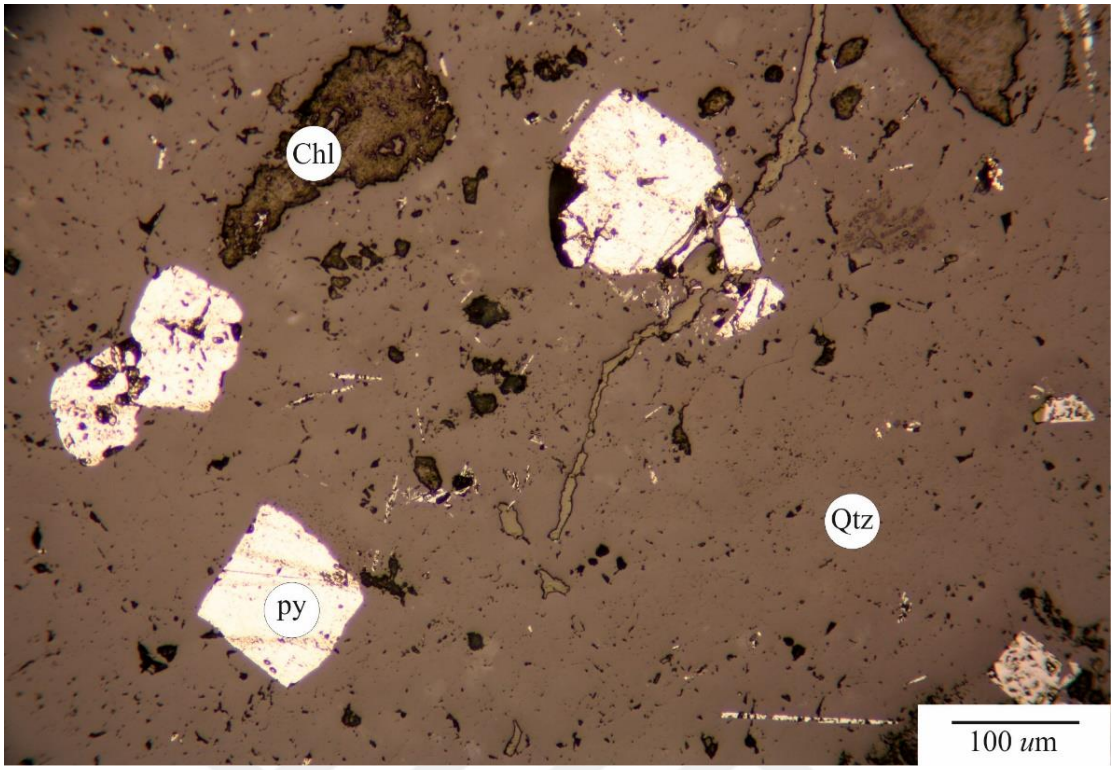

Figure 4.5. Disseminated textures of pyrites within gangue minerals. (Chl: Chlorite, Qtz: Quartz, Py: Pyrite)

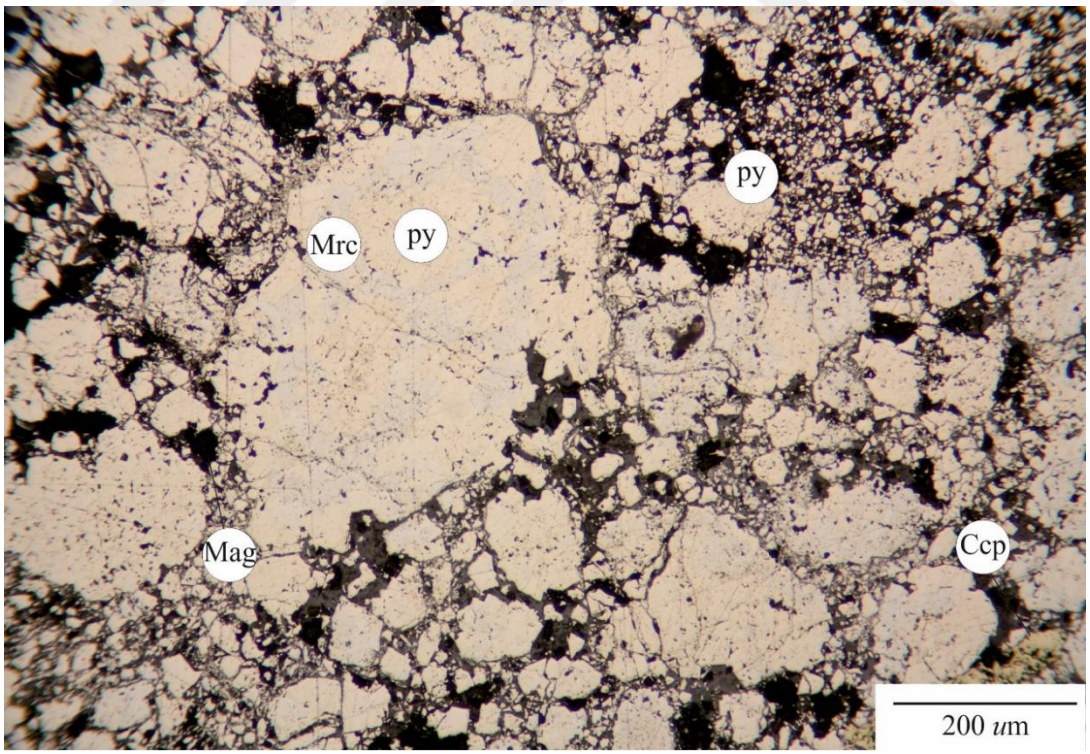

Figure 4.6. Marcasites formed within and along the pyrites boundaries. (Ccp: Chalcopyrite, Mag: Magnetite, Mrc: Marcasite, Py: Pyrite)

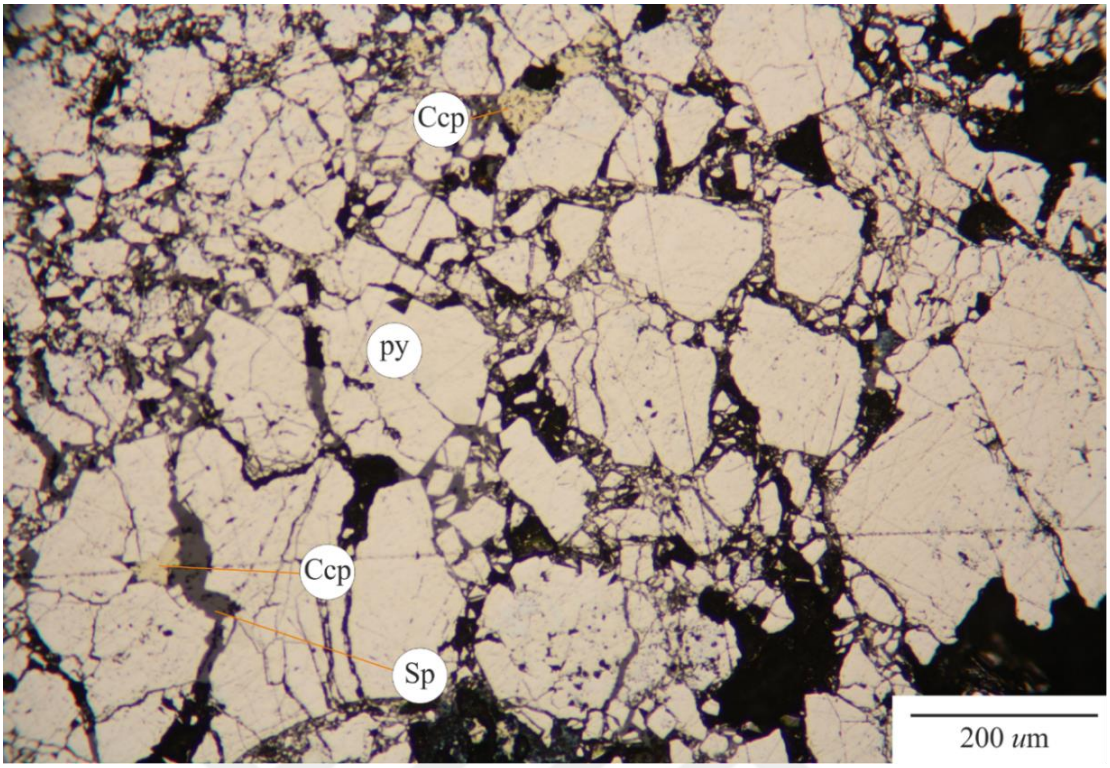

Figure 4.7. Cataclastic texture of pyrites with chalcopyrite and in the spaces between the pyrites. (Ccp: Chalcopyrite, Py: Pyrite, Sp: Sphalerite)

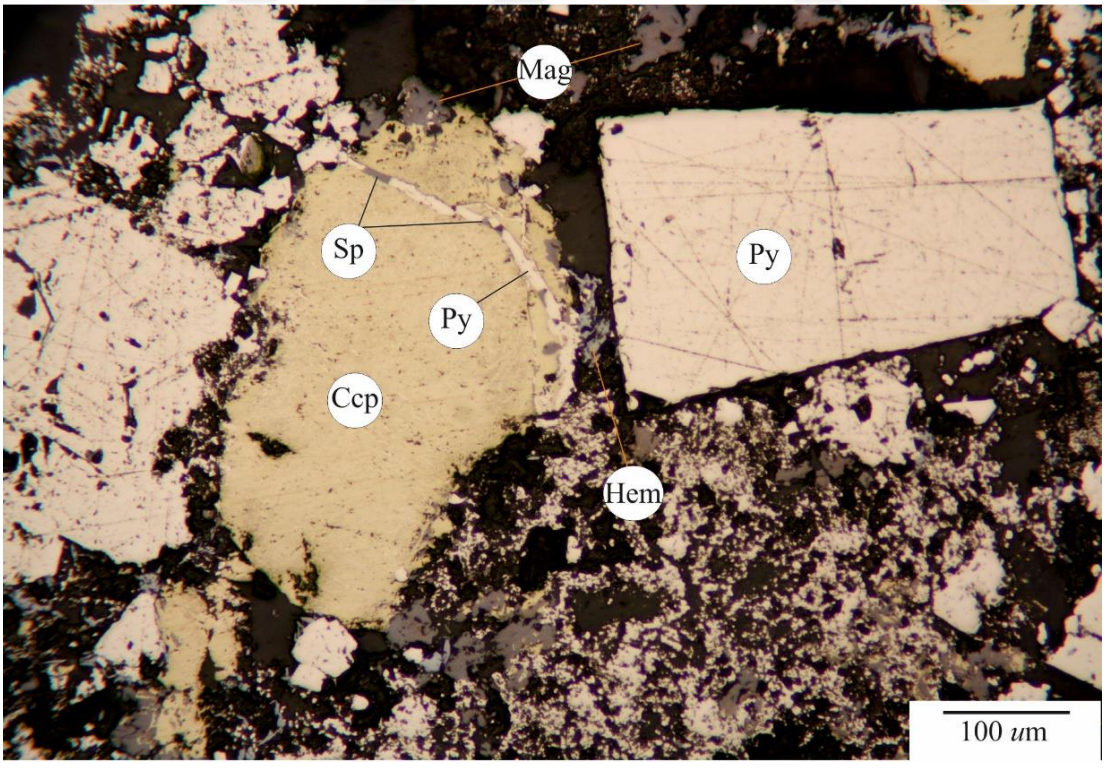

Figure 4.8. Crosscutting textures of pyrites and sphalerites through chalcopyrite. (Ccp: Chalcopyrite, Mag: Magnetite Py: Pyrite, Sp: Sphalerite)

Sphalerite is a rare sulphide mineral occurring in the Ortaklar Deposit. It is found more abundantly in the upper section of the ore zone and in small grain sizes (50-70 microns) mostly along the boundaries of pyrites and chalcopyrites but do intersect the chalcopyrites at certain locations as shown in figure 4.8.

Black in colour in hand specimen, soft, hygroscopic and sooty, magnetite is one of the primary phases occurring throughout the deposit, and forms usually large anhedral grains without any characteristic morphology and orientation. Its abundance is a feature that distinguishes the Ortaklar Deposit from all other types of VMS deposits. Boxwork textures of laths of magnetite composed of cellular crisscross laths of magnetite in a matrix of gangue minerals (Fig 4.11) are found at the supergene zones of the mineralized area close to the gossan.

Secondary enrichment is well developed within the Ortaklar mineralized zone, which is characterised by thick and extensive gossan formations. As a direct consequence of these gossan formations, secondary minerals are also abundant. Represented in decreasing order by chalcocite and covellite, the secondary sulphides have no preferential occurrence with respect to localisation and are found in cracks and rims of chalcopyrite as replacement veins and pockets. (Fig. 4.9). Bornite is less abundant found to be replacing the chalcopyrites and pyrites at certain locations as late stage mineralization (Fig. 4.9).

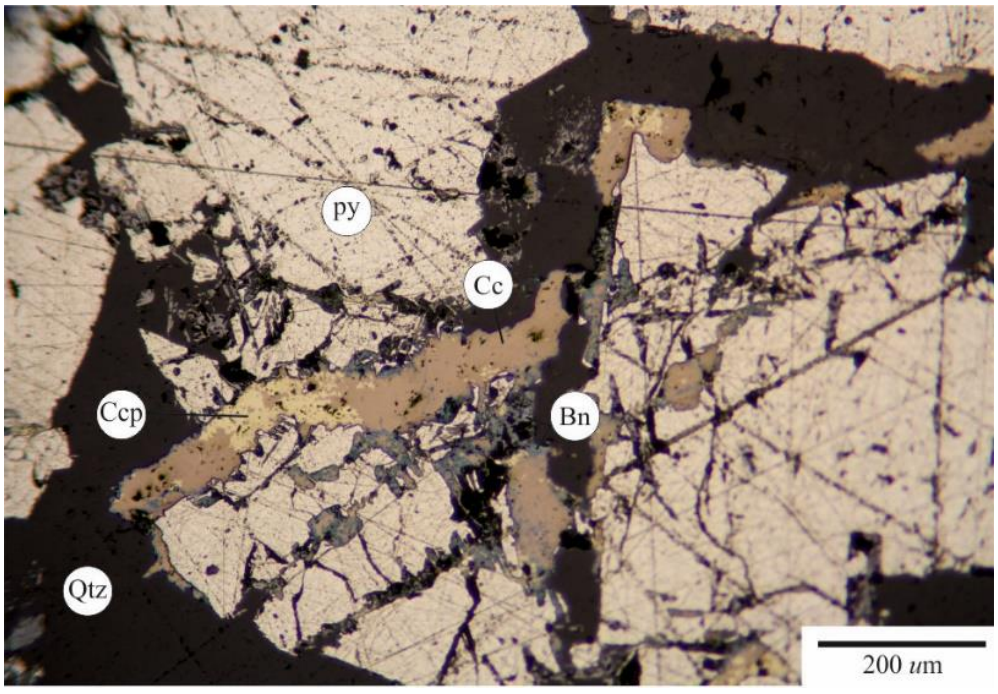

Figure 4.9. Secondary enrichment within cracks and rims of sulphide minerals. (Bn: Bornite, Ccp: Chalcopyrite, Qtz: Quartz, Py: Pyrite)

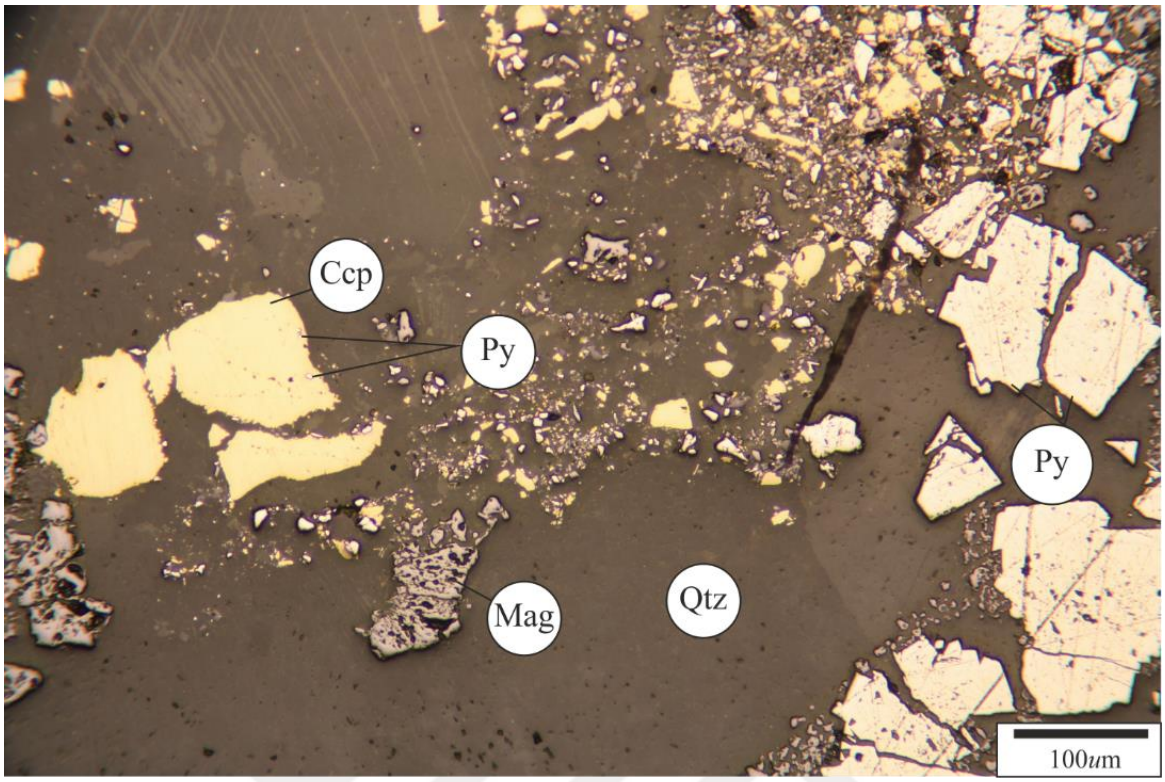

Figure 4.10. Brecciated cataclastic pyrite with magnetite and chalcopyrite. (Ccp: Chalcopyrite, Qtz: Quartz, Mag: Magnetite, Py: Pyrite)

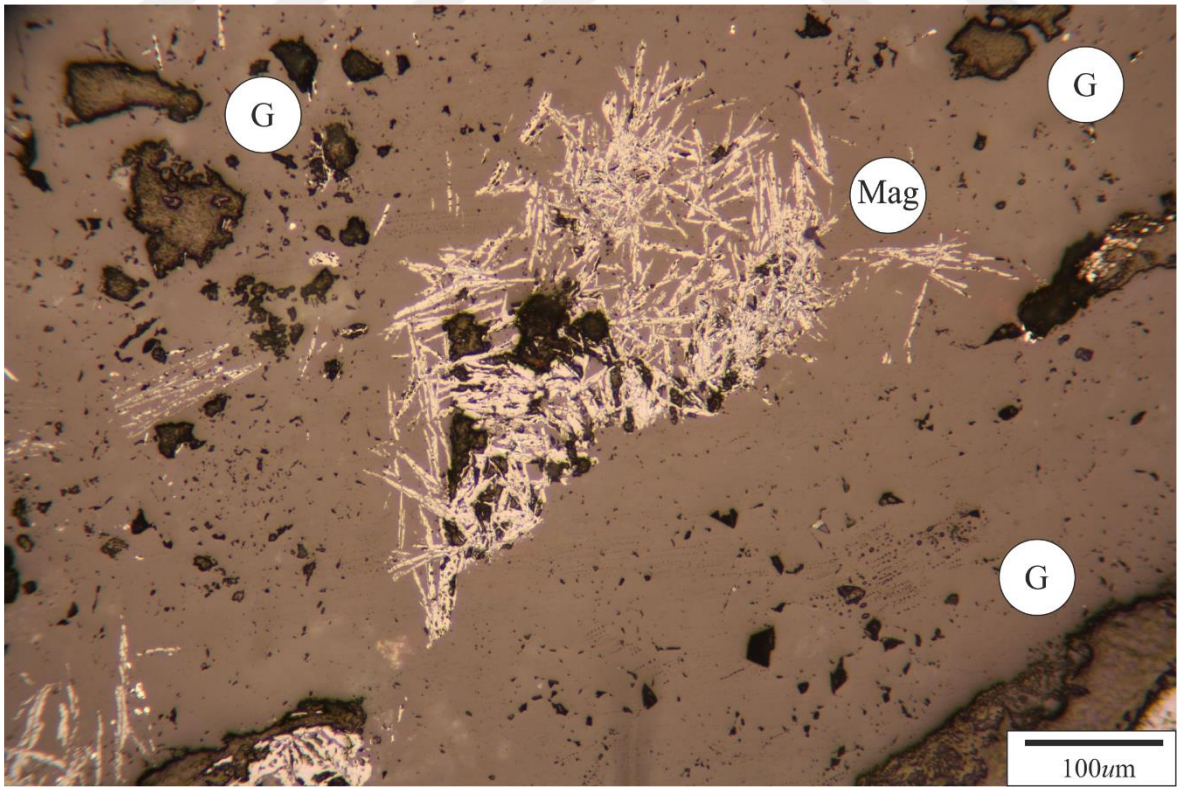

Figure 4.11. Microscopic view of boxwork texture exhibited by magnetites. (G: Gangue, Mag: Magnetite)

Secondary oxides and carbonates represented by limonite and hematite, and malachite and azurite, respectively, are more abundant than secondary sulphides and are encountered abundantly on the surface of the oxidation zone. Microscopic examination of these oxide minerals as well as magnetite indicates that oxidation process is even more complex and widespread than that observed on the surface. Detailed petrographic examination of such minerals show that magnetites are converted to hematite, martite and maghemite as well as goethite, and limonite.

Gangue minerals consist mainly of quartz, carbonates and chlorite with minor pyroxenes. Quartz is rare as expected due do the mafic character of the host rock. Calcite and chlorite are ubiquitous in the stockwork zone. Magnesites are patchy and usually occur as veins crosscutting oxide minerals, mainly magnetite. In such crosscutting veins and veinlets, it is accompanied by chlorites, indicating the mobility and hence enrichment of magnesium in the solution following the main phases of ore deposition.

4.3.2. Mineral Paragenesis

The mineral paragenesis of the VMS deposit of Ortaklar was created from the conclusions drawn from petrologic studies of wall rocks, ore-microscopic studies and microprobe analysis. Conclusions for the ore minerals, gangue minerals and alteration mineral patterns were drawn from a combination of all these studies. Over 50 sulphide and oxide polished sections prepared from 15 different parts of the Ortaklar mine area were studied. The observed primary minerals were pyrite, marcasite, magnetite and chalcopyrite. Sphalerite and bornite also occur in rare quantities, with chlorite, carbonates and lesser amount of quartz representing the gangue minerals as indicated below (table 4.1). Hematite was observed to be a common oxidation product of some magnetites. Maghemite were observed as a late stage mineralization phase occurring as products of low temperature oxidation of iron oxides. Minor amounts of azurite, malachite, covellite, goethite, limonite and chalcocite were also observed as products of supergene alteration.

Table 4.1. Mineral paragenesis sequence of the Ortaklar Deposit.

Mineral	**Stage 1**	**Stage 2**	**Stage 3 (Supergene alteration)**
Pyrite	—	—	
Marcasite		—	—
Magnetite	—		
Chalcopyrite		—	
Sphalerite		—	
Hematite			—
Maghemite			—
Bornite			—
Covellite			—
Chalcocite			—
Geothite			—
Azurite			—
Malachite			—
Limonite			—

4.4. Hydrothermal Alteration

In the Ortaklar Deposit system, intense hydrothermal alteration halo surrounds the NE-SW trending thrust fault zone. It was difficult to identify rock samples that have undergone only one type of alteration in the study area. Most of the rock samples have undergone more than one episodes of alteration. The hydrothermal alteration pattern was studied based on detailed petrographic examination and chemical analysis of samples collected from two representative drill holes (hole id: S52 and S56)) in addition to hand samples collected from the open pit and underground in order to determine the mineral combinations and chemical changes within the mineralized area.

These drill holes are about 200 m away from each other with different azimuth and dip values. One of the drill holes (S52) cut through a mineralized zone while the other (S56) is barren even though it cuts through a zone very close to an ore lens known by using GEOVIA Surpac windows software to model the ore lens after extraction. Chemical analysis obtained from selected samples were used to calculate the mass changes that occurred during the hydrothermal alteration.

The Ortaklar Deposit portrays a greenschist metamorphism with the igneous rocks containing a mineral assemblage composed of chlorite+albite+quartz+ epidote+sericite+amphibole+pyrite. Propylitic alteration, argillic alteration and late stage carbonation occur in the study area. Spillitization of the pillow basalts occurring in the upper zones is extensive in the mineralized area in addition to albitization around the dismembered ore bodies. Serpentinization, chloritization, argillic alteration, calcification, epidotization minor silicification and sericitation occur in varying degrees throughout the study area. The deep green coloured volcanics in Ortaklar are due to extensive chloritization and epidotization.

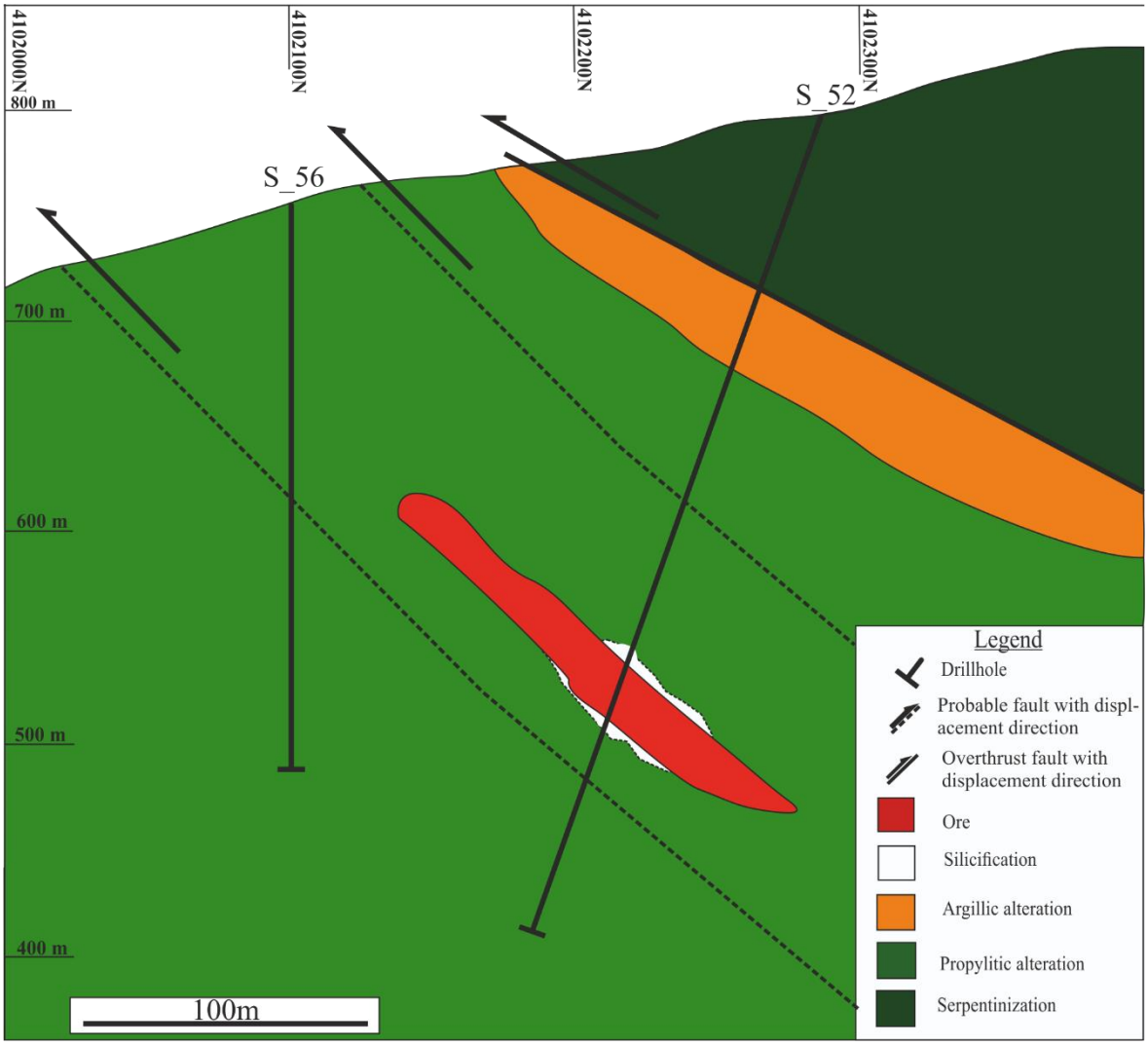

Figure 4.12. Cross section showing the dominant vertical alteration pattern associated with the Ortaklar Deposits. Vertical values are for meters above sea level. Ore modelled using mine data obtained after extraction and modelling it using Surpac.

4.4.1. Propylitic Alteration

Propylitic alteration characterised by the addition of H_2O and CO_2 and locally S with no appreciable H^+ metasomatism tends to be more pervasive towards the inner zones of the Ortaklar Deposit, or, in other words, towards the heat/hydrothermal source. The affected rocks in these zones have mostly undergone a combination of epidotization + chloritisation + carbonatization + sericitization + spillitization. Spilitization is mainly characterized by enrichment in Na_2O, elevated modal plagioclase and epidote segregations.

Chloritization is found to be occurring close to the mineralized zones affecting mostly basaltic and gabbroic rocks, this is characterised by the occurrence of secondary chlorites formed because of hydrothermal alteration of mafic minerals as well as plagioclase within these rocks. They are light green to deep green coloured rocks occurring in the central and southern part of the study area. Under the microscope, these rocks are made up of euhedrally formed grains of plagioclase, pyroxenes, clay, carbonates and opaque minerals exhibiting ophitic texture with the euhedral plagioclase minerals altered into chlorites. Chlorites formed this way are green looking micaceous and globular masses with scaly forms as shown in figure 4.13, assume the shape of the original precursor minerals.

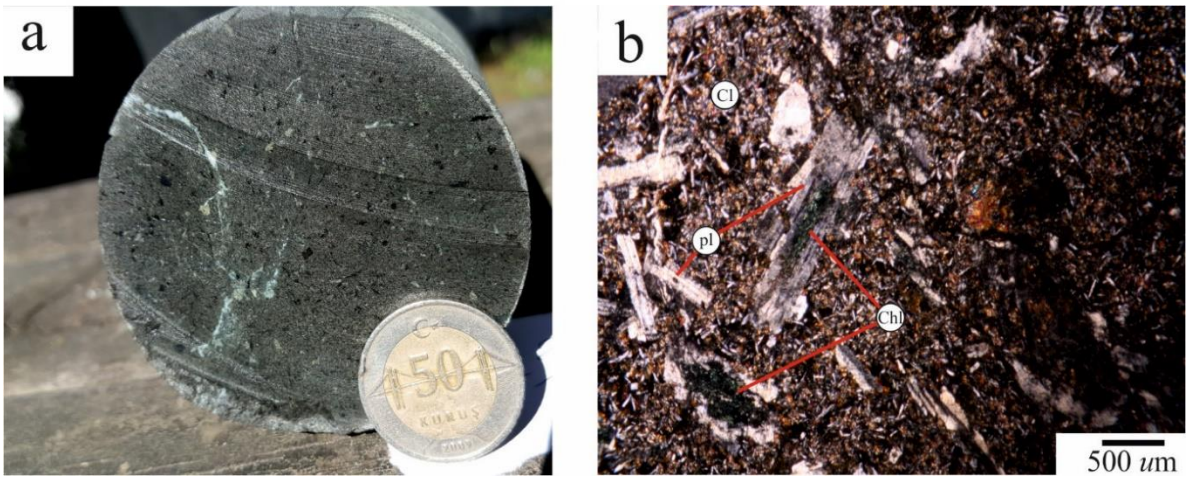

Figure 4.13. Pictures of chloritic altered rock sample showing a chloritized rock in hand specimen (a) and its microscopic view under the crossed polars (b). (Cl: Clay, chl, Chlorite, pl: Plagioclase)

Epidotization occurs especially within the spilitized basalts and sheeted dykes located very close to the ore. These rocks are dark green to bluish green in colour and friable. Their friability increases with respect to distance to the ore. Thus, the closer the ore, the more friable the rock is. Under the microscope, the epidotized rocks are fine to medium grained with varying degree of hydrothermal alteration converting the plagioclase in isolated patches to epidotes, with or without chlorites and with some opaque minerals (Fig 4.14).

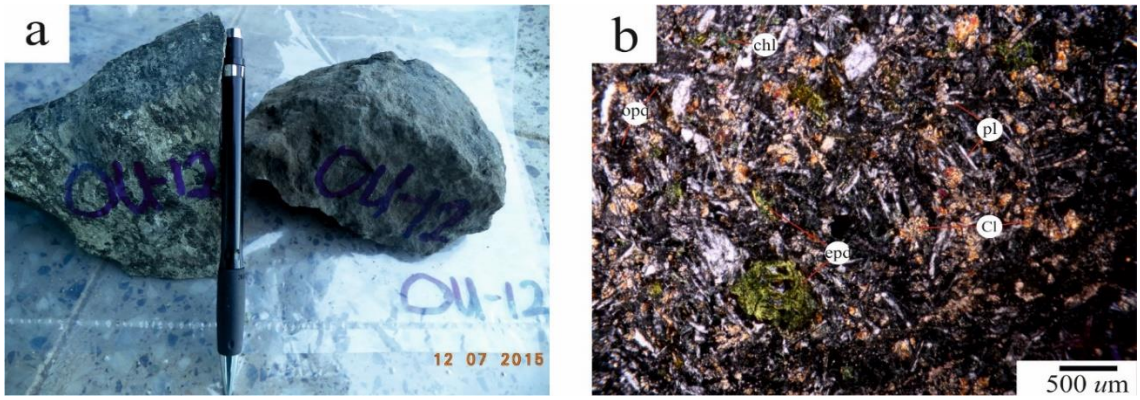

Figure 4.14. Pictures of propyllitically altered rock sample showing an epidotized, chloritized and carbonatized rock in hand specimen (a) and its microscopic view under the crossed polars (b). (chl: Chlorite, cl: Clay, epd: Epidote, pl: plagioclase)

4.4.2. Argillic Alteration

Occurring mostly in the central and southern zone of the study area, argillic alteration obliterates the primary minerals of most rock units giving rise to light brown to greenish grey rocks identified by their friability and softness. These rocks are seen to be highly affected by the alteration where no relict textures for the rocks are seen. They are characterized by clay minerals replacing the minerals prior to the alteration. This type of alteration affects the hanging wall in the mineralized zone and mostly they cover the upper units of the Upper Triassic units in the central and southern zones of the study area. Relict products of previous alterations such as sericite and amphiboles are seen within this unit (fig 4.15b).

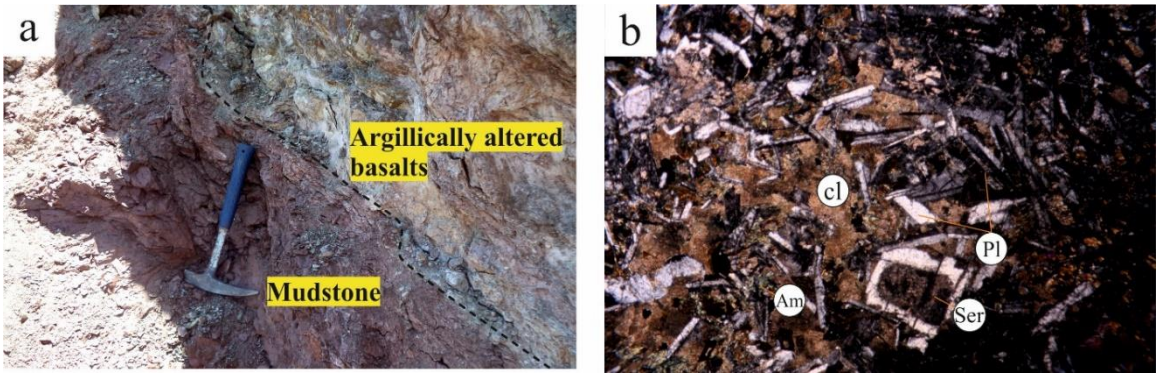

Figure 4.15. Field view (a) and microscopic view (b) of the argillic alteration. (Am: Amphibole, Cl: Clay, Pl: Plagioclase, Ser: Serpentine)

4.4.3. Silicification

The introduction of SiO_2 or alteration of minerals such as feldspars into quartz as a result of hydrothermal fluid flow is common in most VMS deposits and also found in the Ortaklar Deposit, though in small quantities. Silicification in the Ortaklar Deposit is limited in its occurrence and can be found locally within underground samples and drillcores. It is common in the stockwork zone where few sulphides are interspersed with gangue minerals such as chlorite and quatrz as shown in figure 4.16.

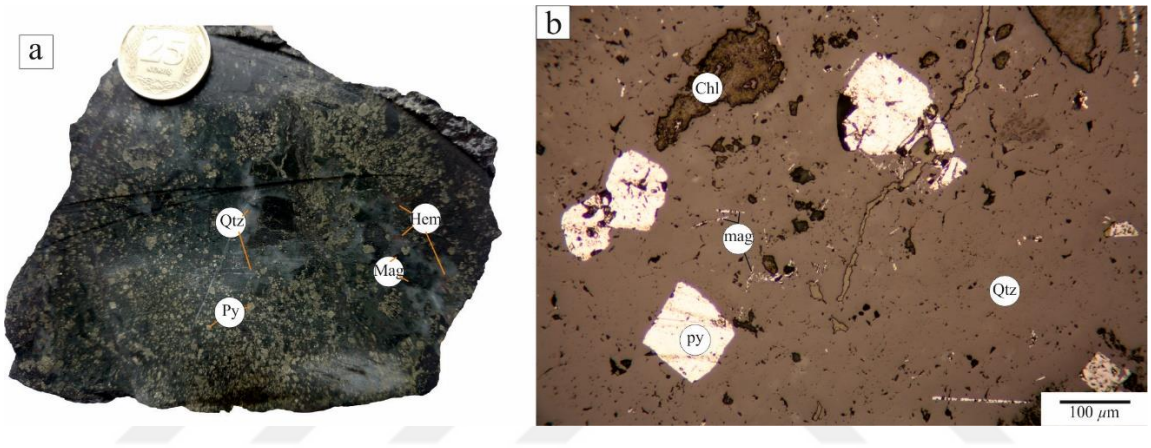

Figure 4.16. Field view (a) and microscopic view (b) of a silicified rock sample. (Chl: Chlorite, Qtz: Quartz, Mag: magnetite, Py: Pyrite)

4.4.4. Other Alterations

Serpentinization

Serpentinization is confined to the ultramafic rocks occurring at the northern part of the study area. The serpentinized rocks are greenish-grey in colour, hard, smooth and have slippery surfaces in the northwest of the study area. In the central and north eastern part, they are very hard, green looking and coarse grained with rough surfaces (Fig. 3.4). Under the microscope, the serpentine minerals are found to have completely replaced the precursors olivine and the pyroxenes. In some samples, the alteration leaves no relicts of the primary minerals present before the alteration. These rocks have a meshed texture characterized by the growth of serpentine minerals along curved fractures and grain boundaries of olivine and pyroxenes (Fig. 3.4).

Oxidation

Oxidation is rather ubiqutous and occurs due to supergene weathering of the primary ore at the Ortaklar Deposit. Composed mainly of azurite, malachite, hematite, geothite, limonite, gypsum and chalcedony, such zones of oxidation cover the ore zones as a cap and form well developed gossans (Fig. 4.17), a very useful mineralogical guide to lead to the mineralisation in the area. These gossan-rich zones contain sandy grains of azurites and malachites and lenses of limonites and hematites interspersed within the area.

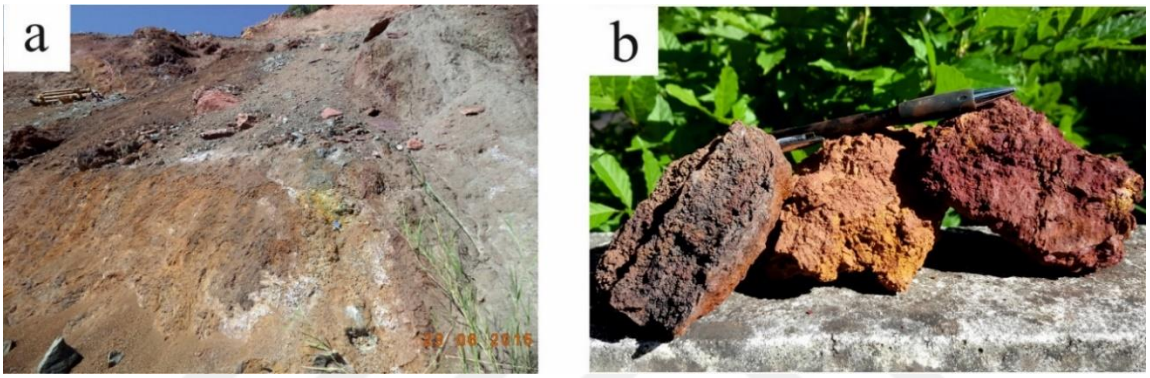

Figure 4.17. Megascopic and micrsocopic view of the oxidation zone. A) Field view of the oxidation zone in the eastern part of the study area. B) Hand size samples of limonite, hematite and geothite taken from part of the oxidation zone.

4.5. Mass Change Calculations

Different methods have been used for the calculation of quantitative elemental mass changes in mineral deposits' alteration over the years. Gresen (1962) used the volume factor. Grant (1986), revising the Gresen's method, made possible the variation of elements and oxides to be easily illustrated on the isocon diagram. Using the immobile elements method, MacLean and Kranidiotis (1987) calculated the mass and chemical changes associated with altered rocks based on a well-defined chemically homogeneous parent rock. MacLean (1990) modified this method to calculate chemical, mass and volume changes associated with altered rock with a multiple or fractionated rock series precursors. Huston (1993) modified Grant's isocon method to improve the presentation of the isocon diagram and to determine volume and mass changes associated with the altered rocks relative to a least altered equivalent. In this study, the method of Huston (1993) and the method of MacLean and Kranidiotis (1987) were used to calculate the relative and absolute mass changes respectively associated with the alteration occurring in the Ortaklar Deposit using the approach of Yaylali-Abanuz and Tüysüz (2010).

The isocon method (Grant, 1986; Huston, 1993; Huston and Cuzon, 1994) was used to determine the elements that behaved immobile during the hydrothermal alteration processes as the first step. One way to understand these elements is to use statistics by using correlations coefficients, since the elements that have had no or very little change as a result of alteration of rocks are expected to produce very high correlations between them. Such an exercise based on all elements known to be immobile or much less mobile compared to others (such as REE, Ti, Zr, Nb, Hf, Ta, Al, etc;) showed that Zr and Ti_2O produced rather high correlations between themselves. However, Ti_2O produced high correlations with, Y and Zr, proving Ti_2O to be the least immobile element producing highest correlation coefficient with Zr in the Ortaklar Deposit as shown in figure 4.18.

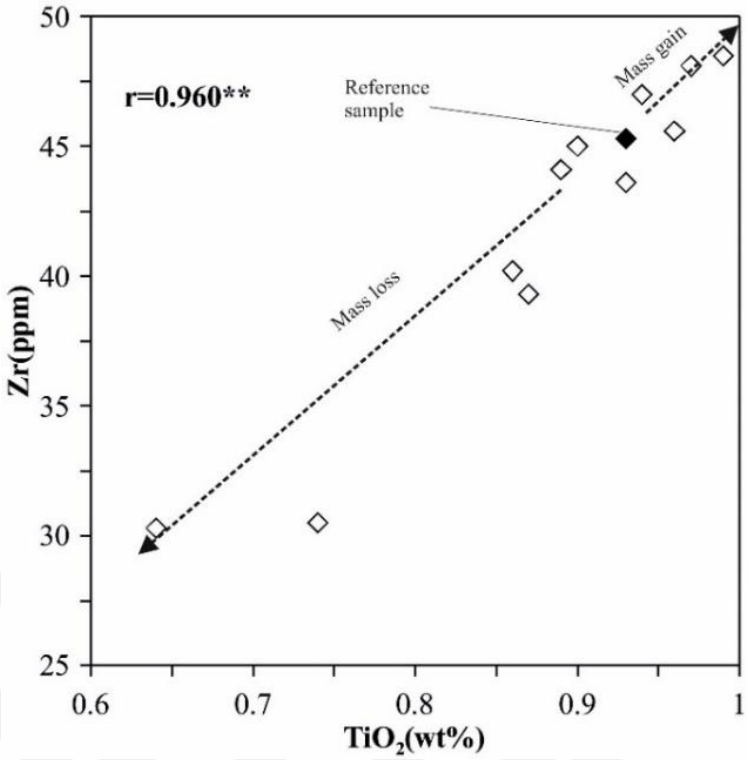

Figure 4.18. Binary diagram showing the correlations between Zr and Ti_2O

To calculate the relative mass changes occurring within the hydrothermally altered rocks, first the isocon was constructed by plotting the element concentration in the least altered basalt sample OU.15 versus the average concentration of the average of the altered samples where the whole rock data are evaluated on a log-log based isocon diagram. This was followed by determining the element that underwent relative mass gain and mass loss. The slope of the isocon was calculated to be 0.947. The net mass change was then calculated from the formula:

$$\Delta M^a\,(\%) = 100(1/m-1) \qquad (4.1)$$

and found to be 5.573%.

The isocon slope can be used to estimate net mass change, and elemental mass changes as shown in figure 4.19.

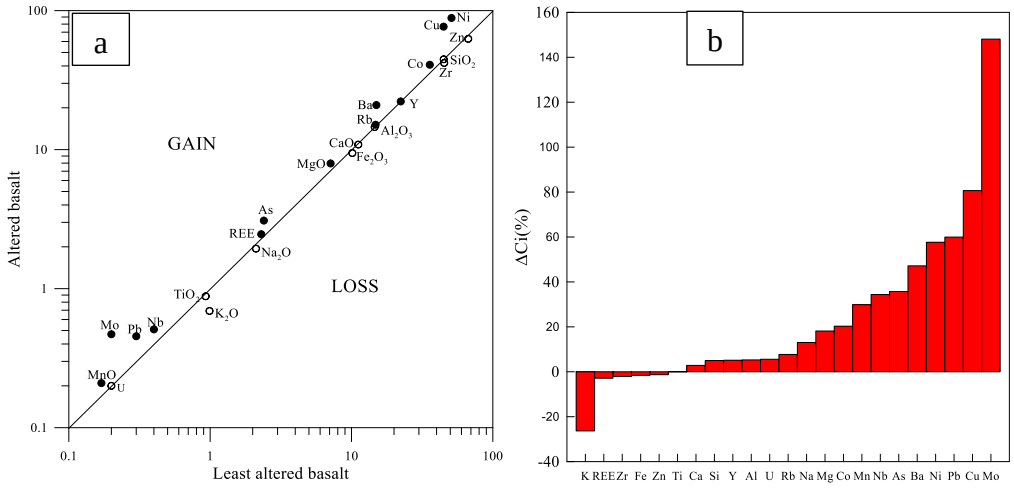

Figure 4.19. a) Diagrams showing the elemental mass loss and gains. A) isocon diagram between altered basalt and least altered basalt. B) relative mass changes in altered basalt.

If no net mass change occurred during alteration the isocon slope is one. Relative mass changes may be estimated from the isocon. Elements that gained mass during alteration plot above the isocon, and those that lost mass plot below the line.

Relative mass changes (RMC) are related to the measured composition of the least altered sample by the formulae:

$$RMC\ (\%) = 100[Ci^a/\ (mCi°) - 1] \quad (4.2)$$

Where Ci^a is the concentration of the element in the altered sample, Ci^o is the concentration of the element in the least altered sample and m is the calculated slope. Interpretation of the isocon diagram basically has two limitations: (1) mass changes are calibrated against a least-altered equivalent, which may or may not be the parent rock to the altered rock, and (2) the least-altered equivalent may have internal variations in composition independent of alteration.

Absolute Mass change calculation was also applied to the altered rocks by using single precursor method of MacLean and Kranidiotis (1987). In this method, Ti_2O was used as the 'immobile element' due to its heterogeneity and high correlation coefficient. For this mass-balance calculations, the means of anhydrous equivalent of the least altered sample was recalculated using MacLean and Kranidiotis (1987) method. The gains and losses were calculated by first using a starting mass of 100g of the least altered basalt and the established immobility of TiO_2 during the alteration.

This is followed by calculating the analytical values to obtained the mass changes in reference to 100g of the least altered basalt (table 4.2) and the established immobile element TiO_2 using the equation below for SiO_2:

SiO_2= (SiO_2 (wt%)/TiO_2 (wt %)) altered rocks x TiO_2 (g, least altered basalt) (4.3)

Using the above equation, calculations were done for each element (ΔCi(g/100g)) (table 4.6) and in order to determine the absolute mass gains and losses (ΔC), least altered gabbro elemental composition were subtracted from the composition of the RC values of altered basalt obtained (table 4.7)

Table 4.2. The result of chemical analysis of the least altered sample and mass change calculations. Ci^o: (Elemental concentration in the least altered sample; Cia: Average concentration of ith element in the altered rock; ΔCi(%): Relative mass changes of elements; Ci^o(g/100): Net mass changes of elements; Major oxides %, Trace elements in mg/kg)

Elements	Ci^o	Ci^a	Ci^o(g/100)	ΔCi(%)	ΔCi(g/100g)
SiO_2	44.93	44.68	48.67	4.99	51.10
Al_2O_3	14.58	14.54	15.79	5.28	16.63
Fe_2O_3	10.14	9.45	10.98	-1.59	10.81
MgO	7.11	7.96	7.70	18.14	9.10
CaO	11.17	10.88	12.10	2.84	12.44
Na_2O	2.30	2.46	2.49	13.04	2.82
K_2O	0.99	0.69	1.07	-26.32	0.79
TiO_2	0.93	0.88	1.01	0.00	1.01
MnO	0.17	0.21	0.18	29.85	0.24
SUM	92.32	91.75	100		104.93
Ba	15.00	20.91	15.00	47.16	23.91
Co	35.80	40.79	35.80	20.29	46.65
REE	2.11	1.94	2.11	-2.85	2.22
Nb	0.40	0.51	0.40	34.37	0.58
Rb	14.80	15.10	14.80	7.71	17.27
U	0.20	0.20	0.20	5.57	0.23
Zr	45.30	42.02	45.30	-2.08	48.05
Mo	0.20	0.47	0.20	148.10	0.54
Cu	44.80	76.66	44.80	80.66	87.67
Pb	0.30	0.45	0.30	59.96	0.52
Zn	67.00	62.64	67.00	-1.30	71.63
Ni	51.00	88.55	51.00	57.66	101.27
As	2.40	3.09	2.40	35.74	3.53
Y	22.30	22.21	22.30	5.14	25.40

The relationship between the elemental loss and gains were plotted to identify the relationship between the alteration patterns and mineralization. Decrease in Na_2O and CaO are considered to be as a result of decomposition of plagioclase. A negative correlation can be seen between the Na_2O + CaO and the the sum of the ore elements Cu+Zn+Pb. This shows that the fluids responsible for the plagioclase alteration also carries ore elements to the altering environment as can be seen in figure 4.20a.

The increase in Fe_2O_3 and MgO can be attributed to chloritization of the affected rock samples. The relationship between Fe_2O_3 +MgO and Cu+Zn+Pb shows a positive correlation. Thus the variation diagram (fig 4.20c) shows a direct relationship between chloritization and mineralization. Also this diagram shows probable two stages of chloritization and mineralization with the mineralization being higher in one stage.

There is a positive correlation between SiO_2 and sum of the mineralizing elements. This variation diagram shows that there was mineralization during the silicification alteration process. Although there seem to be no considerable relationship between the silicification and chloritization (fig 4.20d) the variation diagrams shows a positive correlation between the mineralizing elements and both silicification and chloritization. However, within figure 4.20c, there seem to be a chloritization poor stage of fluid interaction with the wall rocks. This stage might have been accompanied by the silicification.

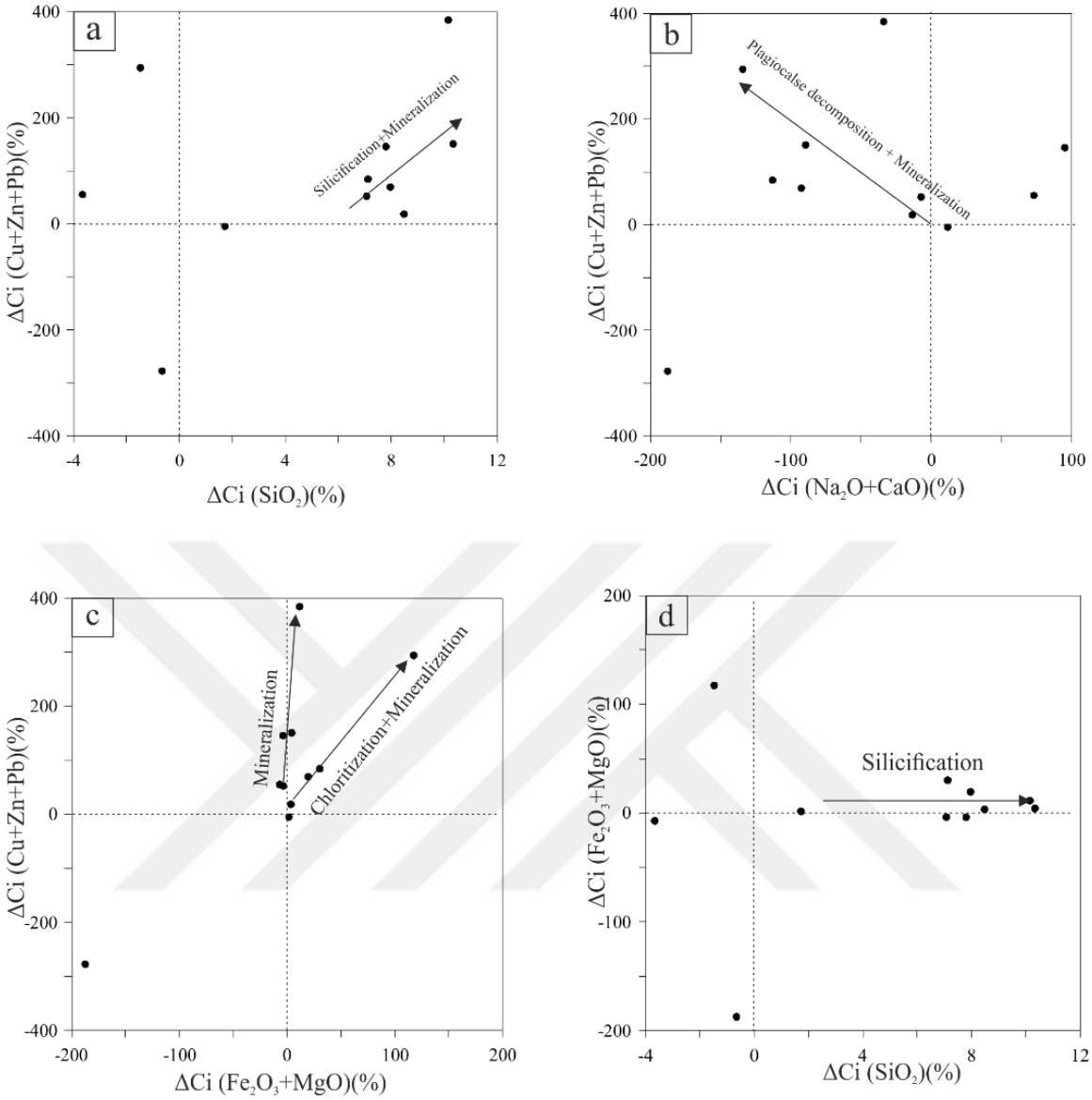

Figure 4.20. Elemental mass changes occurring in association with ore deposition within the hydrothermally altered rocks of the Ortaklar Deposit.

5. ORE GEOCHEMISTRY

Microprobe analyses were performed on sulphides and oxides in addition to the wall rock minerals associated with mineralization of the Ortakar VMS deposit. These analyses were interpreted to provide substantial evidence about the ore genesis and the evolution of the ore-forming fluids. Characterization of possible chemical changes associated with the sulphide and oxide phases in different types of ore were made by collecting samples from four different drill holes and six hand specimens from the underground to represent the mineralisation stages of the ore types.

5.1. Pyrite and Marcasite

Pyrite is the most abundant ore mineral in the Ortaklar Deposit and occurs in all types of ores. It is accompanied by its polymorph (marcasite) at certain locations. Ore petrographic examination of the samples helped identify marcasite in association with pyrite. Microprobe analyses of such phases supported the presence of two different polymorphs of FeS_2 based on colour inferences, shapes and symmetry, although no geochemical differences were detected in either stage of pyrite formation. Trace amounts of arsenic (As) (up to 0.04 wt.%) and zinc (Zn) (up to 0.036 wt.%) were detected in the pyrite. The As content was quite invariable, ranging from undetectable values to 0.036 wt%, with an average of 0.009 wt%. Up to 0.036 wt.% Zn was also detected in some pyrite grains. The Lead (Pb) contents in pyrites from all the pyrite ore types were always below detection limit, except one grain, which gave a value of 0.004 wt%.

Limited range of S, Fe and Cu occur within the pyrites. Sulphur (S) values range from 52.015 wt% to 53.126 wt % with an average of 52.730 wt%, Iron (Fe) contents range from 46.246 wt% to 42.882 wt% with an average of 46.611 wt% and the Copper (Cu) contents range from below detection limit (b.d.l) to 0.232 wt% with an average of 0.050 wt% as shown in table 5.1.

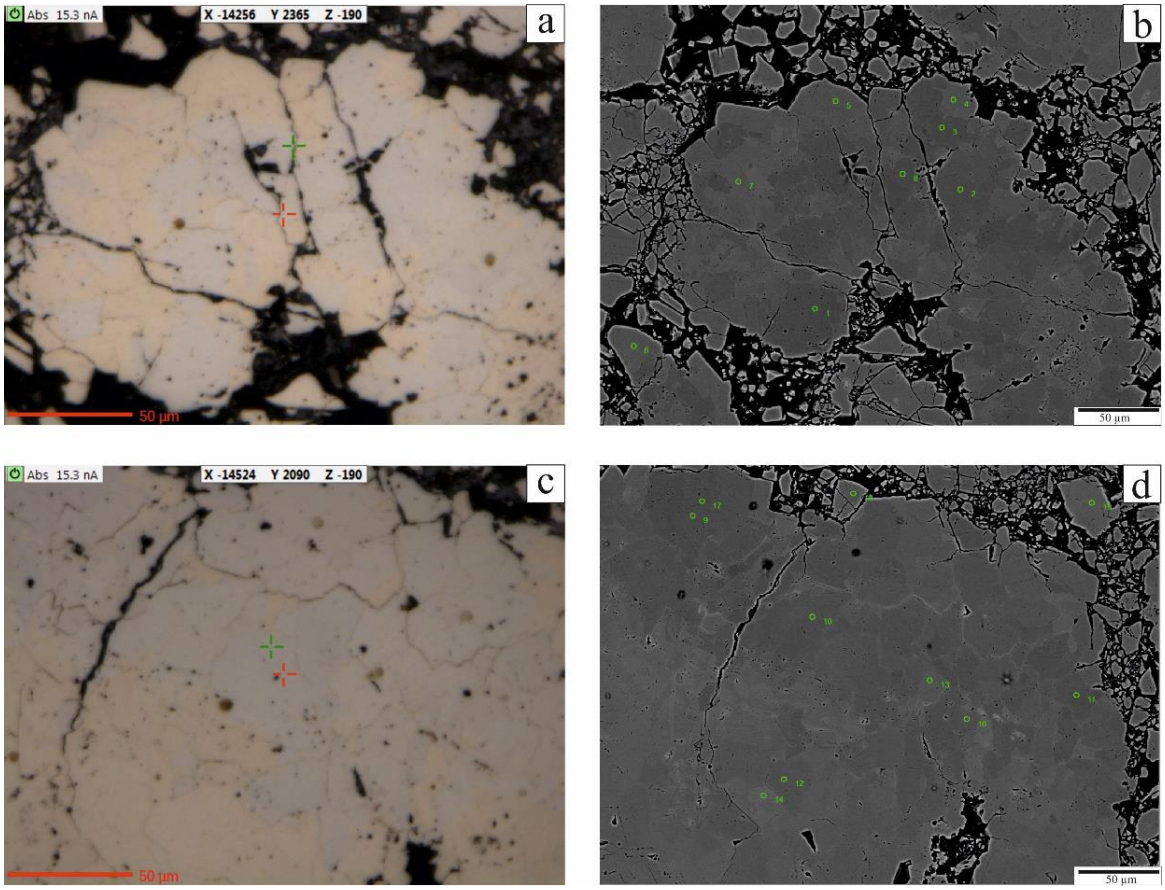

Figure 5.1. Coloured image and Back-scattered electron image of pyrite and marcasite of the analysed area of the ore from the Ortaklar Deposit.

Table 5.1. Results of the representative electron microprobe analysis of the pyrites from sample OU8.

DataSet/Point	S	Fe	Co	Ni	Cu	Zn	As	Pb	Mo	Ag	Cd	Sb	Total
1/1.	52.863	46.491	b.d.l	0.001	0.028	b.d.l	0.002	b.d.l	b.d.l	0.002	0.021	b.d.l	99.409
2/1.	52.015	46.246	b.d.l	b.d.l	0.013	0.008	0.040	b.d.l	b.d.l	b.d.l	0.013	b.d.l	98.335
3/1.	52.987	46.574	b.d.l	0.006	0.020	0.019	0.007	b.d.l	b.d.l	0.014	b.d.l	0.021	99.648
4/1.	52.396	46.407	b.d.l	b.d.l	0.232	0.005	0.016	b.d.l	0.101	b.d.l	0.008	0.020	99.186
5/1.	52.837	46.882	0.005	b.d.l	0.039	0.026	0.034	b.d.l	b.d.l	b.d.l	b.d.l	b.d.l	99.824
6/1.	52.658	46.669	b.d.l	0.008	0.125	0.036	0.015	b.d.l	b.d.l	b.d.l	0.008	b.d.l	99.519
7/1.	52.492	46.462	0.002	0.008	0.017	0.022	0.013	b.d.l	b.d.l	b.d.l	0.010	b.d.l	99.027
8/1.	52.492	46.788	b.d.l	0.004	0.018	b.d.l	0.006	b.d.l	b.d.l	b.d.l	b.d.l	b.d.l	99.307
9/1.	52.835	46.587	0.001	b.d.l	0.035	0.004	0.014	b.d.l	0.025	0.022	b.d.l	b.d.l	99.522
10/1.	52.999	46.711	b.d.l	0.018	b.d.l	b.d.l	0.036	b.d.l	b.d.l	b.d.l	b.d.l	0.002	99.765
11/1.	52.730	46.647	b.d.l	b.d.l	0.035	b.d.l	0.006	b.d.l	b.d.l	0.016	0.004	0.011	99.449
12/1.	52.745	46.754	b.d.l	b.d.l	0.032	b.d.l	0.021	b.d.l	0.148	0.029	b.d.l	b.d.l	99.728
13/1.	52.781	46.688	0.001	b.d.l	0.028	0.005	0.021	b.d.l	0.027	0.011	b.d.l	b.d.l	99.564
14/1.	52.747	46.844	0.008	0.004	0.030	0.001	0.008	0.004	b.d.l	b.d.l	b.d.l	b.d.l	99.647
15/1.	52.952	46.619	0.003	b.d.l	0.048	0.003	b.d.l	b.d.l	0.036	0.006	b.d.l	0.019	99.685
16/1.	52.752	46.465	b.d.l	0.004	0.127	0.026	0.002	b.d.l	b.d.l	0.030	b.d.l	b.d.l	99.405
17/1.	53.126	46.547	b.d.l	b.d.l	0.017	b.d.l	b.d.l	b.d.l	b.d.l	0.028	b.d.l	b.d.l	99.718
Average	52.730	46.611	0.003	0.007	0.053	0.014	0.016	0.004	0.067	0.018	0.011	0.015	99.455
STD	0.266	0.166	0.003	0.005	0.059	0.012	0.012	Undefined	0.055	0.010	0.006	0.008	0.359

5.2. Magnetite

Magnetite, the second most abundant ore mineral in the Ortaklar Fe-Cu-Au deposit contain very limited range of FeO contents (91.48 wt% - 92.05 wt%) but less variable contents in MgO ranging from 0.03 wt% to 0.35 wt% as shown in table 5.6. Up to 0.50 wt% Al_2O_3 were also detected in some magnetite grains. The SiO_2 contents range from 0.11 wt.% to 0.65 wt% which probably occur within the crystal lattice.

5.3. Chalcopyrite

The chalcopyrite data obtained from the electron microprobe analysis show that, the Zn, Pb and Ag contents were all below detection limit. The Fe, Cu and S contents have limited ranges as shown in table 5.2. The mole percent (mol%) calculated for the average of these analyses (table 5.3) shows that the mineral present at that particular area is chalcopyrite with metals to sulphur (Fe:Cu:S) ratio approximately 1:1:2.

5.4. Sphalerite

Sphalerite EPMA data shows a limited range of values for Zn and S with high contents. The Pb contents is below detection limit. After Zn and S, Fe and Cu are the most abundant elements occupying the crystal lattice of the analysed points as shown in table 5.5.

5.5. Bornite

From the electron microprobe analyses, the Zn contents in the bornite were measured to be below detection limit (b.d.l). No significant amounts of Ag enrichment were observed in all the bornite samples (table 5.6). However, limited range of Fe, Cu and S contents occur within the bornite grains. The bornites have average contents of Fe, Cu and S as 11.46 wt.%, 61.38 wt.% and 25.67 wt.% respectively. The calculated mole percentage of the average values (table 5.7) indicates that the mineral is bornite with Cu: Fe: S ratio of approximately 5:1:4.

Table 5.2. Results of representative electron microprobe analysis of the magnetites found in sample S4.4

DataSet/Point	MgO	Al_2O_3	CaO	TiO_2	Cr_2O_3	FeO	SiO_2	V_2O_3	MnO	NiO	ZnO	Total
40/1.	0.052	0.234	0.023	0.005	b.d.l	91.979	0.358	0.007	0.04	0.012	b.d.l	92.704
41/1.	0.351	0.286	0.003	0.027	0.003	91.802	0.649	0.009	0.034	b.d.l	0.016	93.171
42/1.	0.072	0.298	0.021	0.018	0.005	92.052	0.113	0.008	b.d.l	b.d.l	b.d.l	92.575
43/1.	0.035	0.352	0.006	0.018	b.d.l	91.479	0.145	0.007	b.d.l	0.022	0.029	92.077
44/1.	0.058	0.499	0.005	0.003	0.004	91.796	0.254	0.01	0.028	0.005	b.d.l	92.639
Average	0.114	0.334	0.012	0.014	0.004	91.822	0.304	0.008	0.034	0.013	0.023	92.633
STD	0.133	0.101	0.010	0.010	0.001	0.222	0.216	0.001	0.006	0.009	0.009	0.390

Table 5.3. Results of the representative electron microprobe analysis of the chalcopyrite found in sample S4.4

DataSet/Point	S	Fe	Co	Ni	Cu	Zn	As	Pb	Mo	Ag	Cd	Sb	Total
52/1.	34.135	30.050	b.d.l	0.002	34.041	b.d.l	b.d.l	b.d.l	b.d.l	b.d.l	0.016	0.005	98.086
55/1.	34.468	30.204	b.d.l	b.d.l	34.049	b.d.l	b.d.l	b.d.l	0.034	b.d.l	0.003	b.d.l	98.649
56/1.	34.132	30.164	0.021	0.002	34.090	b.d.l	0.011	b.d.l	0.070	b.d.l	b.d.l	0.004	98.334
Average	34.245	30.139	0.021	0.002	34.060	b.d.l	0.011	b.d.l	0.052	b.d.l	0.010	0.005	98.356
STD	0.193	0.080	0.000	0.000	0.026	Undefined	0.000	Undefined	0.025	Undefined	0.009	0.001	0.282

Table 5.4 Mole percentage calculations of the chalcopyrites

Element	weight %	Molecular Weight	Amount (n)	Mole %
Fe	30.139	55.845	0.540	25.176
Cu	34.060	63.546	0.536	25.003
S	34.245	32.065	1.068	49.820
Total	98.444	151.456	2.144	100.000

Table 5.5: Results of the representative electron microprobe analysis of the sphalerite found in sample OU.8

DataSet/Point	S	Fe	Co	Ni	Cu	Zn	As	Pb	Mo	Ag	Cd	Sb	Total
27/1.	32.589	0.805	b.d.l	b.d.l	0.243	65.893	b.d.l	b.d.l	b.d.l	0.014	0.036	b.d.l	99.579
28/1.	32.263	0.478	0.004	0.015	0.123	66.468	b.d.l	b.d.l	0.156	b.d.l	b.d.l	0.013	99.52
29/1.	32.651	0.644	0.010	0.003	0.217	66.040	0.045	b.d.l	b.d.l	0.012	b.d.l	b.d.l	99.622
30/1.	32.710	0.851	b.d.l	b.d.l	0.481	65.774	b.d.l	b.d.l	0.032	0.004	0.013	0.011	99.876
Average	32.553	0.695	0.007	0.009	0.266	66.044	0.045	b.d.l	0.094	0.010	0.025	0.012	99.649
STD	0.200	0.169	0.004	0.008	0.152	0.303	Undefined	Undefined	0.088	0.005	0.016	0.001	0.157

Table 5.6 Results of representative electron microprobe analysis of the bornite found in sample S4.4

DataSet/Point	S	Fe	Co	Ni	Cu	Zn	As	Pb	Mo	Ag	Cd	Sb	Total
51/1.	25.385	11.618	b.d.l	0.007	60.693	b.d.l	0.041	b.d.l	b.d.l	b.d.l	b.d.l	0.016	97.487
53/1.	25.529	11.605	b.d.l	0.005	61.896	b.d.l	0.007	b.d.l	0.013	b.d.l	b.d.l	b.d.l	98.957
54/1.	25.642	11.414	b.d.l	0.01	61.658	b.d.l	0.047	b.d.l	0.048	0.005	b.d.l	b.d.l	98.594
57/1.	26.139	11.196	b.d.l	b.d.l	61.289	b.d.l	b.d.l	b.d.l	b.d.l	b.d.l	b.d.l	0.009	98.426
Average	25.674	11.458	0.000	0.007	61.384	0.000	0.032	0.000	0.031	0.005	0.000	0.013	98.366
STD	0.328	0.198	0.000	0.003	0.524	0.000	0.022	0.000	0.025	0.000	0.000	0.005	0.626

Table 5.7. Mole percentage calculation of the bornites.

Element	weight %	Molecular Weight	Amount (n)	Mole %
Fe	11.458	55.845	0.205	10.406
Cu	61.384	63.546	0.966	48.989
S	25.674	32.065	0.801	40.606
Total	98.516	151.456	1.972	100.000

5.6. Gangue Minerals

5.6.1. Chlorite

Chlorite is one of the main gangue minerals found in the Ortaklar Deposit, occurs both as a primary mineral within the host basalts, and as a secondary product related to propylitic alteration associated with the mineralisation. The chlorites analysis from selected propylitic alteration shows relatively higher contents of Fe as compared to the Mg. Variations in the Fe and Mg contents are noticeable at the core and edges of the grain. Toward the core of the grain chlorite compositions become more Mg-rich and less Fe-rich as shown in table 5.8 and figure 5.2. The chlorite grains give variable values for Ti, Mn and Cr.

Table 5.8 Results of representative electron microprobe analysis of the chlorites found in sample S52.3

	Points of measurements								
	1/1.	2/1.	3/1.	4/1.	5/1.	6/1.	7/1.	8/1.	9/1.
SiO_2	28.97	30.08	28.05	29.16	29.08	29.07	29.72	29.10	29.45
TiO_2	0.00	0.01	0.01	0.01	0.00	0.01	0.01	0.01	0.00
Al_2O_3	14.73	14.85	16.13	15.64	15.26	15.28	14.39	14.83	14.62
FeO	26.56	25.16	25.48	25.52	25.36	24.28	26.15	25.81	25.67
MnO	0.05	0.09	0.05	0.05	0.08	0.11	0.08	0.06	0.03
MgO	15.12	15.45	14.18	15.05	15.17	15.23	14.68	15.14	14.53
H_2O	11.11	11.28	11.00	11.21	11.15	11.10	11.16	11.13	11.10
Total	96.54	96.93	94.90	96.62	96.11	95.08	96.18	96.08	95.40
Si	3.12	3.19	3.06	3.12	3.13	3.14	3.19	3.13	3.18
Al^{IV}	0.88	0.81	0.94	0.88	0.87	0.86	0.81	0.87	0.82
Al^{VI}	1.00	1.05	1.13	1.09	1.06	1.08	1.02	1.02	1.05
Mg	2.43	2.44	2.31	2.40	2.43	2.45	2.35	2.43	2.34
Fe	2.40	2.23	2.32	2.28	2.28	2.19	2.35	2.32	2.32
Mn	0.00	0.01	0.01	0.00	0.01	0.01	0.01	0.01	0.00
Ti	0.00	0.00	0.00	0.00	0.00	0.00	0.00	0.00	0.00
Octahedral cations	5.83	5.73	5.77	5.78	5.77	5.73	5.72	5.78	5.71
Octahedral vacant	0.17	0.27	0.23	0.22	0.23	0.27	0.28	0.22	0.29
Fe/(Fe+Mg)	0.50	0.48	0.50	0.49	0.48	0.47	0.50	0.49	0.50

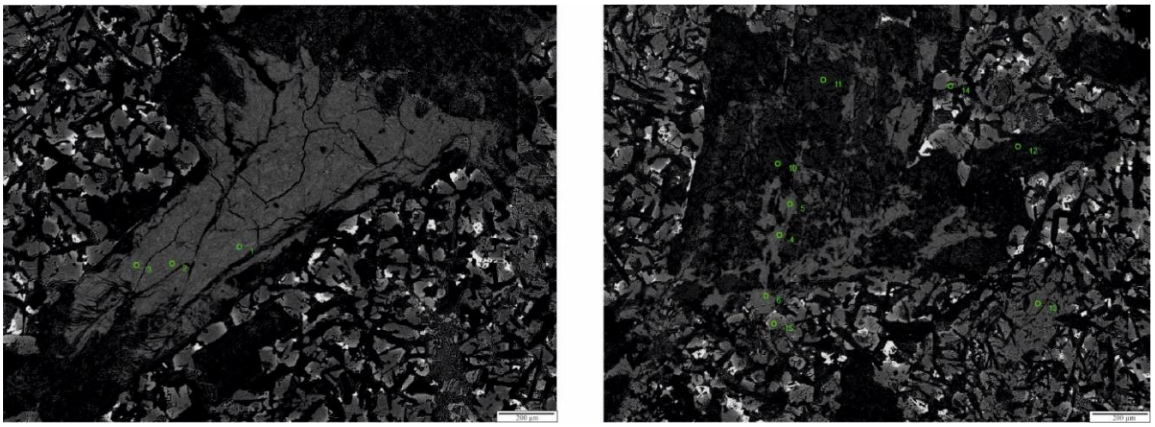

Figure 5.2. Back-scattered electron image of the chlorite

Attempts were made to classify the chlorites based on the EPMA data obtained. In doing this, all Fe data were assumed to be Fe^{2+} in calculating the normative formula as any attempt to calculate a formula from this type of data will only give, for chlorites, an approximate crystallochemical formula, and will require some assumptions (Zane and Weiss, 1998). Studies by Foster (1962); and Zane and Weiss (1998) support this assumption. Based on 154 analyses by Foster, (1962) and 20 analyses by Zane and Weiss (1998), it was concluded that Fe^{2+} /Fe^{3+} ratio is greater than 99.96% in all their analysed samples by wet chemical analyses although there are possibilities of ore mineral impurities occurrences in chlorite concentrates. Not only that, Mossbauer's data indicates that in most cases Fe^{3+} contents only represent low percentage (10 ± 5 wt%) of Fe_{tot} in rock forming chlorites and that it is slightly higher only in highly oxidized assemblages (Dyar et al, 1992). Using WinCcac (Yavuz et al, 2015), in reference to Zane and Weiss (1998) diagram for chlorite classifications, the chlorites from the propylitic zone of the Ortaklar Deposit plotted in Type 1 (Trioctahedral) chlorites, in between Mg-chlorite and Fe-chlorite as shown in figure 5.3.

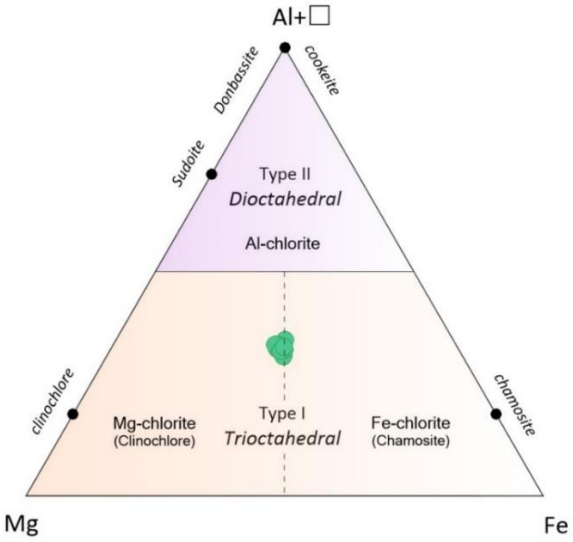

Figure 5.3. The compositional fields of chlorites of the basic igneous rocks from the Ortaklar Deposit after Zane and Weiss (1998). (Mg, Fe (Octahedral); Al (total + octahedral vacancy))

The composition of the chlorites were determined based on 14-atoms of oxygen assuming all Fe to be ferrous (Ruiz Cruz and NIieto, 2006). The chlorites plotted in the Clinochlore zone around the clinochlore-chamosite boundary.

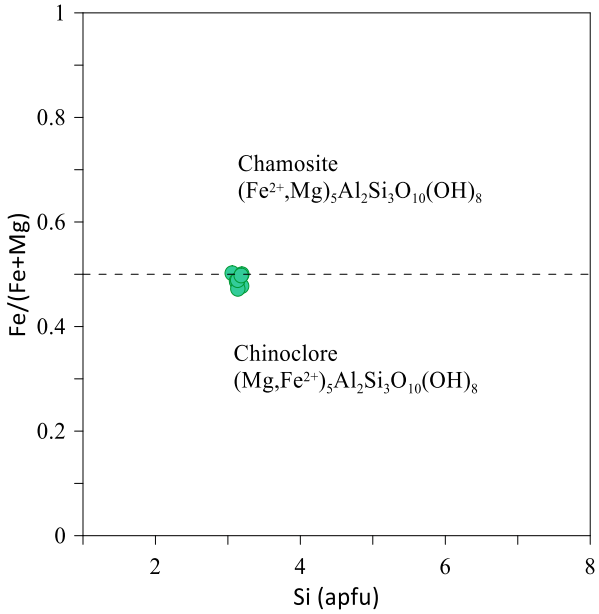

Figure 5.4. Results of EMPA analysis of the chlorite from basic igneous rocks of Ortaklar Deposit in a Fe/(Fe+Mg) versus Si diagram (Ruiz Cruz and NIieto, 2006).

Foster (1962) devised a systematic of chlorite classification based on ionic replacement of Al by Si in the tetrahedral sheet and Mg^{2+} by Fe^{2+} in the octahedral sheet on the relation $Fe^{2+}/ (Fe^{2+} + Mg^{2+})$ vs Al^{IV}. This was applied to the chlorites' data from the Ortaklar Deposit to identify the species of chlorite found. After plotting this, it was clear that the chlorites are all Diabantite except one that plotted in the Brunsvigite region.

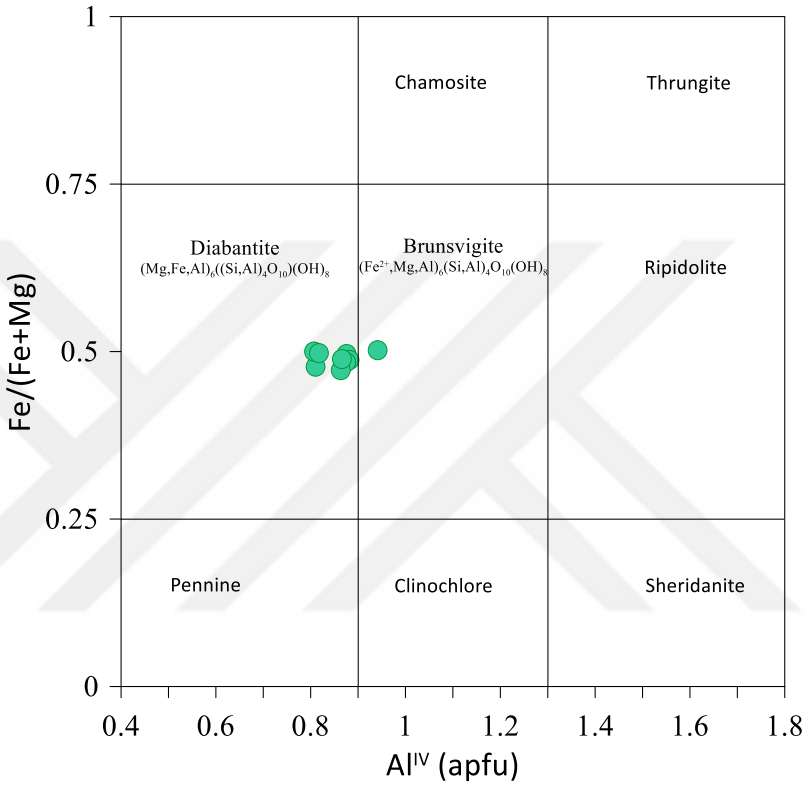

Figure 5.5. Results of EMPA analysis of the chlorite from the basic igneous rocks of the Ortaklar Deposit in a Fe/(Fe +Mg) versus Al diagram (Foster, 1962).

5.6.2. Carbonates

Carbonates form a major part of the gangue phases of the Ortaklar Deposit systems. Obtained microprobe data reflects the presence of minute quantities of carbonates such as ankerites and siderites with the first group in table 5.8 being probably ankerites and group 2 probably siderite. These minerals have a low total probably due to the absence of the analytical values of CO_2. It can be seen that the 'siderite' are rich in ZnO as compared to the 'ankerite'.

Table 5.9. Results of representative analysis of probable ankerite and siderite.

Point	MgO	Al_2O_3	CaO	TiO_2	Cr_2O_3	FeO	SiO_2	V_2O_3	MnO	NiO	ZnO	Total
45/1.	0.516	0.003	6.162	0.000	0.000	50.939	0.016	0.000	1.158	0.006	0.610	59.391
48/1.	0.657	0.105	6.046	0.003	0.003	50.473	0.150	0.000	1.451	0.000	0.347	59.227
Average	0.587	0.054	6.104	0.002	0.002	50.706	0.083	0.000	1.305	0.003	0.479	59.309

46/1.	0.000	0.013	0.163	0.000	0.000	56.798	0.027	0.008	0.519	0.000	2.836	60.346
47/1.	0.005	0.022	0.182	0.000	0.001	58.228	0.000	0.000	0.566	0.012	1.964	60.958
49/1.	0.051	0.000	0.719	0.011	0.000	56.130	0.000	0.005	0.607	0.013	2.742	60.260
Average	0.019	0.012	0.355	0.004	0.000	57.052	0.009	0.004	0.564	0.008	2.514	60.521

5.7. Stable Isotopes

5.7.1. Sulphur (S) Isotope

To determine the source of sulphur associated with the ore minerals of Ortaklar Deposit, sulphur isotope analysis was carried out on selected sulphide minerals from different parts and depths of the mine. Seven different groups of pyrites and five groups of chalcopyrite mineral separates were selected and sent for analysis. The obtained results are summarized in table 5.9.

Table 5.10. Results of $\delta^{34}S$ from Ortaklar Deposit.

Sample No.	Sample ID	Mineralogy	Texture	$\delta^{34}S$	Depth (m)
OP17	S1	Pyrite	Massive	2.5	43
SK35.10	S2	Pyrite	Massive	2.7	58.6
S6.9	S3	Pyrite	Massive	2.6	40
S52.22	S4	Pyrite	Disseminated	3.8	126
OU2	S5	Pyrite	Disseminated	4.6	3.3
OU5	S6	Pyrite	Disseminated	4.4	4.5
S4.9	S7	Pyrite	Brecciated	0.6	274.6
S52.22	S8	Chalcopyrite	Massive	0.5	67
OU.10	S9	Chalcopyrite	Massive	3.6	85
S52.27	S10	Chalcopyrite	Massive	3.0	268.9
OU12	S11	Chalcopyrite	Brecciated	2.7	274.6
S52.19	S12	Chalcopyrite	Brecciated	2.6	284.8

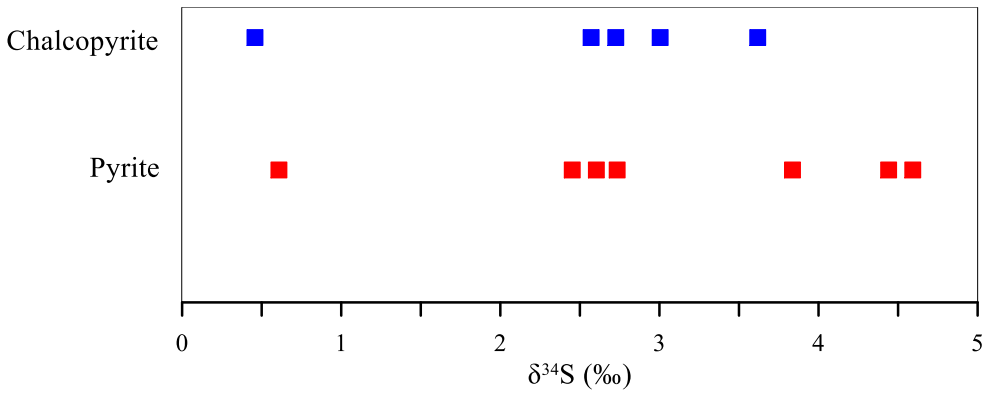

Figure 5.6. Plot of pyrites and chalcopyrites $\delta^{34}S$ values

The heaviest sulphur isotope value at Ortaklar Deposit comes from disseminated pyrite that occurs in magnetite-chlorite–quartz-altered rocks in the stratigraphically shallowest parts of the mineralized area at a depth of 3.30 metres. This pyrite has a $\delta^{34}S$ value of 4.6‰ (Fig 5.3).

As depicted in figure 5.6, significant differences in $\delta^{34}S$ occur between the textural types and stratigraphic depths of the analysed samples. For the textural changes and its associated $\delta^{34}S$ values, it can be seen that, the range of the massive sulphides ($\delta^{34}S$=0.5-3.6‰; n=6) and the brecciated sulphides ($\delta^{34}S$=0.6-2.7‰) are almost identical. However, disseminated pyrite mostly within massive magnetite have somewhat heavier $\delta^{34}S$ values ($\delta^{34}S$=3.8-4.6‰; n=3). The $\delta^{34}S$ values becomes heavier with reducing depth.

Different researchers have extensively studied variations in sulphur isotopic values and general $\delta^{34}S$ values have been assigned based on geological environments, rock types, and ore deposit type (Ohmoto and Rye, 1979; Field and Fifarek, 1985; Hoefs, 1987; Solomon et.al., 2004). Comparison of these sulphur isotope data were made with that of Ortaklar Deposit.

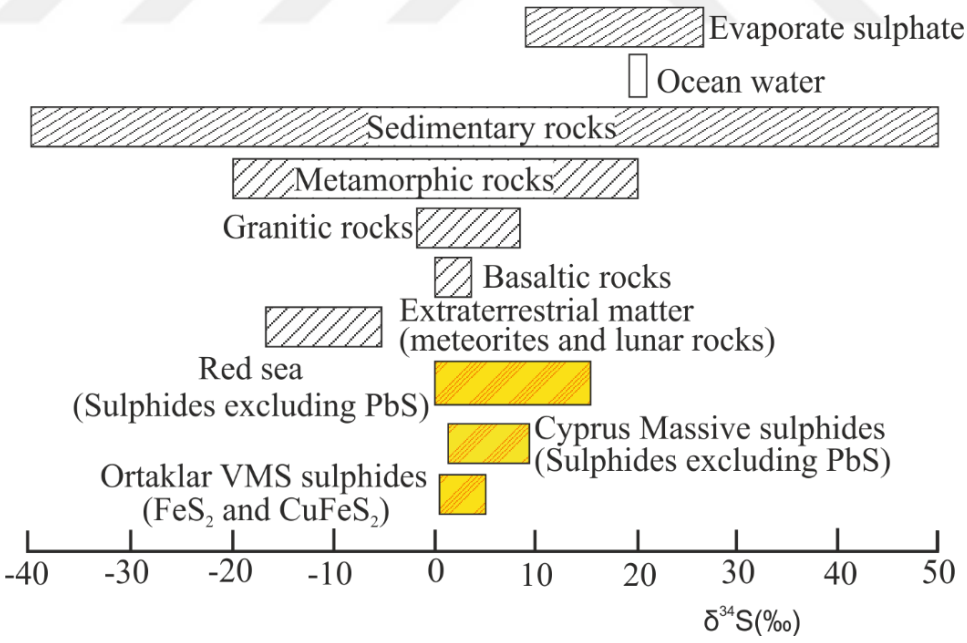

Figure 5.7. $^{34}S/^{32}S$ distribution based on geological environments, rock types, and ore deposit type in comparison to $\delta^{34}S$ isotope distribution of Ortaklar suşphides (δ-variations in ‰ relative to Canyon Diablo troilite) modified from (Hoefs, 1973). Cyprus Massive sulphide data are from Rye and Ohmoto (1974), Red sea sulphide data are from Kaplan et al (1969); and Shanks and Bischoff, (1975).

Basaltic rocks have limited variations in comparison to the other rock types and shows a range closer to the CDT. The basaltic rocks serve as representative values to magmatic sulphur (Hoefs, 1987), as they represent true magmatic phases without any involvement from other crustal sources. The sulphur isotope data obtained from the Ortaklar ore lens fall within the metamorphic and granitic rocks range; and coincides with the narrow range of basaltic rocks. In comparison to stratiform VMS deposits worldwide, the $\delta^{34}S$ values from the Ortaklar Deposit are almost identical to those from other Cyprus type VMS deposits, and coincide with the lowermost values of the Red Sea type (recent) sulphides (Fig 5.7).

5.7.2. Oxygen (O) and Hydrogen (H) Isotopes

For the determination of the source and temperature of the ore forming fluid in Ortaklar, oxygen isotope analysis was carried out on four selected quartz samples, and six magnetite samples from different parts of the mine area. The massive texture with presence of magnetites within the ore samples made the samples nearly opaque and highly unsuitable for fluid inclusion studies. However, water was extracted from fluid inclusions found within these four selected, well-cleaned quartz samples and analysed for H isotopes. Results of these analyses are given in table 5.10.

Table 5.11. Results of $\delta^{18}O$ from magnetite and quartz, and $\delta^{2}H$ of water extracted from fluid inclusions in quartz from the Ortaklar Deposit. (na: not analysed)

Sample No.	Sample ID	Mineralogy	$\delta^{18}O$ ‰	$\delta^{2}H$ ‰
OP17	Z1	Quartz	19.2	-62.3
S76.4	Z2	Quartz	28.9	-52.5
S6.4	Z3	Quartz	8.9	-73.1
S4.9	Z4	Quartz	9.6	-59.1
S8.4	Z5	Magnetite	5.3	na
S6.4	Z7	Magnetite	4.5	na
S4.9	Z8	Magnetite	-1.8	na
S8.3	Z9	Magnetite	-0.4	na
S52.27	Z10	Magnetite	-5.0	na
S52.19	Z11	Magnetite	-3.9	na

The ^{18}O isotope data for the quartz range from 8.9-28.9‰ as shown in figure 5.8. Magnetites samples gave ^{18}O isotopic data range of -5.0-5.3‰. The ^{2}H isotopic data for the water extracted from the fluid inclusions in the quartz samples range from -52 to-73‰. Isotopic data of the magnetites are less variable than the quartz as shown in figure 5.8.

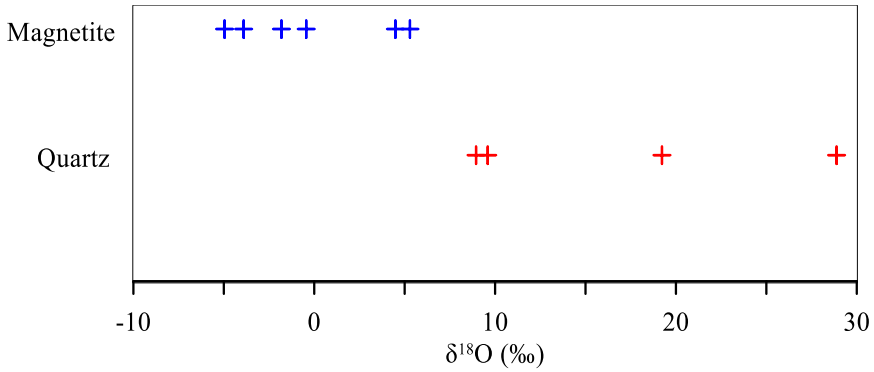

Figure 5.8. Plot of $\delta^{18}O$ of quartz and magnetites from the Ortaklar Deposit

The $\delta^{18}O$ ‰ of the quartz and magnetites show no overlap between their values and the magnetites have lower $\delta^{18}O$ ‰ values (Fig 5.9). Intra-mineral $\delta^{18}O$ ‰ differences occur within the magnetites and the quartz. In the magnetite, difference between the $\delta^{18}O$‰ at the same level tends to be wider while there is a decrease in the $\delta^{18}O$ ‰ values at deeper parts of the ore zone. Difference in $\delta^{18}O$ ‰ of quartz are rather small at shallow levels and larger at deeper zones.

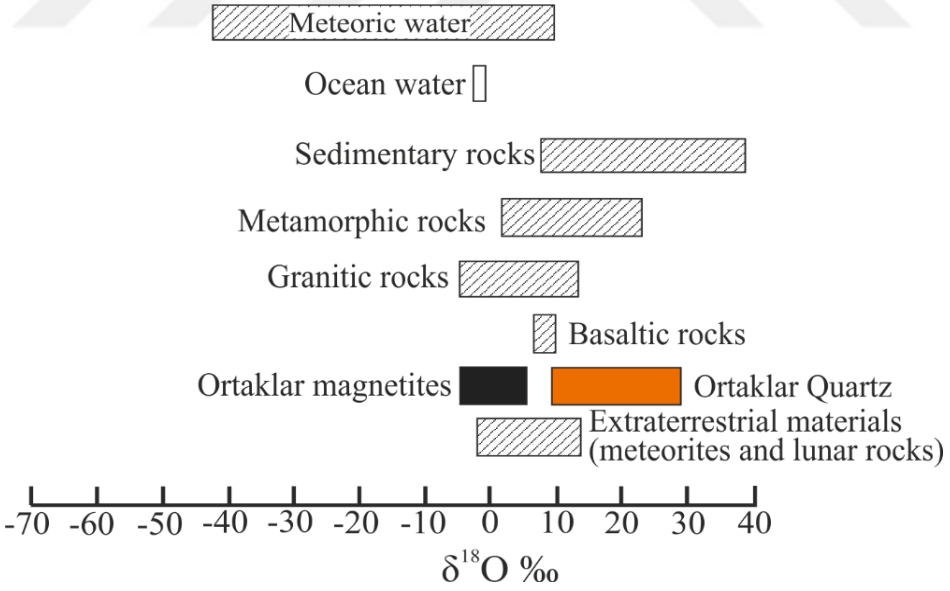

Figure 5.9. $^{18}O/^{16}O$ ratios distribution based on geological environments and rock types in comparison to$^{18}O/^{16}O$ ratios distribution of quartz and magnetites of the ore from the Ortaklar Deposit (δ-variations in ‰ relative to SMOW) modified from Hoefs (1973).

The δ^2H ‰ values of the water from the fluid inclusions extracted from the quartz are plotted in figure 5.10. The data shows a δ^2H ‰ values range between -73 to -52 ‰.

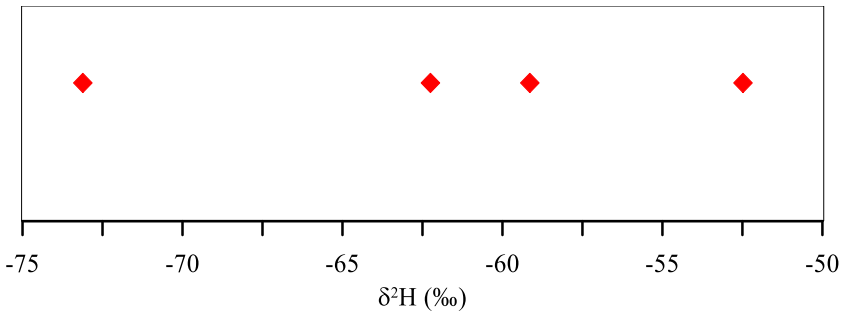

Figure 5.10. Plot of δ^2H values obtained from water found in fluid inclusions of quartz from the Ortaklar Deposit.

These obtained $\delta^{18}O$ and δ^2H isotopic values were compared to already established ranges by researchers (Hoefs, 1973) based on rock types as shown in figure 5.11

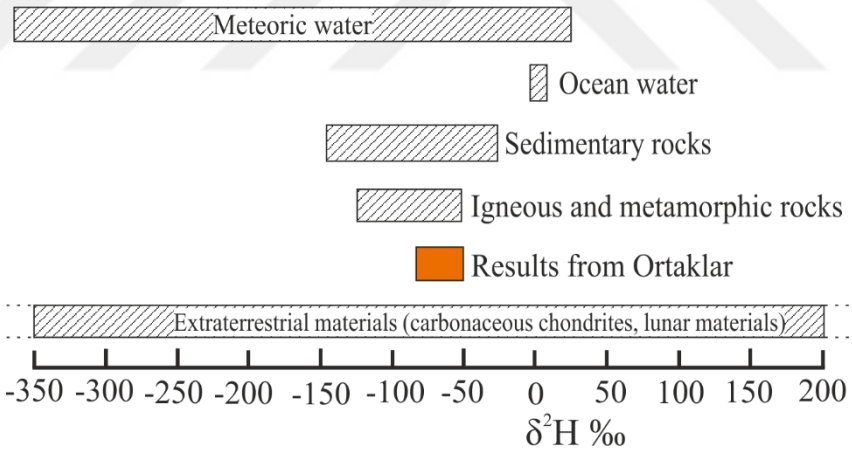

Figure 5.11. D/H ratios of some important terrestrial compounds in comparison to D/H ratios distribution of water extracted from inclusion in quartz from the ore of the Ortaklar Deposit (δ-variations in ‰ relative to SMOW) modified from Hoefs (1973).

6. DISCUSSIONS

6.1. Tectonics and Depositional Environment

The Ortaklar Deposit has a simple geological and mineralogical paragenesis however, these have been complicated by series of alterations and tectonism. The general geology of the area is made up of remnants of Tethyan seaways (Varol et al, 2011) and its oceanic crust known as ophiolites and ophiolite melanges coupled by hydrothermal alterations, sulphides and magnetite ore formations. South East Anatolia suture belt in which the study area falls is a region bounded by the Anatolide-Tauride terrain to the north and the Arabian plate to the south. The study area made up of ophiolite nappe and tectonic imbrications composed of Upper Triassic-Lower Cretaceous volcanics and sedimentary units. The northern part of the area consist of ophiolite nappe made up of serpentinites overthrusting a the imbricated zone popular called the Koçali melange zone made up of isotropic gabbros, spillitic basalts, dolerites and basalts; and sedimentary units made up of pelagic limestone, radiolariate, mudstone, cherts and marbles.

The area is characterized by E-W trending tectonic units separated from each other by north dipping thrust planes. These thrust planes are steep and have non-linear trend. A major NE-SW and northerly dipping thrust fault marks the boundary between the serpentinites and the volcano-sedimentary units along which most of the ore lens can be found. Most ophiolite hosted VMS deposits cluster along a paleohorizon. This paleohorizon defines the termination of intense magmatic activity along the spreading centers of the seafloor and it is usually a contact formed between the volcanic rocks formed by magmatic eruptions in higher volumes at the spreading centre during fast spreading and those formed by more intermittent eruptions on and off-axis during intermediate spreading (Galley and Koski, 1999). According to Galley and Koski (1999), igneous rocks in the lower zones of ophiolite hosted VMS systems usually undergo greenschist-amphibolite facies metamorphism characterised by actinolite + hornblende + ca plagioclase + magnetite + titanite while the igneous rocks in upper zones undergoe greenschist facies metamorphism characterised by chlorite + quartz + albite + epidote + pyrite + actinolite. This cool, relatively permeable area were intruded by hot impermeable dikes resulting in high temperature reaction between the feeder systems, trapped sea water, deeply circulating seawater and possibly exholved magmatic fluids because of the increased temperature.

Hydrothermal alterations have affected the study area on a large scale. Propylitic alteration has affected most of the volcanic units in which the affected rocks have mostly undergone a combination of epidotization + chloritisation + carbonatization + sericitization + spillitization. Argillic alteration occurs mostly in the central and southern zone of the study area obliterating most rock units' colours and textures giving rise to light brown to greyish green rocks. Silicification is common in the stockwork zone where few sulphides are interspersed with gangue minerals such as plagioclase and pyroxenes in the quartz matrix. Sulphur and Iron mineralization dominates the ore formations both in the hypogene and supergene zones of ore mineralization.

The hypogene zone is composed of mostly pyrite, chalcopyrite, sphalerite and magnetite whiles the supergene zones are made up of chalcocite, covellite, hematite, maghemite, goethite, azurite, malachite and limonite. The magnetite is fine-grained with sooty and hygroscopic texture. It is found as brecciated masses within the sulphides having angular fragments as shown in figure 6.1 and forms part of the matrixes of the ore. The pyrite is massive and in some parts rounded within a brecciated ore lens making up the majority of the sulphides. The rounded fragments of the pyrite might be attributed to shearing, rotation and attrition of originally angular sulphidic ore fragments during their transport following the deposition of ore (Clark, 1990). The gangue minerals associated with the ore formations are chlorites, carbonates and quartz.

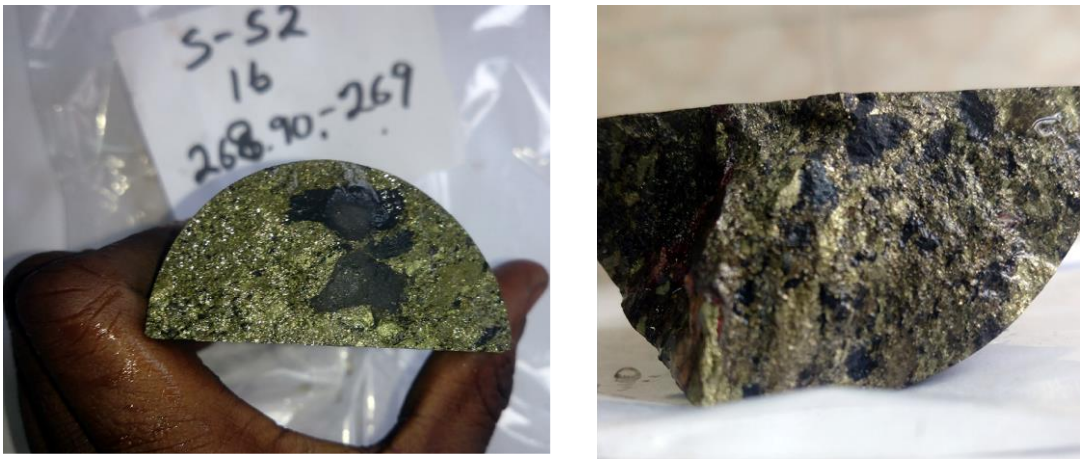

Figure 6.1. Brecciated sample of magnetite with angular fragments.

The volcanic rocks from the study area showed a Mid Ocean Ridge Basalt affinity (MORB) plotting directly in the N-MORB region of Zr/4, Nb*2, Y ternary diagram of

Meschede (1986) and the Ti vs V diagram of Shervais (1982). Volcanic sequences erupted at modem oceanic ridges consist of mainly normal mid-ocean ridge basalt (N-MORB). Melt generation possibly occurred in fore arc, back arc, or possibly below the arc itself (extensional arc settings). Ophiolite complexes are therefore likely to represent any number of extensional environments in which mafic rich ocean floor is generated with/without the accompaniment of ore deposition. To delineate the overall ophiolite sequence and determine the positions of the rocks within the rock suite occurring in the study area will require expansion of the study area followed by detailed geological mapping, sampling and chemical analysis.

6.2. Thermometric Properties

6.2.1. Oxygen Isotope Geothermometry

Even though quartz-magnetite fractionation is not widely used due to its high oxygen fugacity rendering it unable to record peak temperatures (Rollinson, 1993) using the $\delta^{18}O$-data, it is possible to calculate equilibrium temperatures for mineral pairs of magnetite-quartz. To determine the temperature of formation of the H_2O involved in the mineralization, the equation obtained for quartz-magnetite pairs from (Chiba et al., 1989) was applied to the $\delta^{18}O$ data (If the $\Delta\delta$ for any mineral pair is more than 10) as;

$$1000InC = 6.29\ (10^6/T^2) \quad (6.1)$$

$$\text{Where } C = ((1000 + \delta_A) / (1000 + \delta_B)) \quad (6.2)$$

Outliers were then eliminated from the obtained values using Thompson tau technique. This was followed by using box-and-whiskers in addition to TRIMMEAN function from excel to obtain the average of the obtained trimmed data. The results obtained are shown in table 6.1 below.

Table 6.1. Calculated oxygen isotope geothermometries from quartz-magnetite fractionation of the Ortaklar Deposit (Chiba et al., 1989)

Sample Pairs	**Mineral Combination**	**$\Delta\delta^{18}O$ (‰)**	**T (^{O}C)**
Z1-Z11	Qtz-Mgt	23	250
Z1-Z8	Qtz-Mgt	21	276
Z1-Z9	Qtz-Mgt	20	295
Z1-Z7	Qtz-Mgt	15	384
Z4-Z10	Qtz-Mgt	15	385
Z1-Z6	Qtz-Mgt	14	403
Z3-Z10	Qtz-Mgt	14	400
Z4-Z11	Qtz-Mgt	14	410
Z3-Z11	Qtz-Mgt	13	427
Average		16	359

In identifying the origin and history of the H_2O in the hydrothermal fluid, the best application lies with using D/H and $^{18}O/^{16}O$ analyses (Taylor, 1997). The isotopic analyses of quartz and magnetite combined with the calculations of temperature of formations and calculations of D/H and $^{18}O/^{16}O$ ratios of water in equilibrium with the mineral assemblages

at their temperature of formation were used to delineate the source of the H_2O. Using the relationship between quartz and water, the ^{18}O isotope values of the water were calculated from Clayton, O'Neil, and Mayeda (1972) as;

$$10^3 \ln\alpha = {}^{18}O(qtz) - {}^{18}O(H_2O) = 3.38(10^6/T^2) - 2.90 \quad (6.3)$$

Table 6.2. Calculated Oxygen isotopes of formational H_2O from Clayton, O'Neil, and Mayeda (1972)

Sample No.	**Sample ID**	**Mineralogy**	**δ^2H ‰**	**$\delta^{18}O$ (H_2O) ‰**
OP17	ZH1	quartz incl.	-62	13.67
S76.4	ZH2	quartz incl.	-52	23.32
S6.4	ZH3	quartz incl.	-73	3.39
S4.9	ZH4	quartz incl.	-59	4.03

The two main sources of hydrothermal fluids of VMS deposits are circulating seawater and magmatic water (Misra, 1999). Calculated ^{18}O composition obtained for the water in equilibrium with the quartz ranges from 3.34 to 13.62 per mil. There are two far ranges in these results due to the fact that OP17 and S76.4 come from the stockwork zone whiles S6.4 and S4.9 come from the massive zone of the deposit. The D/H and ^{18}O isotopic data from the stockwork zone points to a more evolved metamorphic source of the hydrothermal fluids as the fluid had more time to interact with the immediate environment and the data from the massive zone point closer to the magmatic source of the hydrothermal fluid. Accordingly, it can be easily ascertain that the source of the H_2O might have been magmatic water that was later modified to some extend by interacting with the underlying rocks.

6.2.2. Sulphur Isotope Geothermometry

Isotopic equilibrium constants, which are primary functions of the temperature between two known sulphur minerals, can be used to estimate the equilibration temperature of ore forming fluids. Using accurately known isotopic equilibrium constant between specific compounds as a function of temperature, the equilibration temperature can be estimated by measuring the difference in their ^{34}S isotopic values (Ohmoto and Rye, 1979). Furthermore the sulphur isotope thermometry defined by Rye and Ohmotto (1979) derived from the isotopic equilibrium constants between mineral pairs can be used to calculate the temperature of mineralization. Accordingly, attempts were made to calculate the temperature of mineralization of the ore forming fluids using the data obtained from the stable isotope analysis of the Ortaklar Deposit. To be able to use this method, certain criteria has to be met; at the time of formation, the mineral pairs must be in equilibrium, after formation there should not be any isotopical interaction and changes between these mineral pairs. Also during minerals selection for analyses, the minerals must be completely separated from each other. In this study, pyrite and chalcopyrite mineral pairs were selected and analysed as they met the above criteria. The sulphur isotope thermometry between pyrite and chalcopyrite according to Rye and Ohmotto (1979) was applied to the obtained data as;

$$T\,(K) = \frac{(0.67 \pm 0.04) \times 10^3}{(^{34}S_{pyrite} - {}^{34}S_{chalcopyrite})^{1/2}} \qquad (6.4)$$

During the microscopic studies and selection of ore minerals for isotope analysis, it was difficult to identify minerals that were in equilibrium even though individual ore minerals were easily identified. During the calculation, the mineral pairs in equilibrium produced expected results and the non-equilibrium ones gave unusable results. Outliers were then eliminated from the obtained values using Thompson tau technique. This was followed by using box-and-whiskers in addition to TRIMMEAN function from excel to obtain the average of the obtained data. The calculated temperature of mineralization obtained ranges between 202^0C to 364^0C with a mean value of 264^0C (table 6.3). These temperatures fall within the known temperature of mineralization compiled from various Cyprus type VMS deposit and correspond to some extend the temperature of formation obtained from the calculated chlorite thermometry of the propylitic zone of the deposit.

Table 6.3. Calculated sulphur isotope geothermometries from the two common sulphur minerals in the Ortaklar Deposit (Ohmoto and Rye, 1979).

Sample Pairs	**Mineral Combination**	**$\Delta\delta^{34}S$(‰)**	**T^0C**
S6-S9	Py-Ccp	1.99	202±28
S3-S10	Py-Ccp	1.87	218±29
S7-S8	Py-Ccp	1.87	218±29
S3-S8	Py-Ccp	1.72	239±31
S7-S12	Py-Ccp	1.59	260±32
S3-S12	Py-Ccp	1.44	287±33
S1-S10	Py-Ccp	1.27	323±44
S1-S8	Py-Ccp	1.11	364±38
Average		1.61	264±33

6.2.3. Chlorite Geothermometry

WinCcac windows application software (Yavuz et al., 2015) was used for the calculation of the chlorite thermometry (T,°C), WinCcac calculates and classifies rock-forming chlorite analyses based on the 14 oxygens normalization, but uses both 14 and 28 oxygen normalization approaches to estimate the empirical chlorite geothermometers. Various geothermometric parameters have been used to calculate and estimate the temperature of formation and the results are presented in Table 6.4. Although the estimated temperature of formation varies, they appear to have a limited range within all the parameters used. Cathelineau (1988) derived the following relationship between temperature, T^{o}C and Al^{iv}:

$$TC88\text{-}Al^{IV}(°C) = -61.92 + 321.98\ Al^{IV}_{O28} \quad (6.5)$$

With the results shown in column 1 of table 6.4. The method of Cathelineau, (1988) was used as a chlorite geothermometry of general applicability since the value of Al^{iv} appears to be independent of any rock lithology. Kranidiotis and MacLean (1987) modified the Cathelineau and Nieva (I985) expression purely on empirical grounds, to take into account the variation in Fe/(Fe + Mg) in chlorite. They calculated a corrected $A1^{iv}$ value (AIc^{iv}) as follows:

$$Alc^{iv} = Al^{IV}_{O28} + 0.7(Fe/\ [Fe + Mg]) \quad (6.6)$$

From which the temperature in ^{o}C is calculated as:

$$TKML87\text{-}Al^{IV}(°C) = 106\ Alc^{iv} + 18 \quad (6.7)$$

Kranidiotis and MacLean (1987)'s method is applicable to situations where chlorite grows in 'Al-saturated environment,' i.e., in the presence of other aluminous minerals. In addition, it is widely used in ore deposit environment. After using this method, the results are given in table 6.4, column 2.

Jowett (1991) suggested a similar type of correction, derived from an isothermal Fe/(Fe + Mg) normalization based on Salton Sea and Los Azufres chlorite compositions:

$$AIc^{iv} = Al^{IV}_{O14} + 0.1(Fe/\ [Fe + Mg]) \quad (6.8)$$

$$TJ91\text{-}Al^{IV}(°C)T = 319Alc^{iv} - 69 \quad (6.9)$$

Equation 6.8 and 6.9 are applicable to different systems in the range of 150ºC to 325ºC for chlorites with Fe/ [Fe + Mg] values to be <0.6. The temperature values calculated using equation 6.9 is giving in table 6.4 in column 3.

Note that Al^{IV}_{O28} and Al^{IV}_{O14} denote the tetrahedral aluminium contents of trioctahedral chlorite analysis calculated based on 28 oxygen and 14 oxygen respectively.

Table 6.4. Chlorite thermometers of basic igneous rocks from the Ortaklar Deposit calculated using Winccac (2015), $TC_{88\text{-}Al}$ (column 1) from (Cathelineau, 1988), $TJ_{91\text{-}Al^{IV}}$ $TKML_{87\text{-}Al^{IV}}$ (column, 2) from (Kranidiotis and MacLean, 1987); based on the Al^{IV} (apfu) with the Fe/(Fe+Mg) correction factor, (column 3) from (Jowett, 1991) based on the Al (apfu) with the Fe/(Fe+Mg) correction factor.

	1	**2**	**3**
Sample No	**TC88-Al^{IV}(°C)**	**TKML87-Al^{IV}(°C)**	**TJ91-Al^{IV}(°C)**
1/1.	199	225	205
1/2.	198	226	204
1/3.	201	228	208
1/4.	216	236	221
1/5.	217	238	223
1/6.	220	239	226
1/7.	220	240	226
1/8.	222	241	228
1/9.	241	255	247
Average	**215**	**236**	**221**

6.3. Modeling of the Ore Formation

The Ortaklar Deposit formed in a highly tectonised area (ophiolite zone) with continuing breakages in the ore lens' morphology. The area has been affected by severe hydrothermal alteration. According to Galley and Koski (1999), igneous rocks in the lower zones of ophiolite hosted VMS systems usually undergo greenschist-amphibolite facies metamorphism characterised by actinolite+ hornblende+Ca plagioclase + magnetite + titanite while the igneous rocks in upper zones undergo greenschist facies metamorphism characterised by chlorite+quartz+ albite+epidote+ pyrite+ actinolite. This cool, relatively permeable area was intruded by hot impermeable dikes resulting in high temperature reaction between the feeder systems, trapped sea water, deeply circulating seawater and possibly exholved magmatic fluids because of the increased temperature.

Yildirim et al., (2016) concluded after megascopic and optical studies of this deposit (from both the massive and stockwork zone) that there were two stages of mineralization; stage 1 mineralization composed of pyrites, chalcopyrites and sphalerite as sulphide-rich magnetite-poor stage whereas the magnetite-rich and sulphide-poor mineralization formed in the second stage in which sulphides are replaced by magnetite. The pyrite grains exhibits a zoning texture (Yidirim , et al., 2010) which suggest a multiple stage of pyrite formation (İlhan, 2013; Craig et al., 1998; Large et al., 2011). However, in this study, no zoning texture was found to occur in the studied pyrites. The observed main petrographic features of the pyrites studied were their cataclastic texture and presence of marcasites as pseudomorphs.

The thermometric measurements obtained from isotopic and microprobe studies show a range of temperatures. The ^{34}S isotopes obtained values range between +2.5‰ to 4.6‰ with a mean value of +3.3‰, except for two very low values of +0.5‰ for one pyrite sample and 0.6‰ for one chalcopyrite sample. The source of the sulphur extrapolated from the S-isotopic compositions points to a magmatic sulphur probably leached from the ore-forming fluids. The ^{18}O isotope data for the quartz range between 8.9-28.9‰ as shown in figure 5.8. Quartz and magnetite samples gave ^{18}O isotopic data range from -5.0‰ to 8.3‰. The ^{2}H isotopic data for the water extracted from the fluid inclusions in the quartz samples ranges from -52 to-73‰.

Calculated oxygen isotope geothermometry using the isotopic compositions of genetically related quartz and magnetite yield a temperature range of 250–427ºC. Temperatures calculated from sulphur isotope compositions of pyrites and chalcopyrites vary between 202±28 and 364±38ºC. The calculated formational temperature of the chlorite

obtained from the propylitic zone using microprobe analytical results ranges between 225^0C to 255^0C with an average of 236^0C based on the Al^{IV} (apfu) with the Fe/(Fe+Mg) correction factor (column 1 in table 6.4) calculations of Kranidiotis and Maclean (1987). This was chosen because Al^{iv} in chlorite increases with iron enrichment (Fe/Fe + Mg), whereas $A1^{vi}$ remains relatively constant. Changes in Al^{iv} with temperature at constant Fe/Fe + Mg may provide a useful geothermometer (Cathelineau and Nieva, 1985).

Thermometric and barometric data from fluid inclusion studies could not be analysed making it difficult to calculate the depth of formation of this mineral deposit. However, presence of deep-sea pelagic sediments with radiolarite and cherty limestone found in contact with the massive ore body denotes that the depth of seawater is greater than 1000–1500 m (Finlow-Bates and Large, 1978; Henley and Thomley, 1979).

Contrary to the conclusions drawn by Yildirim et al, (2016), calculated geothermometric data, microscopic studies together with mineral paragenetic studies and field observations indicate that ore deposition occurred in two stages. First stage consists of magnetite-rich sulphide-poor ore deposition stage with an average temperature of around 359ºC and a sulphide-rich magnetite-poor second stage having an average temperature of around 264ºC. These stages were followed by a waning stage where the mineralising fluid underwent cooling with the temperatures falling to around 236ºC as marked by chlorites obtained from the propylitic alteration zone. To support this assumption, the following interpretations were made;

Although the magnetite are ubiquitous, they are often seen to include sulphides in the massive magnetite zone as individual masses but not within the matrixes. The massive sulphides zone even without the presence of brecciated magnetite have signature of magnetite in the matrix. These are as a result of late stage sulphidation where the sulphides were deposited in pool of magnetite providing a substrate for the sulphide mineral grains formation.

Naturally occurring marcasite may have a temperature of formation as high as 240°C (Hannington and Scott, 1985), but preservation on a multimillion-year scale seems to require post-depositional temperatures of below about 160°C (Rising, 1973; McKibben and Elders 1985). The marcasite formed under low-temperature, highly acidic conditions by ascending solutions points to a gradual drop and low temperature maintenance of the depositional environment. A late stage introduction of high temperature magnetite which in itself does not favour the formation of sulphides will probably have converted the magnetite back to

sulphides. According to Fleet (1970), Gronvold and Westrum (1976); Kjekshus and Rakke, (1975) marcasite readily inverts to pyrite when heated under vacuum to temperatures above 673 K. Also Rising (1973) concluded that marcasite readily transformed to pyrite above 433 K under hydrothermal reaction conditions.

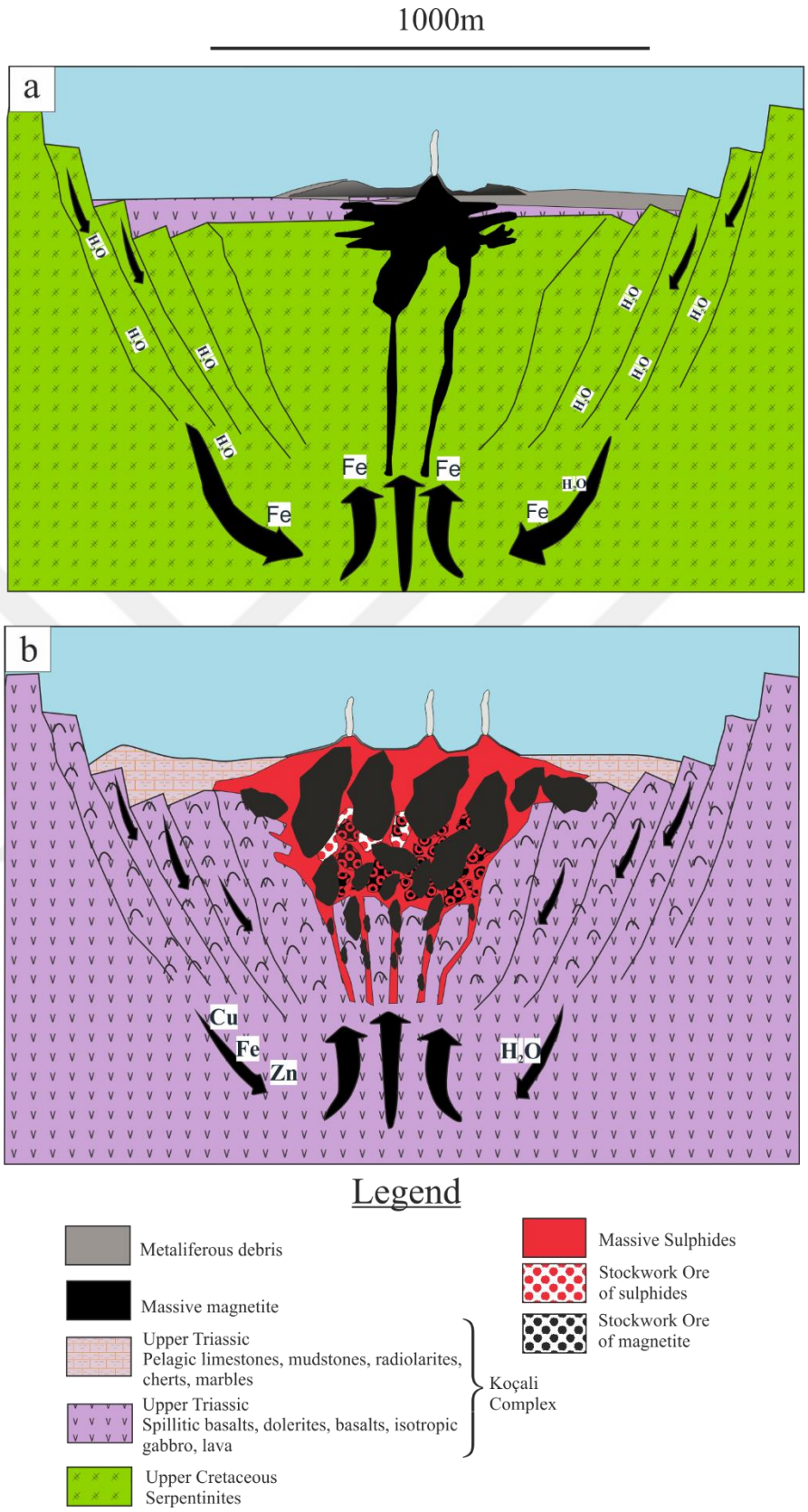

Figure 6.2. A formational model of the Ortaklar Deposit showing the two main mineralisation stages of the Ortaklar Deposit (modified from Pirajno, 2009)

7. CONCLUSIONS

The conclusions drawn based on the geological, mineralogical, structural and geochemical studies of the studied area in South East Anatolia suture belt has been summarised below;

1. The Ortaklar Deposit is found within the Koçali complex made up of Upper Triassic-Lower Cretaceous units consisting of ophiolite nappe made up of serpentinites overthrusting an imbricated zone made up of isotropic gabbros, spillitic basalts, dolerites and basalts; and sedimentary units made up of pelagic limestone, radiolaria, mudstone, cherts and marbles.

2. The mineralization is found within the N-MORB upper Triassic-lower cretaceous volcanic units with occurrences also within the sedimentary units as a result of tectonism and gravitational pull.

3. This is a type of ophiolite hosted Cyprus-type VMS deposit with unusual alteration pattern and mineral paragenesis. This Cyprus type VMS deposit is magnetite rich as opposed to many known deposits of the same type.

4. Hydrothermal alteration has pervasively affected the study area along the NE-SW thrust fault extending to the southern part of the study area. The alteration includes; propylitic alteration, argillic alteration and silification. Supergene alterations such as oxidation also commonly occurs within the study area.

5. The hydrothermally altered rocks underwent elemental mass gains and losses.

6. The mineralization trends in the NE-SW direction with breakages in the ore morphology. The ore has been overturned, dismembered and follow no pattern in the textural properties at most locations, the massive sulphides are found deeper whiles the stockwork are found at shallow levels.

7. The mineralization occurring in the Ortaklar Deposit may have occured in two stages. First stage is a sulphide poor magnetite rich stage whiles sulphide rich magnetite poor mineralization occur in the second stage.

8. The megascopic and microscopic texture and stable isotope thermometry shows that mineralization occurred in two stages. First stage of mineralization consist of high temperature deposition of magnetites whiles the second stage is a sulphide-rich stage.

9. The mineral constituent of this deposit are pyrites, magnetite, chalcopyrite, sphalerite and bornite in decreasing order of content. The gangue minerals associated with the mineralization are mostly chlorites, carbonates and quartz.

10. Massive ore dominates the area with poorly developed stockwork zones. Massive ore consist of pyrites and magnetite whiles the stockwork zone is composed of pyrites, magnetite and gangue minerals.

11. The calculated oxygen isotope geothermometry between quartz and magnetite pairs has a range between $250^{O}C$ to $427^{O}C$ with an average of $359^{O}C$. The sulphur isotope geothermometry between pyrites and chalcopyrite pairs fall between $202^{O}C$ and $364^{O}C$ with an average value of $264^{O}C$. In addition, the calculated chlorite thermometry has a limited range from $225^{O}C$ to $255^{O}C$ with an average $236^{o}C$.

12. The source of hydrothermal fluid responsible for the mineralization and alterations is interpreted to be magmatic fluid, which was later modified to some extend by interacting with underlying rocks and the source of sulphur is interpreted to be leached magmatic sulphur in the ore-forming fluids.

13. For the source of the magnetite, it might have been leached and deposited during the serpentinization of the ultramafic rocks. To support this proposal, further detailed studies and chemical analysis need to be made.

8. REFERENCES

Aagard P., O. J. 2005. Convergence history across Zagros (Iran): constraints from collisional and earlier deformation. International Journal of Earth Sciences Geologische Rundschau, 94, 401–19.

Bahçeci, A., Dağlıoğlu, C., Ateş, M.Z., Kılıçoğlu, G., 1984. Gaziantep Kilis Musabeyli Burç yöresinin manganez ve demir aramaları jeoloji raporu. General Directorate of the Mineral Research and Exploration (Turkey) Report No. 7568 Ankara. (Unpublished).

Barrett, T.J., and MacLean, W.H. 1999. Volcanic sequences, lithogeochemistry, and hydrothermal alteration in some bimodal volcanic-associated massive sulfide systems. In Volcanic-associated massive sulfide deposits: processes and examples in modern and ancient settings. Edited by C.T. Barrie and M.D. Hannington, Reviews in Economic Geology, 8, 101-131.

Bernoulli , D., Weissert, H., and Blome, C. 1990. Evolution of the Triassic Hawasina Basin, central Oman Mountains. In A. Robertson, M. Searle, and A. Ries (Eds.), The geology and tectonics of the Oman Region. 49, 189-202.

Cathelineau, M. 1988. Cation site occupancy in chlorites. Clay Minerals, 23, 471-485.

Cathelineau, M., and Nieva, D. 1985. A chlorite solid solution geothermometer. The Los Azufrez (Mexico) geothermal system. Contributions to Mineralogy and Petrology, 91, 235-244.

Chiba, H., Chacko, T., Clayton, R., and Goldsmith, J. R. 1989. Oxygen isotope fractionations involving diopside, forsterite, magnetite, and calcite: Application to geothermometry. Geochim. Cosmochim. Acta, 53, 2985-2995.

Clark, A. H. 1990. The slump breccias of the Toquepala porphyry Cu–Mo. deposit, Peru: Implications for fragment rounding in hydrothermal breccias. Economic Geology, 85, 1677–1685.

Clayton, R.N. and Mayeda, T.K., 1963. The use of bromine pentafluoride in the extraction of oxygen from oxides and silicates for isotopic analysis, Geochim. Cosmochim. Acta, 27, 43-52.

Clayton, R. N., O'Neil, J. R., and Mayeda, T. K. 1972. Oxygen isotope exchange between quartz and water. Journal Of Geophysical Research, 77(17), 3057–3067.

Craig, J. R., Vokes, F. M., and Solberg, T. N. 1999. Pyrite: physical and chemical textures. Mineral Deposita, 34, 82–101.

De Caritat, P., Hutcheon, I., and Walshe, J. L. 1993. Chlorite geothermometry: a review. Clays and Clay Minerals, 41, 219-239.

Dirik, K., Guncuoglu, M., and Kozlu, H. 1997. General characteristics of pre-Alpine and Alpine Terranes in Turkey: Explanatory notes to the terrane map of Turkey. Annales Geologique de Pays Hellenique, 37, 515–536.

Dyar, M. D., Guidotti, C. V., Harper , G. D., McKibben, M. A., and Saccocia, P. J. 1992. Controls on ferric iron in chlorite. Geolological Society of American Abstracts Programs, 24, 130.

Elmas, A., and Yilmaz , Y. 2003. Development of an oblique subduction zone - Tectonic evolution of the tethys suture zone in southeast Turkey. International Geology Review, 45, 9, 827-840.

El-Sharkawy, M. F. 2000. Talc mineralization of ultramafic affinity in the Eastern Desert of Egypt. Mineralium Deposita, 35, 346-363.

Finlow-Bates, T., and Large, D. L. 1978. Water depth as a major control on the formation of submarine exhalative ore deposits. Geol. Jahrb., D 30, 27–39.

Fleet, M. E. 1970. Structural aspects ofthe marcasite-pyrite transformation. Canadian Mineralogist, 10, 225-231.

Floyd , P. A., and Winchester, J. A. 1975. Magma type and tectonic setting discrimination using immobile elements. Earth and Planetary Science Letters, 27, 211-218.

Foster, M. D. 1962. Interpretation of the composition and classification of chlorites. US Geol. Surv. Prof. Paper, 414A 27.

Fry, B., and Chumchal, M.M. 2011. Sulfur stable isotope indicators of residency in estuarine fish. Limnol. Oceanogr., 56, 5, 1563–1576.

Galley, A. G., and Koski, R. A. 1999. Setting and characteristics of ophiolite-hosted volcanogenic massive sulfide deposits. In C. T. Barrie, and M. D. Hannington (Eds.), Volcanic-Associated Massive Sulfide Deposits: Processes and Examples in Modern and Ancient Settings. Reviews in Economic Geology, 8, 215-236.

Gencuoğlu, M. C., and Turhan, N. 1984. Geology of the Bitlis metamorphic belt, in O. Tekeli and M.C. Göncüoğlu (eds) Geology of the Taurus Belt. Proceedings of the International Symposium on the Geology of The Taurus belt. Ankara: Mineral Research and Exploration Institute of Turkey. 237-244.

Grant, J. A. 1986. The Isocon Diagram A Simple Solution to Gresens' Equation for Metasomatic Alteration. Economic Geology, 81, 1976-1982.

Gresen, R. L. 1962. Composition-Volume relationship of metasomatism. Chemical Geology, 2, 47-65.

Gronvold, F., and Westrum , E. F. 1976. Heat capacities of iron disulfides. Thermodynamics of marcasite from 5 to 700 K, pyrite from 300 to 780 K, and the transformation of marcasite to pyrite. Journal of Chemical Thermodynamics, 8, 1039-1048.

Güvench , T. 1963. Gaziantep-Kilis bölgesi stratigrafis. MTA Jeoloji Etüdleri Dairesi rapor arşivi.

Hannington, M. D., and Scott, S. D. 1985. A caldera-hosted silica-sulfate-sulfide deposit, Axial Seamount, central Juan de Fuca Ridge, N.E. Pacific Ocean. G.A.C.-M.A.C. Joint Ann. Mtg. Prog. Abstr. 10, A24.

Henley, R. W., and Thomley, P. 1979. Some geothermal aspects of polymetallic massive sulfide formation. Econ. Geol., 74, 1600–1612.

Hillier, S., and Velde, B. 1991. Octahedral occupancy and chemical composition of diagenetic (low-temperature) chlorites. Clay Minerals, 26, 149-168.

Hoefs, J. 1973. Stable Isotope Geochemistry. New York: Springer-Verlag Berlin Heidelberg.

Huston, D. L., 1993. The effect of alteration and metamorphism on wall rocks to the Balcooma and Dry River South volcanic-hosted massive sulfide deposits,Queensland, Australia. Journal of Geochemzcal Exploratton, 48, 277-307.

Huston, D. L., and Cozens, G. J. 1994. The geochemistry and alteration of the White Devil porphyry: Mineral. Deposita, 29, 275-287.

İlhan, S. 2013. The Origin of Massive Sulfide Deposits Within The Kocali Complex (Adıyaman): PhD Thesis. (in Turkish with English Abstract), Institute of Natural And Applied Sciences. Çukurova University, Adana/Turkey.

Jowett, E. C. 1991. Fitting iron and magnesium into the hydrothermal chlorite geothermometer. Geol. Assoc. Can. – Mineral. Assoc. Can. – Soc. Econ. Geol., Program Abstr, 16, A62.

Kaplan, I. R., Sweeney, R. E., and Nissembaum, A., 1969. Sulfur isotopes studies on Red Sea geothermal brines and sediments. In E. T. Degens, and D. A. Ross (Eds.), Hot Brines and Recent Heavy Metal Deposits in the Red Sea. Springer-Verlag, 474-498.

Kavalieris, I., Walshe, J. L., Halley, S., and Harrold,, B. P., 1990. Dome-related gold mineralization in the Pani Volcanic Complex, North Sulawesi, Indonesia: a study of geologic relations, fluid inclusions, and chlorite compositions. Economic Geology, 85, 1208-1225.

Kazmin V., R. L., Kazmin, V., Ricou , L. E., and Sbortshikov, I. M. 1986. Structure and evolution of the passive margin of the eastern Tethys. Tectonophysics, 123, 153-179.

Kjekshus, A., and Rakke, T. 1975. Compounds with marcasite type crystal structure. XI. High temperature studies of chalcogenides. Acta Chemica Scandinavica A,, 29, 443-452.

Kohn, M. J., 1999. Why most “dry” rocks should cool “wet”. Am Miner, 84, 570–580.

Kranidiotis, P., and MacLean, W., 1987. Systematic of of chlorite alteration the Phelps Dodge massive sulfide deposit, Matagami, Quebec. Economic Geology, 82, 1898-1911.

Kuşcu, G., and Friedman, R., 2013. Late Cretaceous to middle Eocene magmatism and metallogeny of a portion of the Southeastern Anatolian Orogenic Belt, east central Turkey. Economic Geology, 108, 641-666.

Large, R. R., Bull, S. W., and Maslennikov, V. V., 2011. A carbonaceous sedimentary source-rock model for Carlin-type and orogenic gold deposits. Econ. Geol., 106, 331–358.

Le Maitre, W., Bateman, P., Dudek, A., Keller, J., and Et al., 1989. A Classification of Igneous rocks and Glossary of Term Recommendations of the International Union of Geological Science Subcommission on the Systematics of Igneous Rock. Blackwell Scientific.

MacLean, W. H., 1990. Mass change calculations in altered rock series. Mineralium Deposita, 25, 44–49.

MacLean, W. H., and Kranidiotis, P., 1987. Immobile elements as monitors of mass transfer in hydrothermal alteration; Phelps Dodge massive sulfide deposit, Matagami, Quebec. Economic Geology, 82, 951-962.

McDonough, W. F., and Sun, S. S., 1995. Composition of the Earth. Chemical Geology, 120, 223-253.

McKibben , M. A., and Elders, W. A., 1985. Fe-Zn-Cu-Pb mineralization in the Salton Sea geothermal system. Econ. Geol., 80, 539-559.

Meschede, M., 1986. A method of discriminating between different types of mid-ocean ridge basalts and continental tholeiites with the Nb-Zr-Y diagram. Chemical Geology., 56, 207-218.

Misra, K. 1999. Understanding Mineral Deposits. Dordrecht, Boston, Mass: Kluwer Academic Publishers. 845.

Nail Yıldırıma, C. D., 2016. A magnetite-rich Cyprus-type VMS deposit in Ortaklar: A unique VMS style in the Tethyan metallogenic belt, Gaziantep, Turkey. Ore Geology Reviews, 79, 425-442.

Ohmoto, H., and Rye, R. O., 1979. Isotopes of Sulfur and Carbon. In H. L. Barnes (Ed.), Geochemistry of Hydrotermal Ore Deposits. John Wiley and Sons, 509-567.

Okay, A. I., 2008. Geology of Turkey: A Synopsis. Anschnitt, 21, 19-42.

Okay, A. I., and Tüysüz, O., 1999. Tethyan sutures of northern Turkey. In "The Mediterranean Basins: Tertiary extension within the Alpine orogen". (L. J. B. Durand, Ed.) Geological Society, London, Special Publications, 156, 475-515.

Pearce, J. A., 1982. Trace elements characteristics of lavas from destructive plate boundaries. In E. S. Thorpe (Ed.), Andesites. New York: Wiley, 525-548

Pearce, J. A., 1983. Role of the subcoontinental lithosphere in magma genesis at active continental margins. In C. J. Hawkeswoth , and M. J. Norry (Eds.), Continental basalts and Mantle Xenoliths. Shiva, Nantwitch, 230-249.

Perincek, D., 1978. Geological investigation and petroleum prospects of the region between Celikhan-Sincik-Kocali (city ofAdiyaman). Ph.D. Thesis, Istanbul Univ., TPAO Report, 1250. (in Turkish, unpublished).

Perincek, D., 1979. Geological investigation of the Çelikhan-Sincik- Koçali area (Adıyaman Province). İst. Üniv. Fen. Ed. Mec., Seri. B, 127–147.

Perincek, D., 1979a. Interrelation of the Arabian and Anatolian plates. Guidebook for excursion B, First Geol. Congr. Middle East. The Geol. Soc. Turkey, 34.

Perincek, D., 1979b. Geological investigation of the region between Celikhan-Sincik-Kocali (city of Adiyaman). TPAO Report, 1394. (in Turkish, unpublished).

Perinçek, D., 1990. Hakkari ili ve dolayının stratigrafisi Güneydoğu Anadolu Türkiye. Türkiye Petrol Jeologları Derneği Bülteni, 2, 21-68.

Pirajno, F., 2009. Hydrothermal Processes and Mineral Systems. Berlin: Springer.

Ramdohr, P., 1981. The Ore Minerals and Their Intergrowth. New York: Pergamon Press.

Ricou, L. E., and Marcoux, J. 1980. Organisation générale et role structural des radiolarites et des ophiolites le long du système alpino-méditerranéen. Bull. Soc. Géol. France, 7, l-14.

Rigo de Reghi, M., and Cortesini, A., 1964. Gravity and Tectonics in Foothills Structure Belt of Southeast Turkey. American Association of Petroleum Geology Bulletin, 8, 1911-1937.

Rising, B. A., 1973. Phase relations among pyrite, marcasite, and pyrrhotite below 300°C. Ph.D. thesis, PA: The Pennsylvania State University, University Park, 192.

Robertson , A., Ustaömer, T., Parlak, O., Ünlügenç, U., Taslı, K., and İnan, N., 2006. The Berit transect of the Tauride thrust belt, S. Turkey: Late Cretaceous–Early Cenozoic accretionary/ collisional processes related to closure of the southern Neotethys. Journal of Asian Earth Sciences, 27, 108–145.

Robertson, A. F., Parlak, O., Rızaoğlu, T., Unlügenç, U., İnan, N., Taslı, K., and Ustaömer, T., 2007. Tectonic evolution of the South Tethyan ocean: evidence from the Eastern Taurus Mountains (Elazığ region, SE Turkey). in: A.C. Ries, R.W.H. Butler, R.H. Graham (Eds.), Deformation of the Continental Crust: The Legacy of Mike Coward, Geological Society, London, Special Publications, 272, 231–270.

Robertson, A. P., 2007. Tectonic evolution of the South Tethyan Ocean: evidence from the Eastern Taurus Mountains (Elazığ region, SE Turkey). In A. Reis, R. Butler, and R. Graham (Eds.), Deformation of the Continental Crust. The Legacy of Mike Coward. Geological Society, London, 272, 231–270.

Robertson, A. U., 2004. Testing models of Late Palaeozoic-early Mesozoic orogeny: support for an evolving. Geological Society of London., 161, 501–511.

Rolland, Y.,Sosson, M.,Adamia, Sh.,Sadradze, N., 2011. Prolonged Variscan to Alpine historyan of an active Eurasian margin (Georgia, Armenia) revealed by 40Ar/39Ar dating. Gondwana Research, 20, 798–815.

Rollinson, H. R., 1993. Using geochemical data: evaluation, presentation, interpretation. New York: Techn., Longman Scient. John Wiley and Sons, 352.

Rollinson, H. R., 1993. Using geochemical data: Evaluation, presentation, interpretation (6th ed.). Harlow, Essex, England: Longman Scientific and Technical.

Ruiz Cruz, M. D., and NIieto, J. M., 2006. Chemical and structural evolution of "metamorphic vermiculite" in metaclastic rocks of the Betic Cordillera, Málaga, Spain a synthesis. Canadian Mineralogist, 44, 249-265.

Rye, R. O., and Ohmoto, H., 1974. Sulfur and Carbon Isotopes and Ore Genesis A Review. Economic Geology, 69, 826-842.

Savostin, L.A., Sibuet, J.-C., Zonenshain, L.P., Le Pichon, X., Roulet, M.-J.,. 1986. Kinematic evolution of the Tethys belt from the Atlantic ocean to the Pamir since the Triassic. Tectonophysics, 123, 1–35.

Sengör, C., and Yilmaz, Y., 1981. Tethyan Evolution Of Turkey: A Plate Tectonic Approach. Tectonophysics, 75, 181-241.

Senel, M., 2002. The Geological map of Turkey, Sheet Hatay, 1:500 000. Ankara: Directorate of Mineral Explorations (MTA).

Shanks, W. C., and Bischoff, I. L., 1975. Sulfur isotopes and sulfide deposition in the Red Sea geothermal. Geol Soc. Am. Annu. Mtg. (abstract) Programs, 1266.

Shervais, M., 1982., Ti-V plots and the petrogenesis of modern and ophiolitic lavas. Earth Plan. Sci. Lett., 59, 101-118.

Sun, S. S., and Mc Donough , W. F., 1989. Chemical and isotopic systematics of oceanic basalts: implications for mantle composition and processes. In A. Saunders, and J. Norry (Eds.), Magmatism in the ocean basin. 42, 313-345.

Sungurlu, O., 1972. Geology of the region between Golbasi-Gerger district-VI TPAO Rept. 802. in Turkish, unpublished.

Sungurlu, O., 1974. VI. Bölge kuzey sahalarının jeolojisi. Türkiye ikinci petrol kongresi, 85-107.

Taylor, H. P., 1997. Oxygen and hydrogen isotope relationships in hydrothermal mineral deposits. In H. L. Barnes (Ed.), Geochemistry of hydrothermal ore deposits. New York: John Wiley and Sons. 229–302.

Terlemez, H., Şentürk, K., Ateş, Ş., Ümengen, M., and Oral, A., 1992. Gaziantep dolayının ve Pazarcık-şakçagöz-Kilis-Elbeyli-Oğuzeli arasının jeolojisi. Ankara: yayınlanmamış.

Tuna, D., 1973. VI. Bölge litostratigrafi birimleri adlamasının açıklayıcı raporu:. Ankara: Unpublished.

Ulu, U., Genc, Ş., Giray, S., Metin, Y. and Çörekçioğlu, E., 1991. Belveren-Araban-Yavuzeli-Nizip-Birecik dolayının jeolojisi ve Senozoyik yaşlı volkanik kayaçların petrolojisi ve bölgesel yayılımı. Maden Tetkik ve Arama Raporu No: 9226. Ankara: Unpublished.

Varol, E., Bedi, Y., Tekin, U., and Uzunçimen, S., 2011. Geochemical and petrological characteristics of late Triassic basic volcanic rocks from the Koçali Complex; SE Turkey: implications for the Triassic evolution of southern Tethys. Ofioliti, 36, 101–115.

Wilson, H., and Krummenercher, R., 1957. Geology and Oil Prospects of The Gaziantep Region, Southeast Turkey. TPOA Report No.839 (unpublished).

Winchester, J. A., and Floyd, P. A., 1977. Geochemical discrimination of different magma series and their differentiation products using immobile elements. Chemical Geology, 20, 325-343.

Xie, X., Byerly, G. R., and Ferrell, R. J., 1997. IIb trioctahedral chlorite from the Barberton greenstone belt: crystal structure and rock composition constraints with implications to geothermometry. Contributions to Mineralogy and Petrology, 126, 275-291.

Yavuz , F., Kumral, M., Karakaya, N., Karakaya, M. Ç., and Yildirim, D. K., 2015. A Windows program for chlorite calculation and classification. Computers and Geosciences, 81, 101–113.

Yaylali Abanuz G. and Tüysüz N., 2010, Chemical, mineralogical, and mass-change examinations across a gold bearing vein zone in the Akoluk area, Ordu, NE Turkey", Neues Jahrbuch Fur Mineralogie-Abhandlungen, 1, 11-22.

Yildirim , N., Ay, Y., Çakır, C., İlhan, S., Dönmez, C., and Yıldırım, E., 2010. Koçali Ofiyolitik Karmaşığı'nın Metalojenik (Cu-Au) Önemi. IV. Ulusal Jeokimya Sempozyum Bildirileri, Elazığ, 79-80.

Yildirim, N., Dönmez, C., Kang, J., Lee, I., Pirajno, F., Yildirim, E., and Chang, S., 2016. A magnetite-rich Cyprus-type VMS deposit in Ortaklar: A unique VMS style in the Tethyan metallogenic belt, Gaziantep, Turkey. Ore Geology Reviews, 79, 425–442.

Yiğitbaş, E. and Yılmaz, Y., 1996, Post-late Cretaceous strike-slip tectonics and its implications on the Southeast Anatolian orogen - Turkey. International Geology Review, (SCI), 38, 9, 818-831.

Yilmaz, E., and Duran , O., 1997. Güneydoğu Anadolu Bölgesi otokton ve allokton birimler stratigrafi adlama kılavuzu "Lexicon". Türkiye Petrolleri A.O. Araştırma Merkezi grubu Başkanlığı, Eğitim Yayınları, 460.

Yilmaz, Y., 1990. Comparisons of young volcanic association of western and eastern Anotolia formed under a compressional regime: a review. Journal of Volcanology and Geothermal Research, 44, 69-87.

Yilmaz, Y., 1993. New evidence and model on the evolution of the southeast Anatolian orogen. Geological Society of America Bulletin, 105, 252-271.

Yilmaz, Y., and Yiğitbaş, E., 1990. SE Anadolu'nun farklı ofiyolitik-metamorfik birlikleri ve bunlarin jeolojik evrimdeki rolü. Eighth Petroleum Congress of Turkey, Ankara. 128-140

Yilmaz, Y., and Yıldırım, M., 1991. Güneydoğu Anadolu orojenik kuşağının ekaylı zonu. Türkiye Petrol Jeologları Derneği Bülteni, 3, 57-73.

Yoldemir, O., 1987. Suvarlı-Haydarlı-Narlı-Gaziantep arasında kalan alanın jeolojisi, TPAO Arama Grubu Rapor no. 275,. Ankara.

Yoldemir, O., 1988. Sakçagoz, Kartal, Yaylacık (Gaziantep batısı) cıvarının jeolojisi, yapısal durumu ve petrol olanakları. TPOA Rapor No 2453, Ankara.

Zane, A., and Weiss, Z., 1998. A procedure for classifying rock-forming chlorites based on microprobe data. Rendiconti Lincei, 9, 51–56.

Zang, W., and Fyfe, W. S., 1995. Chloritization of the hydrothermally altered bedrock at the Igarapé Bahia gold deposit, Carajás, Brazil. Mineralium Deposita, 30, 30-38.

9. APPENDICES

Table 9.1. Results of the chemical analysis of volcanic rocks from Ortaklar

Sample type	Sample	Depth	SiO_2	Al_2O_3	Fe_2O_3	MgO	CaO	Na_2O	K_2O	TiO_2	P_2O_5	MnO	Cr_2O_3	LOI	Sum
		metres (m)	%	%	%	%	%	%	%	%	%	%	%	%	%
Drill core Samples	**S52.1**	170.3	42.28	14.86	10.65	6.62	10.41	2.97	1.39	0.97	0.08	0.22	0.058	9.3	99.79
	S523	214.9	46.96	16.73	9.24	7.27	11.46	2.62	0.02	0.96	0.06	0.24	0.032	4.2	99.79
	S52.10	393.9	45.57	14.72	9.78	6.36	11.02	3.59	0.83	0.99	0.07	0.23	0.060	6.6	99.80
	S52.36	336.8	41.00	13.87	8.99	6.69	11.39	2.97	1.55	0.89	0.08	0.31	0.042	12.0	99.80
	S52.40	345.4	43.29	13.06	9.34	7.02	13.02	2.11	0.83	0.74	0.06	0.20	0.055	10.1	99.81
	S52.42	365.8	46.88	15.40	8.85	8.03	11.69	2.58	0.52	0.93	0.06	0.19	0.059	4.6	99.78
	SK33.7	168.6	46.17	15.65	9.51	7.03	12.16	2.36	0.67	0.90	0.06	0.15	0.048	5.1	99.80
	S56.7	31.6	48.30	16.09	9.49	6.47	11.83	2.94	0.10	0.90	0.06	0.19	0.053	3.4	99.79
	S56.8	61.1	45.59	14.05	9.25	9.02	9.09	2.63	0.01	0.87	0.05	0.16	0.048	9.0	99.76
	S56.10	96.5	41.93	11.89	9.75	14.53	6.84	1.06	0.01	0.64	0.04	0.19	0.084	12.7	99.69
	S56.17	238.6	46.59	13.29	9.38	9.99	11.53	1.63	<0.01	0.76	0.05	0.18	0.099	6.2	99.75
	S56.18	244.4	45.95	14.72	8.85	8.58	11.03	2.23	0.03	0.86	0.05	0.16	0.048	7.2	99.76
	S56.21	256.5	35.04	12.34	15.49	7.68	12.00	1.02	0.81	0.56	0.05	0.33	0.030	14.3	99.64
Hand Samples	**OU9**	82	43.13	15.28	7.12	7.01	10.91	0.43	0.18	0.60	0.03	0.12	0.045	14.9	99.81
	OU12	120	45.88	14.99	9.76	6.37	11.58	1.97	1.74	0.94	0.07	0.25	0.049	6.2	99.80
	OU15	125	44.93	14.58	10.14	7.11	11.17	2.30	0.99	0.93	0.07	0.17	0.047	7.4	99.79
	OP3	85	40.56	14.99	7.54	7.48	14.22	1.92	0.60	0.65	0.03	0.14	0.055	11.6	99.80

Continuation of the Table 9.1.

Sample type	Sample	Depth	Ba	Be	Co	Cs	Ga	Hf	Nb	Rb	Sn	Sr	Ta	Th	U	V	W	Zr	Y
		metres (m)	ppm	ppm	ppm	ppm	ppm	ppm	ppm	ppm	ppm	ppm	ppm	ppm	ppm	ppm	ppm	ppm	ppm
Drillcore Samples	**S52.1**	170.3	22	<1	46.2	0.7	13.6	1.4	0.7	18.0	<1	121.5	<0.1	<0.2	<0.1	291	<0.5	48.1	25.3
	S52.3	214.9	10	<1	38.8	<0.1	15.8	1.3	0.7	<0.1	<1	134.9	<0.1	<0.2	<0.1	268	<0.5	45.6	22.8
	S52.10	393.9	23	<1	43.3	0.4	12.2	1.6	0.6	11.9	<1	162.9	<0.1	<0.2	<0.1	275	<0.5	48.5	24.9
	S52.36	336.8	44	<1	39.6	0.6	12.5	1.3	0.7	17.2	<1	132.5	<0.1	<0.2	<0.1	243	<0.5	44.1	22.6
	S52.40	345.4	26	<1	39.4	<0.1	12.0	1.0	0.5	13.8	<1	116.6	<0.1	<0.2	<0.1	236	<0.5	30.5	20.3
	S52.42	365.8	16	<1	50.3	<0.1	14.0	1.4	0.5	5.9	<1	138.4	<0.1	<0.2	<0.1	262	<0.5	43.6	21.5
	SK33.7	168.6	22	<1	33.2	0.3	12.9	1.4	0.6	17.9	<1	129.5	<0.1	<0.2	0.2	250	<0.5	45.0	21.2
	S56.7	31.6	18	2	36.6	<0.1	14.4	1.6	0.2	1.6	<1	185.3	<0.1	<0.2	<0.1	282	<0.5	41.1	23.4
	S56.8	61.1	9	<1	39.0	<0.1	12.0	1.2	0.4	<0.1	<1	164.5	<0.1	<0.2	<0.1	262	<0.5	39.3	20.9
	S56.10	96.5	12	<1	41.4	<0.1	9.9	1.0	0.2	<0.1	<1	78.0	<0.1	<0.2	<0.1	192	<0.5	30.3	18.0
	S56.17	238.6	11	<1	53.7	<0.1	11.3	1.1	0.2	<0.1	<1	111.0	<0.1	<0.2	<0.1	238	<0.5	35.5	19.4
	S56.18	244.4	33	<1	40.1	<0.1	12.4	1.3	0.3	<0.1	<1	179.9	<0.1	<0.2	<0.1	265	<0.5	40.2	21.9
	S56.21	256.5	5	<1	66.2	<0.1	11.0	0.8	<0.1	2.9	<1	26.9	<0.1	<0.2	1.1	142	<0.5	28.2	14.4
Hand Samples	**OU.9**	82	7	<1	33.6	<0.1	16.3	0.9	<0.1	2.8	<1	62.6	<0.1	<0.2	<0.1	218	<0.5	25.6	15.5
	OU.12	120	13	<1	37.4	0.4	14.3	1.4	0.4	21.0	<1	123.4	<0.1	<0.2	0.2	270	<0.5	47.0	24.9
	OU.15	125	15	<1	35.8	0.3	12.9	1.3	0.4	14.8	<1	180.9	<0.1	<0.2	0.2	272	<0.5	45.3	22.3
	OP.3	85	18	<1	39.1	<0.1	12.4	0.9	0.1	5.6	<1	146.7	<0.1	<0.2	<0.1	203	<0.5	29.5	16.4

Continuation of the Table 9.1.

Sample type	Sample	Depth	La	Ce	Pr	Nd	Sm	Eu	Gd	Tb	Dy	Ho	Er	Tm	Yb	Lu	Total REE	LREE /HREE	Eu/Eu*
		metres (m)	ppm	ppm	ppm	ppm	ppm	ppm	ppm	ppm	ppm	ppm	ppm	ppm	ppm	ppm	ppm		
Drillcore Samples	**S52.1**	170.3	1.9	4.1	0.93	5.4	2.25	0.82	3.34	0.63	4.32	0.93	2.85	0.43	2.61	0.41	104.32	0.99	0.15
	S52.3	214.9	1.5	4.3	0.86	4.4	1.86	0.75	3.02	0.59	3.79	0.85	2.57	0.38	2.66	0.4	96.33	0.96	0.15
	S52.10	393.9	1.9	5.1	0.87	5.3	1.94	0.81	3.19	0.62	4.26	0.98	2.72	0.41	2.57	0.42	104.49	1.05	0.16
	S52.36	336.8	2.2	4.1	0.9	5.3	2.06	0.75	2.81	0.58	4.01	0.9	2.74	0.39	2.41	0.41	96.26	1.07	0.15
	S52.40	345.4	1	3.2	0.64	3.5	1.46	0.57	2.49	0.47	3.43	0.73	2.21	0.32	2.04	0.31	73.17	0.86	0.14
	S52.42	365.8	1.3	4.1	0.82	4.9	1.88	0.75	2.95	0.57	3.97	0.82	2.68	0.39	2.48	0.39	93.1	0.96	0.16
	SK33.7	168.6	1.6	4	0.81	5	1.78	0.71	2.94	0.58	3.83	0.83	2.59	0.36	2.42	0.37	94.02	1.00	0.15
	S56.7	31.6	1.4	4.6	0.81	5.1	1.91	0.74	3.09	0.58	3.8	0.86	2.72	0.38	2.4	0.38	93.27	1.02	0.15
	S56.8	61.1	1.3	3.8	0.72	4.4	1.71	0.71	2.78	0.55	3.45	0.8	2.49	0.37	2.27	0.37	85.92	0.97	0.16
	S56.10	96.5	1.1	2.6	0.56	3.1	1.21	0.57	2.2	0.45	2.84	0.66	2.08	0.28	1.85	0.3	68.1	0.86	0.17
	S56.17	238.6	1.2	3.5	0.63	4	1.47	0.61	2.49	0.49	3.22	0.7	2.15	0.32	2.1	0.32	78.1	0.97	0.15
	S56.18	244.4	1.2	3.5	0.71	4.9	1.88	0.71	2.91	0.56	3.63	0.84	2.44	0.38	2.43	0.36	88.55	0.95	0.15
	S56.21	256.5	2	2.6	0.46	2.7	1.21	0.3	1.74	0.35	2.4	0.53	1.68	0.27	1.71	0.26	60.81	1.04	0.10
Hand Samples	**OU.9**	82	0.9	2.1	0.47	2.8	1.15	0.45	1.89	0.38	2.46	0.53	1.69	0.26	1.75	0.26	58.19	0.85	0.15
	OU.12	120	1.6	4.2	0.88	5.1	1.88	0.75	3.22	0.61	3.98	0.89	2.91	0.41	2.55	0.38	101.26	0.96	0.15
	OU.15	125	2.1	4.2	0.82	5.3	2.02	0.76	2.95	0.59	4.07	0.85	2.58	0.36	2.55	0.39	97.14	1.06	0.15
	OP.3	85	0.9	2.5	0.53	2.9	1.27	0.52	2.21	0.43	2.83	0.6	1.78	0.27	1.9	0.27	64.81	0.84	0.15

Continuation of the Table 9.1.

Sample type	Sample	Depth	Cu	Pb	Zn	Ni	As	Cd	Sb	Bi	Ag	Au	Hg	Tl	Se
		metres (m)	ppm	ppm	ppm	ppm	ppm	ppm	ppm	ppm	ppm	ppb	ppm	ppm	ppm
Drillcore Samples	**S52.1**	170.3	86.3	0.6	106	74.7	8.3	0.4	0.1	<0.1	<0.1	1.0	<0.01	<0.1	<0.5
	S52.3	214.9	83.2	0.5	50	58.8	<0.5	0.2	<0.1	<0.1	<0.1	1.3	<0.01	0.5	<0.5
	S52.10	393.9	49.0	0.4	61	69.4	4.4	<0.1	<0.1	<0.1	<0.1	<0.5	<0.01	<0.1	<0.5
	S52.36	336.8	59.1	0.3	70	53.0	4.1	<0.1	<0.1	<0.1	<0.1	0.6	<0.01	<0.1	<0.5
	S52.40	345.4	62.0	0.2	50	78.3	0.7	<0.1	<0.1	<0.1	<0.1	<0.5	0.01	<0.1	<0.5
	S52.42	365.8	96.2	1.1	45	133.8	1.3	<0.1	<0.1	<0.1	<0.1	0.9	<0.01	<0.1	<0.5
	SK33.7	168.6	61.6	0.3	43	39.9	<0.5	<0.1	<0.1	<0.1	<0.1	<0.5	0.01	<0.1	<0.5
	S56.7	31.6	72.1	0.2	40	66.2	2.5	<0.1	<0.1	<0.1	<0.1	2.1	0.03	0.2	<0.5
	S56.8	61.1	82.2	0.3	54	79.4	<0.5	<0.1	<0.1	<0.1	<0.1	0.5	<0.01	<0.1	<0.5
	S56.10	96.5	82.2	0.7	98	280.7	0.6	0.1	<0.1	<0.1	<0.1	2.0	0.01	<0.1	<0.5
	S56.17	238.6	91.1	0.2	42	264.1	<0.5	<0.1	<0.1	<0.1	<0.1	1.3	<0.01	<0.1	<0.5
	S56.18	244.4	81.2	0.3	46	62.4	<0.5	<0.1	<0.1	<0.1	<0.1	<0.5	<0.01	<0.1	<0.5
	S56.21	256.5	40.3	1.5	1606	98.0	3.6	4.0	<0.1	<0.1	<0.1	18.3	<0.01	<0.1	<0.5
Hand Samples	**OU.9**	82	59.3	1.2	59	92.1	1.3	0.5	<0.1	<0.1	<0.1	<0.5	<0.01	<0.1	<0.5
	OU.12	120	100.3	0.3	66	43.7	2.2	<0.1	<0.1	<0.1	<0.1	0.9	<0.01	<0.1	<0.5
	OU.15	125	44.8	0.3	67	51.0	2.4	<0.1	<0.1	<0.1	<0.1	<0.5	<0.01	<0.1	<0.5
	OP.3	85	74.5	0.5	42	104.3	7.3	0.9	0.2	<0.1	<0.1	<0.5	<0.01	<0.1	<0.5

Table 9.2. Detection limits of all elements analysed

Element	SiO_2	Al_2O_3	Fe_2O_3	CaO	MgO	Na_2O	K_2O	MnO	TiO_2	P_2O_5	Cr_2O_3
Detection Limit	0.01%	0.01%	0.04%	0.01%	0.01%	0.01%	0.04%	0.01%	0.01%	0.01%	0.002%

Element	Ba	Ag	As	Au	Bi	Cd	Cu	Hg	Mo	Ni	Pb
Detection Limit	5 ppm	0.1 ppm	0.5 ppm	0.5 ppb	0.1 ppm	0.1 ppm	0.1 ppm	0.01 ppm	0.1 ppm	0.1 ppm	0.1 ppm

Element	Sb	Se	Tl	Zn	Be	Ce	Co	Cs	Dy	Er	Eu
Detection Limit	0.1 ppm	0.5 ppm	0.1 ppm	1 ppm	1 ppm	0.1 ppm	0.2 ppm	0.1 ppm	0.05 ppm	0.03 ppm	0.02 ppm

Element	Ga	Gd	Hf	Ho	La	Lu	Nb	Nd	Ni	Pr	Rb
Detection Limit	0.5 ppm	0.05 ppm	0.1 ppm	0.02 ppm	0.1 ppm	0.01 ppm	0.1 ppm	0.3 ppm	20 ppm	0.02 ppm	0.1 ppm

Element	Sc	Sm	Sn	Sr	Ta	Tb	Th	Tm	U	V	W
Detection Limit	1 ppm	0.05 ppm	1 ppm	0.5 ppm	0.1 ppm	0.01 ppm	0.2 ppm	0.01 ppm	0.1 ppm	8 ppm	0.5 ppm

Element	Y	Yb	Zr
Detection Limit	0.1 ppm	0.05 ppm	0.1 ppm

RÉSUMÉ

Born on 25-10-1987, Huseini ZAKARIA completed his primary education at Khalid Ibn Walid primary and continued to GHATECO junior high school in Koforidua, Ghana. He then proceeded to Pope John Senior High School and Junior Seminary to pursue his senior high school education as a General Science student also in Koforidua, Ghana. After completion he gained admission to University of Ghana in Accra, Ghana and finally graduated in 2012 with a BSc in Geology. In 2014, he began his studies at Karadeniz Technical University in Trabzon, Turkey as a Masters student in Geological Engineering. He speaks fluent English, has intermediate proficiency in Turkish and a beginner in Russian language.